Title
HIGH TEMPERATURE DEFORMATION OF MgO

Author
Dokko, Chung.

Publication Date
1975-11-01

LBL-3979
c.1

HIGH TEMPERATURE DEFORMATION OF MgO

Chung Dokko
(Ph. D. thesis)

November 1975

Prepared for the U. S. Energy Research and
Development Administration under Contract W-7405-ENG-48

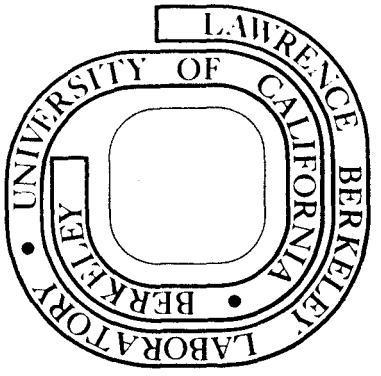

LBL-3979
c.1

DISCLAIMER

HIGH TEMPERATURE DEFORMATION OF MgO

Contents

HIGH TEMPERATURE DEFORMATION OF MgO

Chung Dokko

Materials and Molecular Research Division, Lawrence Berkeley Laboratory
and Department of Materials Science and Engineering,
University of California, Berkeley, California 94720

ABSTRACT

The deformation and recovery of both single crystals (⟨100⟩, ⟨110⟩, ⟨111⟩ and Ni-doped ⟨100⟩) and fully dense polycrystals (with grain sizes ranging from 4 to 160 μm) of MgO were studied under compressive stress-strain and creep testing conditions at 1200°C (0.48 Tm) and 1400°C (0.55 Tm). Emphasis was placed on the aspects relevant to ductility such as recovery contribution and the role of grain boundaries. Correlations were sought between stress-strain and creep results, and between deformation and recovery rates measured during stress-strain tests. It was found that no polycrystals were harder than a ⟨111⟩ crystal, nor softer than a ⟨100⟩ crystal, which represented dislocation glide on the more difficult and the less difficult slip planes, respectively. Plastic anisotropy between these slip planes decreased and polycrystalline ductility increased with decreasing strain rate as well as increasing temperature. Simultaneous activation of all five independent slip systems did not lead to a large ductility. A maximum ductility was observed for the smallest grain size under given testing conditions. Fine-grained specimens (<15 μm) were susceptible to rapid recovery and accommodation aided by dislocation climb. Steady flow or fracture stress, however, exhibited little dependence on the grain size except when diffusional creep or premature failure

occurred. In addition to slip on both planes and dislocation-climb-aided accommodation, intergranular separation is suggested as a mode of accommodation, although it was accompanied by weakening effects. Significance of grain boundary nature, per se, was indicated by variability of the mechanical behavior as a function of prior annealing history for the same grain size.

I. INTRODUCTION

Dislocation glide or slip is an important deformation mechanism for ceramic materials when a diffusional deformation mechanism of Nabarro[1]-Herring[2] or Coble[3] type cannot produce fast deformation. For MgO, slip occurs in <110> directions on {110} and {100} planes to provide 2 and 3 independent slip systems, respectively. Simultaneous operation of 5 independent slip systems, often referred to as the von Mises[4] requirement, would allow a general shape change of a polycrystalline body without resulting in the loss of grain boundary coherence. Hulse et al.[5] have shown previously that the critical resolved shear stress for secondary slip on {100} planes is considerably greater than that for primary slip on {110} planes. Consequently, the stress must be raised to the level necessary for the secondary slip before all 5 independent slip systems become operative.

Provided that primary slip can take place before the secondary slip systems are activated, stress concentrations might develop at grain boundaries in association with dislocation pileup. If the grain boundaries are not strongly bonded, then the stress concentration could result in intergranular separation (IGS) before the critical resolved shear stress for the secondary slip systems is reached. It seems likely that IGS would be followed by premature failure. However, several workers have noted in various types of ceramic materials such as UO_2,[6,7] ZrO_2,[8] and Al_2O_3[9,10] that these were crept at a steady state while IGS

occurred. These observations suggest that some limited, even stable, flow is possible in spite of the failure to satisfy the von Mises requirement.

On the other hand, fulfillment of the von Mises requirement is not a sufficient condition for unlimited ductility. Stresses will continue to build up at barriers to dislocation motion unless the removal of dislocations from the head of the pileup takes place as fast as the accumulation of dislocations. Under such circumstances, weakness of the grain boundaries as barriers would increase the likelihood of IGS and hence of a limited ductility.

Dislocations leave the glide plane by thermally-activated processes such as cross-slip and climb. According to Weertman's model,[11] they can be subsequently annihilated upon encountering the dislocations of opposite sign on the new glide plane. Both removal from the head of a pileup and subsequent annihilation of dislocations can occur during deformation (dynamic recovery) as well as during static recovery to cause softening effects. Furthermore, this process may preempt crack nucleation. Thus, ductility might be expected to increase as a result of dynamic recovery. The study of recovery phenomenon has an particular relevance to ceramic materials, since they become plastic at elevated temperatures where the contribution of dynamic recovery should also be significant.

Any thermally-activated process is time- or strain-rate-dependent. The effect of strain rate could be not only a quantitative

but also a qualitative one such as a change in the deformation mechanism. Thus, it was of interest to see whether the stress-strain curves obtained at relatively high strain rates could be used to predict, or be correlated with, the creep behaivor at lower strain rates.

Hence, the major objective of the present work are:

a) to study the role of the grain boundary in high-temperature deformation and the relation between single crystal and poly-crystalline specimens,

b) to study the role of dynamic recovery in high-temperature deformation, and

c) to seek a correlation between the stress-strain and the creep behavior and to study the effects of strain rate.

II. EXPERIMENTAL PROCEDURE

A. Preparation and Characterization of Specimens

Both single and polycrystalline specimens of parallelepiped shape with dimensions of 0.15×0.15×0.30 inches were parpared.

1. Single Crystal Specimens

Two types of single crystals, one undoped and the other doped with 0.8 wt% NiO, were obtained from the Muscle Shoals Electrochemical Corp., Tuscumbia, Alabama. The cation impurities are reported in Table I(A). The specimens to be loaded along <100> axis were formed by cleaving. The <110> loading axis specimens, flanked by {110} and {100} planes, were cut and cleaved after being oriented on the goniometer using Laue back-reflection X-ray technique. The <111> loading axis specimens, having side faces of {110} and {112} planes, were cut in a similar fashion. Both <110> and <111> specimens were within 1° from their true orientations, and were prepared from undoped crystals only. Machined faces were ground on a series of emery papers down to 4/0 grade. A special jig was used to ensure that the ends were parallel to each other and perpendicular to the side faces. Finally, all single crystal specimens were polished in 85% orthophosphoric acid at 110°C for 2 min.

Ni-doped crystals were apparently affected by the reducing atmosphere during crystal growth. While a major portion used for specimen preparation was transparent and colored light green, the outer portion was opaque and dark colored. Electron microprobe analysis indicated

that this portion contained particles of Ni metal. Thus, it seems possible that the specimens were enriched in cation vacancies by diffusion after they were produced in association with reduction of NiO. Hereafter, the Ni-doped <100> crystals are denoted by N<100>.

A limited number of single crystal specimens were annealed 100h in air at 1400°C prior to testing.

2. Polycrystalline Specimens

Polycrystalline specimens were fully dense and machined from a large disc (7 in. diameter by 3/8 in thickness) provided by Eastman Kodak Company. They were prepared by hot pressing MgO powder with the aid of 2 wt% LiF followed by some unspecified heat treatment to produce transparency. The corresponding impurity contents are listed in Table I(A). The content of Li, although not detected, is presumed to be less than 40 atomic ppm which corresponds to the as-hot-pressed condition of a similar Kodak specimen according to Leipold and Blosser.[12] Test specimens were prepared by following similar procedures used for single crystals. Specimens were then annealed in air at 1400°, 1450°, and 1500°C for various lengths of time; most specimens were annealed at 1500°C and henceforth only the specimens annealed at other temperatures will be so specified. Some specimens, however, were tightly wrapped in thin platinum foil during the anneal. Hereafter, these are designated as "annealed in Pt (wrap)" in contrast to "annealed in air". The

following characteristics were noted in annealed specimens:

(a) The specimens remained essentially transparent except when annealed in air at 1400°C. In this case, numerous cloudy spots were formed and optical microscopy of polished section revealed continuous or discontinuous features on grain boundaries (Figs. 1 (a) and (b)). These features are believed to correspond to intergranular separations indicative of weakened grain boundary cohesion. Day and Stokes[13] have previously made a similar observation, namely, the evolution of porosity during annealing of initially transparent MgO. Electron microprobe analysis (thin window technqiue) failed to indicate the association between these features and fluorine. Therefore, their origin remains unclear at present.

The analysis, however, revealed that corners of small grains were enriched in Si. Thus, it is likely that the liquid phase on the short, constricted grain boundaries (eg., in the center of Fig. 1b) as well as some triple points is associated with Si.

Many F ions are not expected to be in the form of LiF in view of the higher content of F as compared with Li (eg., 2000 vs. 40 ppm after hot pressing, according to Leipold and Blosser[12]). Bulk content of F is reported in Table I(B) for the as-received condition and after annealing at 1500°C. It can be seen that the F concentration decreased steadily during annealing and its removal was delayed by the use of Pt wrap.

The amount of F associated with grain boundaries was estimated

by assuming that all the F ions were accumulated at grain boundaries in the form of a thin "film" with simple cubic packing (see Appendix I). It was found that the amount of F associated with unit areas of grain boundary, as indicated by thickness of the "film", actually increased with grain growth before it decreased (Fig. 2.).

It should also be noted that more F was removed from the specimen annealed in Pt as compared with the specimen annealed in air to give the same grain size. Since the use of Pt wrap would be expected to raise the partial pressure of F and thus retain more F in the specimen, the decrease of F must be attributed to a longer annealing period together with slow grain growth.

(b) Grain size was defined as 1.27 times the average chord length obtained by lineal intercept method. Thus, the grain size ranged from 4μm in the as-received condition to 160μm for the maximum anneal. Hereafter, the specimens with grain sizes of 4 to 15μ m, 25 to 40μm, and 60 to 160μm will be referred to as being fine-grained medium-grained, and coarse-grained, respectively. Otherwise, the grain sizes are specified for the individual specimens.

Behavior of grain growth is depicted in Fig. 3. While the common square law for grain growth was roughly obeyed, some deviations were noted. Regardless of annealing parameters, the grain size tended to be stabilized at ~25μm with respect to further grain growth; this stage was followed by accelerated grain growth corresponding to the extended annealing periods. The Laue X-ray

patterns confirmed that no preferred orientation developed during annealing (Fig. 4). Hence, no apparent change in the physical nature of grain boundaries could be associated with the observed stabilization of grain growth.

It is also shown in Fig. 3 that the use of Pt resulted in retardation of grain growth. Since the use of Pt suppressed the escape of F, it is tempting to conclude that F was responsible for the inhibitive effect of grain growth.

B. Mechanical Testing

All specimens were subjected to identical testing conditions to allow for a valid comparison. An Instron testing machine and the hydraulic loading machine built previously by Hulse and Copley (Apparatus III)[14] were used to obtain stress-strain and creep curves, respectively. A wide range of strain rates differing by four orders of magnitude was thereby covered. The specimens were loaded in compression and in air at 1200° (= 0.48 Tm) and 1400°C (= 0.55 Tm).

Reported in this work are true stresses and true strains. True stress (σ_T) was calculated under the assumption of uniform deformation so that

$$\sigma_T = \frac{P}{A_o}(1-\varepsilon_{eng})$$

where P is the applied load, A_o the original cross-section area, and ε_{eng} the engineering strain. True strain (ε_T) was given by

$\ln (1-\varepsilon_{eng})$.

The specimen was placed in the center of a split furnace with $MoSi_2$ heating elements and held in place by a preload of 1000 psi with Al_2O_3 loading rams while being heated. The rams were protected by Lucalox buttons (3/4 in. diameter by 3/8 in. thick). Thin platinum foils (0.0005 in. thick) were inserted between the specimen and the buttons as a reaction barrier and hence as a lubricant. The specimen was held at the test temperature for 1 h behore testing started.

1. Stress-Strain Tests

The specimens were deformed in an Instron machine at various crosshead speeds to give nominal strain rates ranging from 1×10^{-5} to 3×10^{-4} sec^{-1}. Two types of tests were run. In one type, the test was carried out at a single crosshead speed until fracture was indicated by gradual decrease or sudden drop in load. If fracture was not encountered, the test was simply discontinued at some large strain. In the second type, the test was interrupted either by a change in crosshead speed or by an unloading-reloading sequence.

In the latter sequence, the specimen was unloaded in several steps until the subsequent relaxation curve showed momentarily no change in load with time. This stress corresponded to the so-called "internal" stress below which no deformation could occur (See MacEwen et al.[15]). In a limited number of cases, the specimen was fully unloaded, i.e., to the preload level. The specimen was then allowed to recover before being reloaded.

2. Creep Tests

While the hydraulic machine was able to maintain a constant load, tests were performed at constant true stresses by manually adjusting the applied load in accordance with the instantaneous strain. Whereas some specimens were deformed at a single stress throughout the test in order to establish steady states, the incremental stress technique was applied to others in order to reduce scatter among specimens: the stress was increased everytime steady state was observed. In some instances, however, stress was decreased to check the reproducibility of the previously-obtained steady state. Applied stresses ranged between 2000 and 32,000 psi.

To eliminate possible errors arising from deformation of loading trains, displacements between reference points on the Lucalox buttons caused by deformation of the specimen were monitored as a strain. Such displacements were transferred out to a LVDT via a lever arrangement and recorded continuously. Two sapphire rods used as lever arms had sharp ends which were forced by spring loading to rest in small divots inscribed on the buttons as fiducial marks.

In this work, conventional activation energy was obtained from a ratio of steady creep rates at 1200°C and 1400°C. In some cases, however, activation energy was determined from a ratio of strain rates before and after a small rapid change in temperature made during the test (Dorn's technique[16]). In this case, both an increase and a decrease of 25°C were effected by manual control of the power supply within 10 minutes.

C. After-Test Examination

The deformed specimens were examined visually for their shape and macroscopic fracture path. Before being mounted and polished, surfaces of some selected polycrystalline specimens were examined by an optical and a scanning electron microscope. Laue back-reflection X-ray patterns were taken from some single crystal and fine-grained polycrystalline specimens, using tungsten radiation at 50 kv and 20 ma for 2 min. Deformed <111> specimens were cleaved to expose a (100) plane which was then mounted for optical microscopy. All specimens were mounted in resin and mechanically polished through 1/4μm diamond paste in lapping oil. Single crystal specimens were etched in a solution consisting of two parts of 85% orthophosphoric acid and one part of concentrated sulfuric acid at room temperature for 30 minutes. Polycrystalline specimens were examined for cracks and cavities after mechanical polishing, and subsequently etched in 0.5M solution of $AlCl_3$ maintained at 55°C for 3 minutes.

III. EXPERIMENTAL RESULTS

A. Macroscopic Observation

1. Buckling

Despite all efforts to prevent it, buckling occurred in some <100>, N<100> and <110> single crystals regardless of applied strain rates or stresses. The extent of buckling in <111> single-crystal and polycrystalline specimens, however, was comparatively small or unnoticeable. Preventive measures included:

a) Use of a small aspect ratio: the ratio of 2:1 was selected on the basis of previous work.[17]

b) Careful alignment of loading rams and testing below the pre-determined load for elastic buckling of the loading column itself.

c) Use of specimens with a variation in height less than 0.0002 in. throughout the cross-section and careful alignment with loading rams.

d) Use of a snug fitting alumina tube to confine the sideway movement of Lacalox buttons; this practice, however, was discontinued since buckling still took place by sliding at the interface between the button and the specimen.

With buckling, one or both ends (rather than mid-section) of the specimen had escaped the alignment. Severe buckling that occurred in some <100> and N<100> crystals at later stages of deformation was accompanied by a load maximum on the load-displacement curve.

2. Spreading of Cross Section

In <100> and N<100> single crystals, the occurrence of oblique intersection involved in slip was indicated by spreading of the cross-section in both directions. According to such evidence, the oblique intersections occurred in these crystals deformed at 1400°C, but rarely in the crystals deformed at 1200°C: in the latter case, the cross-section spread only in one direction.

In general, both single crystals and polycrystals were barrelled during deformation, causing non-uniform cross-section areas along the loading axis. Barrelling in a <100> crystal involved lattice bending. This is indicated in Fig. 5 by a curved longitudinal cleavage crack that conformed to the barrelled shape. The cocurrence of lattice bending was subsequently confirmed by the streaks on a Laue pattern (Fig. 6).

In the case of fine-grained polycrystals, however, it was noted that the occurrence of barrelling depended on the testing conditions. Thus, as shown in Fig. 7(b), no barrelling occurred in an as-received polycrystal crept at 1400°C and low strain rates ($<1\times10^{-6}sec^{-1}$). It should be pointed out that this particular specimen was not deformed at a constant stress throughout. Instead, it was subjected to incremental stressing after steady creep occurred at a given stress. Thus, even a slightly "negative" buckling was observed when the same type of specimen was deformed to a greater extent within a given low strain rate region (Fig. 7(c)). On the other hand, this type of specimen was barrelled when deformed at a higher strain rate (i.e. stress-strain tested at $\dot{\varepsilon}>1\times10^{-5}sec^{-1}$) at the same

temperature. In Fig. 7(a), an example of barrelling is shown for a similar type of specimen stress-strain tested ($\dot{\varepsilon}\sim 1\times 10^{-5}\,sec^{-1}$) at 1200°C.

3. Fracture

Deformed single crystals often showed macroscopically visible cracks; these cracks usually emanated from the ends of the specimen and propagated partially into the specimen. Nevertheless, the overall shape of the corresponding stress-strain curve was not seriously affected thereby.

Most polycrystalline specimens lost transparency during deformation. The loss of transparency, however, was not necessarily accompanied by the loss of load-carrying capacity or fracture. For instance, a coarse-grained (~160μm) specimen was found to be opaque at 1% strain, although the corresponding stress-strain curve had no indication of fracture; the curve showed strain hardening up to this point. On the other hand, macrocracks were not visible in coarse-grained specimens deformed beyond a miximum load, indicative of fracture. This behavior was in contrast with medium-grained specimens where macrocracks could be seen clearly under similar conditions.

Concerning the resistance to the loss of transparency, it was observed to be a function of specimen character and testing condition. Thus, when deformed to 1.5% strain at $\dot{\varepsilon}\sim 1\times 10^{-5}\,sec^{-1}$, an as-received specimen remained transparent whereas a slightly coarser-grained (~15μm) specimen turned opaque under the same conditions. On the other hand, the as-received specimen did not

remain transparent at the same strain when deformed at the same temperature but a higher strain rate of 3×10^{-4} sec^{-1}. By the same token, the latter specimen could essentially retain its transparency at 5% strain when deformed at 1200°C and strain rates that were approximately two orders of magnitude lower than the above value.

4. Texture Development

Laue back-reflection X-ray patterns were taken from polycrystalline specimens with a grain size less than 30μm that were tested for stress-strain and creep curves at both test temperatures. For all the cases examined, there was no indication even after true strains as large as 90% that any preferred orientation or texture had developed during deformation.

B. Microscopic Observation

1. Single Crystal Specimens

a. Etch pits. At 1200°C, the general arrangement of etch pits could be characterized by uniformly spaced slip bands that intersected with each other, regardless of specimen types and of strain rates. This is illustrated in Fig. 8(a) for a crept <111> specimen as seen on a (100) plane. In this case, the operative slip planes were identified as {100} planes, since they were parallel to the cleavage cracks that appeared in the same section (not shown). On a localized scale, however, subboundaries were observed to form in the case of a N<100> crystal deformed at $\dot{\varepsilon}\sim1\times10^{-5}$ sec^{-1} (Fig. 9). This may be significant since such observation were not made at all in undoped <100> crystals under

the same conditions.

At 1400°C, slip bands persisted in all stress-strain tested specimens. Specimens crept at low strain rates, however, tended to develop subgrain structures. Thus, in the case of <100> crystals, subgrains did not form when stress-strain tested at $\dot{\varepsilon} \sim 1 \times 10^{-5} sec^{-1}$ (Fig. 10(a)). Whereas they were seen to form locally when crept to a comparable strain at strain rates that were more than an order of magnitude lower (Fig. 10(b)).

As mentioned above, N<100> crystals appeared to be more susceptible to subgrain formation. In Figs. 11(a) and (b), the extent of subgrain development is shown as a function of strain when those crystals were crept at 1400°C and a stress of 8000 psi by 12 and 27%, respectively. At the smaller strain, slip bands coexisted with open-ended subboundaries. These boundaries did not seem capable of blocking edge dislocation since they were freely crossed by slip bands. At the larger strain, the boundaries were fully developed encircling the subgrains, and slip bands could hardly be seen.

It was noted that <111> crystals were most susceptible to formation of subgrains. Thus, even though the subgrain structure shown in Fig. 8(b) corresponds to a specimen crept as much as 50% strain, a similar structure was also observed in another specimen crept by only 3% at lower stresses.

b. Microcracks. The presence of microcracks was revealed in all types of single

crystals crept or stress-strain tested at a low strain rate. Microcracks were observed at 1400°C in a <100> crystal (Fig. 10(a)) and a N<100> crystal (Fig. 11(a)). Since examination of the cross-sections suggested the occurrence of oblique intersections at this temperature, microcracking could be considered as an indication of the difficulty involved in the oblique intersection. Similary, microcracks present in a <110> crystal (Fig. 12(a)) and a <111> crystal (Fig. 12(b)) after creep testing at 1200°C should also be indicative of the intersection difficulty. This interpretation is consistent with the rapid strain-hardening observed during stress-strain tests at the same temperature (Figs. 23 and 22(c), respectively).

It is to be noted, however, that the microcracks tended not to propagate. It seemed that the microcracks were prevented by slip bands from subsequently propagating.

2. Polycrystalline Specimens

a. Grain Growth. Although grain growth by a factor of ~2 could occur in the finest-grained or as-received (4μm) specimens during heating prior to testing, subsequent grain growth during a stress-strain test was found to be rather neglible. A limited further grain growth (by another factor of 2) was encountered in this type of specimen crept for 600h at 1400°C. Another specimen of the same type that was annealed next to the deforming specimen during the same run, however, exhibited a remarkable grain growth, i.e., a factor of 15. Such a large difference suggests that grain size was wather stabilized by simultaneous deformation. Other types of

specimens with a grain size larger than 20μm did not show any noticeable grain growth during creep.

b. Grain Shape. When a polycrystalline specimen was deformed to a large strain, there was a corresponding change in the shape of the grains. Thus, at 1400°C, a fine-grained specimen crept to 5% showed equiaxed grains (Fig. 13(e)), while another specimen of the same type crept to 48% strain tended to develop oval-shaped grains squeezed along the compression axis (Fig. 13(f)). Tendency toward the oval-shaped grains was also noted in a finer-grained specimen crept to 99% strain at the same temperature (Fig. 14(b)).

On the other hand, a medium-grained (annealed in Pt) specimen could be characterized by its tendency to exhibit diamond-shaped grains that were aligned edge to edge at an angle to the compression axis. These features were observed throughout the specimen, although somewhat stronger development was noted along the specimen ends. This behavior was indicated in the specimens crept at 1200°C (Fig. 15(b)), and stress-strain tested at $\dot{\varepsilon}\sim 1\times 10^{-5}\,\mathrm{sec}^{-1}$ or crept at 1400°C (Figs. 15(c) and (d), respectively). Similar behavior was also encountered in a finer-grained (~15μm) specimen stress-strain tested at 1200°C and $\dot{\varepsilon}\sim 1\times 10^{-5}\,\mathrm{sec}^{-1}$ (Fig. 13(b)).

c. Subgrain Formation. Evidence of creep by dislocation motion was provided by subsgrain formation. Most distinct subgrains were developed in coarse-grained specimens crept at 1400°C (Fig 15(b)). Although subgrains did not form and grain boundaries remained smooth at small strains (Fig. 15(a)), development of subgrains with increasing strain was accompanied by corrugation

of the grain boundaries as illustrated in Fig. 16(b). It can be seen that cusps (arrow) formed at the intersection of the grain boundary with a subboundary.

Subgrains were also observed to form in medium-grained specimens that gave rise to diamond-shaped grains (Fig. 15(b) through (d)), and in an initially fine-grained specimen that was crept for a period of 600h at 1400°C, exhibiting oval-shaped grains (Fig. 14(a)). In the latter case, however, subgrains were rather indistinguishable from grains. As indicated in single crystals crept at 1200°C, however, subgrain formation did not appear to be a prerequisite for the steady creep, since subgrains were sometimes absent in a specimen that was crept in the steady state (e.g., Fig. 16(a)).

d. Grain Boundary Sliding. Direct and indirect evidence that grain boundary sliding (GBS) had occurred was obtained in all the specimen types examined. Direct evidence in fine-grained specimens is shown by scanning electron micrographs (Fig. 17(a) and (b)). It can be seen that grains on the surface were squeezed out as a result of GBS. Note also that a grain at the center of Fig. 17(b), for instance, was rotated around the axis which lies nearly in the plane of the photograph; other neighboring grains also slid against the rotating grain and were squeezed further out of the surface.

Also shown in Fig. 17(b) is indirect evidence of GBS, i.e., widening of intergranular separation (IGS). Complete IGS occurred across a single facet of the grain, with the facet

corresponding to the tensile grain boundary that was essentially parallel with the (vertical) compression axis. It is important that the adjacent facet remained coherent while the IGS developed on the tensile facet continued to widen. This evidence attests to the stability of IGS with respect to propagation as a crack. The micrograph also suggests that such widening was associated with GBS on the adjacent facet.

Furthermore, there was indication that IGS was caused by GBS. In Fig. 18(a), one area where no extensive IGS has yet occurred is shown for a medium-grained (annealed in Pt) specimen stress-strain tested at 1200°C and $\dot{\varepsilon} \sim 1 \times 10^{-5} sec^{-1}$. Note that localized deformation (arrows) took place along the extension of the grain boundaries that were favorably oriented for GBS. Such features, termed a "fold" by Chang and Grant,[18] represent an accomodation mechanism for GBS. However, more severe GBS that could not be fully accomodated resulted in IGS, as was observed in different areas of the same specimen (Fig. 18(b)). It can be seen that the separation occurred in spite of the more advanced folding as compared with Fig. 18(a). Once the grains are separated along an edge A, GBS occurs freely along the adjacent edge B. This not only widens the gap at A, but also nucleates IBS at a third edge C. Thus, the IGS spreads (rather than propagates) throughout the body. After extensive development, however, interlinkage of IGS may occur to cause intergranular fracutre (Fig. 15(a)).

e. Intergranular Separation. Complete IGS as described above was most pronounced in the specimens stress-strain tested at a low

temperature or at a high strain rate. IGS was observed as early as at yielding stages. Thus, a fine-grained specimen stress-strain tested at 1200°C and $\dot{\varepsilon}\sim 1\times 10^{-5}\,sec^{-1}$ exhibited IGS as shown in Fig. 13(a), at a strain of 1.5%. In this particular case, the corresponding stress-strain curve showed strain-softening immediately following yielding, although strain-hardening ensued at later stages.

In the case of a coarse-grained specimen, there was a clear indication that IGS contributed directly to the observed strain (at the expense, however, of a volume change of the specimen). Namely, as shown in Fig. 19, a coarse-grained specimen (cloudy prior to testing) stress-strain tested at 1200°C and $\dot{\varepsilon}\sim 5\times 10^{-5}\,sec^{-1}$ exhibited a barrelled shape in which the maximum local deformation at the midsection was also associated with the widest IGS in this specimen.

f. Cavitation. Partial separation of grain boundaries, or cavitation, was characteristic of the specimens stress-strain tested at a high temperature or at a low strain rate. Cavitation occurred in fine-grained as well as coarse-grained specimens. While they were located primarily at triple points, cavities were also noted to form on the grain boundaries. In the case of a coarse-grained specimen (Fig. 16(c)), it could be seen that the cavities were nucleated at the points where the grain boundary was intersected by a subboundary (arrow). However, it was also observed that the extension of IGS could be stabilized by the intersection point (Fig. 16(d)).

In contrast with complete IGS, cavitation did not occur preferentially on the tensile grain boundaries. Absence of cavities inside the grains suggested that grain boundary migration was stabilized by the observed cavities or that the cavities migrated with grain boundaries.

The number of cavities seemed to increase with increasing strain. However, they were not necessarily interlinked even after a large deformation. Such an example is given in Fig. 20(a) for a medium-grained specimen crept to 92%. For a comparable strain, less cavities were present in a specimen deformed at a lower strain rate (cf. (d) vs. (f) in Fig. 13).

g. Cracking. The term of a crack was reserved in this work to describe the separation that extended beyond a grain size. Cracking was found to occur predominantly along intergranular paths, as can be seen in Figs. 14(b) and 15(a). This generally was true regardless of material character and testing conditions.

As shown in Figs. 14(a) and 20(b), however, transgranular cracking was also observed locally in some specimens with a relatively small grain size that were crept to a large strain exhibiting an extremely slow tertiary stage. In these cases, it can be noted that branching or secondary cracking also occurred. Secondary cracks appeared approximately in parallel to, but thinner than the major, continuous crack. Since these specimens did not fail catastrophically despite cracking, it was considered that the secondary cracking was characteristic of the slow fracture (i.e., the slow tertiary stage). It is possible that secondary cracking tended to dissipate the stress concentrations at the tip

of the major crack, thus retartding crack propagation and reducing the immediate damage to the load-carrying capacity of the specimen.

C. Mechanical Behavior

1. Shape of Stress-Strain Curves

True stress-true strain curves presented here are based on the individual readings of load-displacement curves taken at strain interval of 2.5 or 5%. Hence, the small variations within this interval are not indicated. In general, the specimen character was reflected in the shape of stress-strain curves for the same testing conditions. The shape of <100> and N<100> crystals was characterized by gradual yielding followed by approximately linear strain-hardening (Figs. 21(a) and (b)) whereas <111> and <110> single crystals (Figs. 22(c) and 23) exhibited a smooth parabolic shape with initially rapid strain-hardening. In the case of polycrystals, however, various shapes were observed as a function of annealing parameter, particulary when tested at 1200°C (Fig. 24(a)). Also, in addition to the features shown in the figure, medium-grained polycrystals showed "yield drop", yield plateau, or sharp yielding, depending on the annealing condition. Magnitudes of the yield drop are given in Table III. As indicated in Fig. 24(b), however, the effect of material character on the shape of the curve tended to diminish at 1400°C. Yield drops were also absent although the specimen annealed in Pt showed a limited strain-softening. In this figure, it is also shown that polycrystalline stress-strain curves are bracketed by the curves for <100> and <111> single crystals.

Except when premature failure occurred as in coarse-grained polycrystals, all specimens except for N<100> crystals tended to approach a steady state when deformed at 1400°C and $\dot{\varepsilon}\sim 1\times10^{-5}sec^{-1}$. Also, in the case of polycrystals, the curves for fine-grained and medium-grained specimens tended to merge as a steady state was approached (Fig. 24(b)). For the same strain rate but at 1200°C, on the other hand, the tendency toward a steady state was overshadowed by either continued strain-hardening or premature failure except for fine-grined polycrystals. As shown in Fig. 24(a), a fine-grained polycrystal with a grain size of 13μm showed strain-softening immediately following yielding. Similar behavior has been observed previously by Evans et. al.[19] for porous, hot-pressed MgO specimens. This stage, however, was eventually replaced by strain-hardening which led to a brief steady state.

In the case of a finest-grained polycrystal, an apparent steady state occurred followed by another steady state of a shorter duration (Fig. 24(a)). Thus, these polycrystals tended to approach the same flow (or fracture) stress at a large strain. In the case of <110> and <111> single crystals as well as coarse-grained polycrystals, the rate of strain-hardening continued to decrease unitl a maximum stress indicative of fracture was reached. Although the maximum also occurred in annealed <100> and N<100> crystals (Fig.s 22(a) and (b)), this occurrence was attributed to the severe buckling encountered in these particular tests. On the other hand, microcracking that occurred in other tests of these

types of crystals was not generally registered on the corresponding stress-strain curve. In some cases, however, a sharp finite drop of load signifying an extensive cracking was registered at later stages, although the load sprang immediately back to the level that would have been observed in the absence of the drop; one particular observation made with a <100> crystal deformed at 1200°C and $\dot{\varepsilon} \sim 3 \times 10^{-4} sec^{-1}$ is shown in Fig. 21(a).

As shown in Figs. 21(a) and (b), the curve for a <100> crystal became essentially linear beyond yeilding when tested at the highest strain rate. The curve for the lowest strain rate, on the other hand, showed three stages with a maximum slope occurring at the intermediate stage. This behavior is similar to that for NaCl deformed at room temperature.[20] These stages were less noticeable at the higher temperature and in doped crystals.

It can also be seen in Figs. 21(a) and (b) that a Ni-doped crystal strain-hardened less rapidly than an undoped crystal, even though the former crystals yielded at a slightly higher stress. An exception, however, was observed when the test was run at 1400°C and the lowest strain rate. In this case, the doped specimen continued to strain-harden while the undoped specimen reached a steady state.

Although not indicated in the figures presented, serrated curves were observed in the doped crystals; at low or high strain rates for 1200°C and 1400°C, respectively. The serrations were characterized by instantaneous stress drops rather than overshooting above, or oscillations about, the general level of the curve, with

a drop accounting for as much as 5% of the total stress. The serrations were often accompanied by a reduced rate of strain-hardening over a limited strain.

It is worthwhile to note the effect of prior treatment on the stress-strain curve of single crystals observed as a function of material character. Namely, prior annealing of a N<100> crystal resulted in an increased slope of the curve despite the occurrence of severe buckling (Fig. 22(b)) whereas the identical treatment of a undoped <100> crystal did not (Fig. 22(a)). In the case of a <111> crystal, annealing resulted in a general elevation of the stress-strain curve over that of an unannealed specimen and this effect was more appreciable at the lower test temperature (Fig. 22(c)). Similar type of hardening was observed in the case of a <100> crystal as a result of introducing mechanical damage on the surface by grinding the specimen (Fig. 22(a)). This observation suggests that surface effects could persist at a high temperature.

As indicated above, the stress-strain curve of a given specimen type was a sensitive function of the strain rate for the same temperature. The degree and the nature of the sensitivity depended on the type of the specimen. For <100> and N<100> crystals, the general slope of the curve was sensitive to the strain rate. In this case, the doped crystal was more sensitive than the undoped crystal at 1200°C, while the opposite was the case at 1400°C (Figs. 21(a) and (b)). For <111> crystals (Figs. 22(b) and 25)

and fine-grained polycrystals (Figs. 24(a) and 26), an increased strain rate resulted in increased flow stresses which, however, started to decay at early stages. Fine-grained polycrystals exhibited a greater strain-rate-sensitivity than medium-grained specimens. Hence, the former specimen was harder than the latter at $\dot{\varepsilon}\sim 3\times 10^{-4}\,\mathrm{sec}^{-1}$, whereas the opposite was observed at $\dot{\varepsilon}\sim 1\times 10^{-5}\,\mathrm{sec}^{-1}$ (Figs. 24(b) and 25). On the other hand, coarse-grained polycrystals showed an opposite response; the flow stresses were lowered upon an increase in the strain rate (Figs. 24(a) and 26).

In the interrupted stress-strain tests, the response corresponding to a given instantaneous change in the crosshead speed (by a factor of 2.5 to 25) was found to be a function of specimen character. Three types of responses are illustrated in Fig. 27 for an increase in the strain rate. In types A and B, little instant (or elastic) increase in the stress occurred, although the slope of the stress-strain curve either decreased (type A) or increased (type B). In type B, the larger the ratio of the crosshead speeds involved, the larger was the change in the slope. Whereas type C is characterized by some ill-defined instantaneous increase in the stress. In <100> or N <100> crystals, all types were observed depending on the strain of interruption; the type changed from A for small strains through B for intermediate strains to C for large strains. In <111> crystals or polycrystals, on the other hand, only type C was observed.

In another type of test interrupted for recovery to take place, three types of response were observed upon reloading depending also on the specimen character. As shown schematically in Fig. 28, type A represents a transient effect produced by recovery; although flow upon reloading occurred at a stress slightly lower than the stress prior to recovery, the shape of the original stress-strain curve was soon restored. Type B corresponds to a more durable effect i.e., general lowering of the curve over a period of deformation, reminiscent of "ortho-recovery" described by Cherian et al.[21] Type C is of somewhat intermediate nature between types A and B. In <100> and N<100> crystals, all three types appeared, depending on the strain at which the specimen was unloaded; types A, B and C appeared at initial, intermediate and final stages of deformation, respectively. At intermediate stages (between 3 and 15%, approximately), the type B became the more pronounced, the longer the recovery period. Although the original stress-strain curve was eventually restored in most cases, an exception was noted in a N<100> crystal deformed and recovered at the lowest strain rate used and at 1400°C. In this case, an extended recovery resulted in flow at a decreased stress followed, however, by strain-hardening above the level extrapolated from the previous stress-strain curve.

In <110>, <111> crystals and polycrystals, only type C occurred regardless of strains and recovery periods. However, some variations of this type were also noted. Namely, in <111>

crystals deformed at high strain rates and 1200°C, recovery resulted in appearance of the yield drop. As shown in Fig. 29, magnitude of the drop accounted for a few % of the total stress at its maximum which occurred at a small intermediate strain. In the case of fine-grained polycrystals, extended recovery gave rise to a peak stress upon reloading (σ_{max}) which was greater than the stress (σ_o) that was maintained at a steady state prior to recovery (Fig. 30). This behavior was termed "recovery-hardening" and the difference, $\sigma_{max}-\sigma_o$, is reported in Table IV as a function of annealing and testing parameters. For a given testing condition, the effect is shown to be more pronounced for a specimen that was subjected to less extensive annealing prior to testing.

2. Shape of Creep Curves

For both single crystals and polycrystals, a small instantenous straining upon loading was usually followed by a primary stage characterized by monotonously decreasing strain rates, and subsequently by secondary stage or steady state. While it was not observed in single crystals, a pronounced tertiary stage was encountered in a coarse-grained polycrystal crept at 1200°C (Fig. 31). At 1400°C or for finer-grained specimens, this stage was rather unnoticeable. Thus, for instance, a fine-grained or a medium-grained specimen was crept to ~90% in true strain (or ~60% in engineering strain) without a catastropic failure.

Concerning the primary stage, sigmoidal (S-shaped) curves were observed in both single crystals and polycrystals crept under

low stresses and at 1200°C, in particular. It is noteworthy that both undoped and Ni-doped <100> crystals exhibited such behavior when crept at stresses lower than the yield stress: this stress was found to be insensitive to strain rates employed in stress-strain tests (Figs. 32(a) and (b)). For a medium-grained polycrystal, the initial strain rates were so low that there appeared to be an incubation period as indicated in Fig. 31. It should be noted, however, that a fine-grained specimen did not show sigmoidal creep to any noticeable extent.

Primary strain, or the strain at the onset of a steady state, was found to increase with stress and temperature. In Figs. 32(a) and (b), straight lines are drawn to indicate an average trend where primary strain increased with stress raised approximately to the third power. It can be seen that, for the same testing conditions, the primary period was most pronounced for a fine-grained polycrystal, less pronounced for a <100> crystal and least pronounced for a <111> crystal and a medium-grained or a coarse-grained polycrystal. In case of a find-grained polycrystal, apparent steady flow occurred during the primary period until it was terminated by transition to final steady state at a very large strain (Fig. 33).

Absolute strain hardening (h_o) was defined as the ratio of creep stress with respect to instantaneous strain upon initial loading. The results are plotted in Fig. 34 as a function of stress. It is shown that the values for <110>, <111> crystals and polycrystals are considerably higher than those for <100> and N<100> crystals.

3. Yield Stresses

The following remarks are of relevance in presentation of the data. a) The flow stress at 0.2% offset was defined as yield stress. b) In single crystals, Schmid (or stress resolution) factors for primary slip in a <100> and a <110> crystal and for secondary slip in a <111> crystal are 0.5, 0.25 and 0.47 respectively. In this work, however, compressive yeild stresses rather than critical resolved shear stresses are reported. c) For the plots showing temperature-dependency of yield stresses, the stress was normalized respect to the shear modulus (G). The shear moduli for <100> and <110> crystals well as N<100> crystals are the values for a (110) plane, whereas the moduli for <111> crystals are the values for a (110) plane. The same shear moduli were used for both undoped and doped crystals, because of unavailability of doped data in the literature. Also, since the high temperature data for MgO are not available, they were estimated by extrapolating the data obtained at lower temperatures by Chung and Lawrence[22] (Table II). d) When a temperature-dependency was observed, the activation energy (Q) was estimated on the basis of the data for two temperatures employed. Thus,

$$Q = \frac{R \ \ell n \ \frac{\dot{\varepsilon}_2}{\dot{\varepsilon}_1} \frac{T_2}{T_1} \frac{G_1}{G_2}}{\frac{1}{T_1} - \frac{1}{T_2}}$$

where R is the gas constant (or 1.987 cal/K.g mol), $\dot{\varepsilon}_1$ and $\dot{\varepsilon}_2$ the strain rates for a given value of $\frac{\sigma}{G}$ at temperatures T_1 and T_2, respectively, and G_1 and G_2 the shear moduli at T_1 and T_2, respectively. Thus-determined activation energy is reported in Table V together with the stress-dependency. e) In the Instron tests, the real strain rate of the specimen at initial stages of loading differs ignificantly from the nominal strain rate ($\dot{\varepsilon}$), or the crosshead speed divided by the original length of the specimen. Thus, the real instantaneous strain rate for the specimen ($\dot{\varepsilon}_T$) was given by

$$\dot{\varepsilon}_T = \dot{\varepsilon}(1 - \frac{h_N}{E_M}) \simeq (1 - \frac{\Delta P}{\Delta P_E})$$

where h_N is the slope of a tangent to the load-deflection curve at the point of interest in terms of engineering stress per unit strain, E_M the elastic modulus of the machine plus loading trains, ΔP the increment of load along the tangent of interest for a given increment of deflection, ΔP_E the increment of load pertaining to the same increment of deflection in the elastic region. f) The Instron data are plotted together with the creep data. For the latter, the maximum strain rates for a given creep stress were taken from tangents to the strain-time curve either immediately after the instantaneous straining ($\dot{\varepsilon}_i$) or at the stationary point ($\dot{\varepsilon}_{max}$) for those cases where sigmoidal creep was observed. The presented data correspond to the initial loading (prior to incremental stressing) of different specimens. Henceforth, the term of stress-dependency of creep rates will be used interchangeably as the term

of strain-rate-sensitivity of creep stresses.

The Instron data for both <100> (Fig. 34(a)) and N <100> Fig. 35(b)) crystals indicate that their yield stresses were essentially insensitive to strain rates and temperatures within the ranges studied. It was also noted that a doped crystal yielded usually at a slightly higher stress than a undoped one. The creep data, however, in contrast with the Instron data, shows a distinct temperature and strain-rate-dependence. Thus, as shown in Fig. 35(a), for instance, a higher stress must be applied under creep conditions to realize an initial strain rate comparable to that in the stress-strain test.

In comparison with <100> or N<100> crystals, <111> crystals (Fig. 35(c)) as well as polycrystals (Figs. 35(d) and (e)) are more sensitive to strain rates and temperatures. The strain-rate-sensitivity was increased further in a low strain rate region typical of creep rates, while the temperature-dependency appeared to remain unchanged (See also Table V). In Fig. 35(d), a parallelism or an agreement is indicated between <111> crystals and annealed polycrystals, despite the fact that the polycrystalline data represented the specimens with various annealing histories. According to the figure, the annealed polycrystals appear to be somewhat stronger than <111> crystals at 1400°C. However, the disparity would tend to be insignificant if the strain rates were also normalized with respect to G, or if neither the stresses nor the strain rates were normalized. Nevertheless, it was considered significant that the temperature-dependency or the apparent activation energy for polycrystals

tended to be lower than that for <111> crystals (Table V).

Because the behavior of as-received or finest-grained polycrystals was substantially different from that of annealed polycrystals, the data for the former specimens are plotted separately in Fig. 35(c). It is shown that as-received polycrystals exhibited a higher strain-rate-sensitivity (or a lower stress-dependence) in a low strain rate region in comparison with both <111> crystals and annealed polycrystals.

For a given strain rate and temperature, polycrystalline yield stresses measured in stress-strain tests were primarily a function of the grain size. In Figs. 36(b) and (c), these data are plotted against (grain size)$^{-1/2}$ to test the applicability of the well known Hall-Petch relation,

$$\sigma = \sigma_o + k(GS)^{-1/2}$$

where σ is the yield (or flow) stress, σ_o and k the material parameters and GS the grain size. The value of σ_o was taken as the yield stress of the <100> single crystal, inasmuch as it corresponds to the yield stress for the infinitely large grain size. In Fig. 36(a), the data of elastic (or proportional) limits are plotted to show a parallelism between them and yield stresses. It can be seen that the data are in qualitative agreement with the Hall-Petch relation, except for the fine-grained specimens for which a negative deviation from the relation occurred. However, it can be noted that polycrystals were not harder to any appreciable extent than a <111> single crystal.

Thus, an upper limit for the Hall-Petch relation was defined by the yield stress of the <111> crystal corresponding to the critical resolved shear stress of the more difficult slip systems. On the other hand, a lower limit coincided with the yield stress of the <100> crystal representing the less difficult slip systems.

In Figs. 36(b) and (c), it is also shown that the yield stress is not always a unique function of the grain size. Thus, even for a given grain size, yielding could occur at different stresses depending on the annealing parameters used to obtain the grain size of concern. For instance, annealing in air for 170h at 1400°C resulted in a considerably lower yield stress than annealing at a higher temperature would have shown, regardless of test temperature. In this comparison, it should be recalled that the former specimen was cloudy as a result of annealing while all other types of annealed specimens were not. It is also indicated in Fig. 36(b) that a shorter annealing period (70 vs. 110h) in Pt at 1500°C gave rise to a lower yield stress when tested at 1200°C, even though the grain sizes were similar.

Effect of strain rate on the grain-size-dependence of yield stresses is shown in Fig. 36(c). In general, the data tended to obey the Hall-Petch relation at all strain rates with the upper limit always coinciding with the yield stress of a <111> crystal for the corresponding strain rate. As the strain rate was increased, however, the grain size at which the upper limit occurred was shifted to a smaller value. Hence, the fine-grained specimen became the

hardest i.e., yielded at the same stress as a <111> crystal at the highest strain rate used, although it was considerably softer than the latter crystal at lower strain rates. Also, the yielding resistance deteriorated with increasing strain rate, particularly in coarse-grained specimens; deterioration was also observed for medium-grained specimens in response to an increment in strain rate larger than that sufficient to cause similar effects in coarse-grained specimens.

4. Fracture Stresses. For <110>, <111> single crystals and polycrystalline specimens, fracture stress was defined as the maximum stress on a stress-strain curve beyond which the stress decreased at an increasing rate. It may be worthwhile to point out that in compression tests, the stress corresponding to a maximum load is usually smaller than the maximum (true) stress unless the maximum load occurs at a small strain. For <100> and N<100> single crystals, fracture stress was defined as the stress at which the first, abrupt stress drop occurred. In those cases where the steady state was observed without fracture, the steady state flow stress was considered as the fracture stress. In the case of a fine-grain (~15μm) polycrystal that exhibited strain-softening following yielding (Fig. 24(a)), a maximum (or steady flow) stress reached in the later stages was considered as a fracture stress, even though this value was smaller than the yield stress.

While single crystal data are given in Table VI, polycrystalline data are plotted against (grain size)$^{-1/2}$ in Fig. 37. In this figure, the following observations could be made: (a) The

difference between small and medium grain size that was exhibited at the yielding stage has now diminished at both deformation temperatures for those specimens annealed in air at 1500°C prior to testing. (b) In coarse grained materials, however, the fracture stress decreased with increasing grain size as was observed for the yield stress. (c) Among medium grained materials with a comparable grain size, the specimen annealed in Pt fractured at a higher stress than the one annealed in air. The specimen annealed 170h in air at 1400°C fractured at the lowest stress.

The comparison with single crystal data reported in Table VI reveals that: (d) At 1200°C, the highest fracture stress observed for polycrystalline specimens is much lower than the fracture stress for a <111> single crystal and is in the order of the (projected) fracture stress for a <100> crystal. At 1400°C, the highest fracture stress for polycrystalline specimens is still much lower than the fracture stress for a <111> crystal but somewhat higher than the fracture stress (or steady state flow stress) for a <100> crystal.

It may be added that: (e) Coarse grained specimens not only yielded at, but also fractured at, lower stresses under a higher strain rate.

5. Ductilities. Ductility or fracture strain for the stress-strain test was defined as the strain where the above-defined fracture stress was observed. Fracture strain for the creep test was defined as the strain at the end of the steady state.

Ductilities for single crystals observed in stress-strain tests are reported in Table VI as a function of strain rates and temperatures. Ductility, in general, increased with increasing temperature or decreasing strain rate, ranging from 5% to a value exceeding 50%. For a given testing condition, <100> and N<100> crystals were more ductile than <110> and <111> crystals. Nickel dopant tended to enhance the ductility of a <100> crystal, particularly at a low temperature and a high strain rate.

Polycrystalline ductilities are plotted against (grain size)$^{-1/2}$ in Fig. 38 to facilitate a correlation with other plots for yield and fracture stresses shown in Figs. 36 and 37. Ductilities ranged from less than 1% for coarse-grained specimens to more than 50% for the as-received (fine-grained) specimen, depending also on annealing parameters as well as testing conditions. In general, ductility increased with decreasing grain size, increasing temperature, and decreasing strain rate, although some exceptions were also noted.

In further agreement with such generalizations, a crept specimen showed a greater ductility than a stress-strain tested specimen. For instance, ductility of a medium-grained specimen (annealed 110h in Pt at 1500°C) at 1200°C increased from 8% for a strain rate of 1×10^{-5} sec^{-1} to 15% for a steady creep rate of $\sim3\times10^{-7}$ sec^{-1}.

It is also shown in Fig. 38 that ductility was the more sensitive to temperature or strain rate, the finer the grain size. Alternatively,

ductility became more dependent on the grain size with increasing temperature or decreasing strain rate whereas no grain size dependence of ductility could be observed at the highest strain rate used where all specimens showed a ductility of less than 2%, regardless of temperature. Under these conditions, even an as-received polycrystal proved to be less ductile than a <111> crystal, following yielding at the same stress.

As an exception to the above generalization, however, it was noted that coarse-grained specimens showed a slight but distinct increase in ductility with either decreasing temperature or increasing strain rate (Fig. 38). In the same figure, the variability of ductility as a function of annealing parameters is indicated for a given grain size and testing condition. For instance, the cloudy specimens obtained by annealing 170h in air at 1400 C exhibited little ductility as compared with other clear specimens with comparable grain sizes, obtained under different annealing conditions. On the other hand, it should be pointed out that a difference in annealing history did not always lead to different ductilities for the same grain size. Hence, as can be seen in Fig. 24(a), a medium-grained specimen annealed in Pt fractured at essentially the same strain as a medium-grained specimen annealed in air, even though the fracture stress reflected a difference in the specimen character.

6. Recovery Rates

a. Measurement of Static Recovery. The static recovery rate (r_E) was defined as

$$\frac{\sigma_o - \sigma_E}{\Delta t}$$

where σ_o is the stress prior to unloading, σ_E the elastic limit upon reloading and Δt the time elapsed between the moment of interruption and the moment that the specimen was reloaded to elastic limit.

It was necessary to minimize the recovery period (Δt) to avoid gross underestimation of initial recovery rates which should correspond to the dislocation structure obtained during deformation. A preliminary investigation suggested that parallel results can be obtained at different strain rates if different values of Δt were used accordingly. Thus, Δt was reduced from 5 - 10 minutes to 0.5 minutes as the strain rate was increased from 1×10^{-5} to 3×10^{-4} sec^{-1}.

For recovery measurements, the specimen was only partially unloaded to a level slightly below the internal stress. Thus, it was necessary to assess the effect of application of such finite stress on recovery. For this purpose, special tests were made under randomly chosen conditions. In one case, the specimen was completely unloaded, except for the small preload that was necessary to maintain the alignment. In another case, the specimen (and the loading column) was allowed to relax from the deformation stress by stopping the crosshead movement. After the same period of recovery, the specimens were reloaded and the rate of recovery was determined. In Table VII, the corresponding results are presented

to be compared with the values determined by the usual technique where recovery took place under the applied stress slightly less than the internal stress. For all specimen types and testing conditions, it is clear that the application of a small stress did not cause any noticeable change in the recovery rate as long as the applied stress was smaller than the internal stress. This implies that there was indeed no extensive dislocation motion to interfere with recovery under such conditions. However, it can be seen that the recovery under stresses above the internal stress, i.e., during relaxation, resulted in consistently lower rates of recovery than that under lower stresses. This means that the recovery effect was overshadowed by the concurrent strain hardening and therefore, does not corroborate the notion of strain-enhanced recovery.[23]

b. Measurement of Dynamic Recovery. It was desirable to establish whether static recovery rates measured in the absence of strain-hardening could represent dynamic recovery condition. In the case of <100> and N<100> crystals, dynamic recovery rates (r_d) could be measured in the presence of strain-hardening utilizing the relation,

$$h = h_o - \frac{r_d}{\dot{\varepsilon}}$$

where h is the apparent strain hardening, h_o the absolute strain hardening in the absence of recovery contribution, and $\dot{\varepsilon}$ the

strain rate.

Thus, if a change in the applied strain rate is not accompanied by a change in dislocation structure, then the dynamic recovery rate should be given by

$$\frac{h_2-h_1}{1/\dot{\varepsilon}_2-1/\dot{\varepsilon}_1}$$

where $\dot{\varepsilon}_1$ and $\dot{\varepsilon}_2$ are the instantaneous strain rates of the specimen immediately before and after a sudden increase in the crosshead speed, h_1 and h_2 the corresponding rates of strain hardening. It was found that a small increment (2 or 2.5 times) of the crosshead speed was usually sufficient to give a measureable increase in the rates of strain-hardening. Negative responses of type A in Fig. 27 were not utilized.

Thus-determined dynamic recovery rates are compared with static recovery rates in Fig. 39 for two different base strain rates. Since there is excellent agreement between these recovery rates, it was concluded that the simultaneous deformation did not affect the recovery kinetics at least in <100> and N<100> crystals.

Also determined with the dynamic recovery rate was the absolute rate of strain hardening (h_o) given by

$$\frac{h_2-h_1(\dot{\varepsilon}_1/\dot{\varepsilon}_2)}{1-\dot{\varepsilon}_1/\dot{\varepsilon}_2}$$

where the symbols have the same meaning as before. The results are shown in Fig. 34 as a function of flow stress and temperature. It can be seen that the absolute rate of strain-hardening increased with stress which, in turn, increased with strain, thus suggesting increased difficulty of slip at later stages. Furthermore, the higher h_o values at a higher temperature seem to reflect increased oblique intersections. It is also indicated that thus-determined values are quite comparable to the results obtained independently from creep tests.

c. Static Recovery Behavior. For a given strain rate and temperature static recovery rates during the stress-strain test increased rapidly as deformation proceeded or as strain-hardening occurred. Subsequently, the static recovery rate was found to increase with the stress raised to the power n. The recovery rate also increased with increasing temperature. These results are indicated in Fig. 39 through 44 and summarized in Table V for different types of specimens tested.

In <100> and N<100> crystals, however, the recovery rate depended not only on the stress but also on the strain rate at a given temperature. Thus, an increase in the strain rate by a factor of 30 was accompanied by an increase in the recovery rate by a factor of ~3 (Figs. 39 and 40).

In <111> crystals and polycrystals, on the other hand, less dependence on the strain rate was indicated, since the data for different strain rates ranging from 1×10^{-5} to 3×10^{-4} sec^{-1} could be

represented by a single straight line (Fig. 41 and 42(a)) although fine-grained polycrystals deformed at the lowest strain rate at 1400°C tended to deviate from this behavior (Fig. 42(b)).

In addition to stress and strain rate, another factor was indicated in a <100> crystal deformed and recovered at 1200°C and $\dot{\varepsilon} \sim 1 \times 10^{-5} sec^{-1}$. As shown in Fig. 43, three stages could be ascribed to the corresponding recovery data, recalling that an increase in the stress was associated with increasing strain in this case. If a single straight line were drawn through them, however, the corresponding n would be at variance with that for the data either at 1400°C (Fig. 39) or at a higher strain rate (not presented). Similarly, it would also be at variance with the behavior of doped crystals which exhibited a constant n regardless of temperature and strain rate (Fig. 40). On the other hand, it can be noted that there is a correspondence between the break points shown in the plot and the beginning and the end of the second stage exhibited on the continuous stress-strain curve, obtained under the same deformation conditions (Fig. 21(a)). On this basis, it can be seen that the second stage was accompanied by the tendency for recovery to slow down. In Fig. 43, the effect of Ni doping is also shown: while there is no stage-dependence of recovery, a doped crystal recovered more readily than a undoped crystal, particularly at later stages of deformation.

By the same token, the hardening of <111> crystals as a result of prior annealing concurred with an increase in the flow stress

required for a given recovery rate, or equivalently, with an increase in recovery resistance. This observation is in agreement with polycrystalline results. In Figs. 42(a) and (b), it is shown that polycrystals obtained by annealing (in Pt) are more resistant to recovery as compared with as-received polycrystals. This behavior is in accord with the greater flow resistance exhibited by the former type of specimens.

In Fig. 44, static recovery rates as well as flow stresses at the time of interruption (marked by open circles) are plotted as a function of strain for a fine-grained (~10μm) polycrystal. It can be seen that the overall shape of the thus-constructed stress-strain curve is practically identical with that exhibited by the same specimen type (~13μm) in the uninterrupted test (Fig. 24(a)). Of significance are the concurrence of decreasing flow stress and increasing recovery rate following yielding, and the increasing flow stress and decreasing recovery rate at later stages. The slight disparity between the flow stress minimum and the recovery peak is not very surprising, however, considering the simultaneous effect of strain hardening on deformation.

7. Steady State Creep Rates

In presenting data, it is to be pointed out that steady flow stresses observed in stress-strain tests were included in plots of the steady state creep data. Also included are the fracture stresses of a magnitude comparable to the steady flow stresses that were observed for other specimen types under the same testing conditions.

As shown in Figs. 45(a) through (d), the steady-state creep rate for single crystals was found to be proportional to the stress raised to the power n within the observed range of strain rates for all specimen types tested. The values of n or stress-dependency are summarized in Table V. In the case of polycrystals, on the other hand, no single values of n was applicable throughout. Thus, n values of 3 and 4.4 were ascribed to a low stress and a high stress region, respectively, as can be seen in Figs. 46(a) and (b). Fine-grained specimens crept under low stresses at 1400°C, however, exhibited n = 1.

Under other creep conditions, neither grain-size-dependence, nor dependence on prior annealing conditions of the steady creep rate was indicated for polycrystals deformed at a given stress. Similarly, prior annealing of single crystals did not give rise to any noticeable effect on the steady creep rate. Comparison of polycrystalline data with single crystal data represented also in Figs. 46(a) and (b) as dashed lines strongly suggests a correlation between single crystals and polycrystals. Namely, polycrystals tended to be indistinguishable with <100> crystals when crept at 1200°C and under high stresses, in particular. At 1400°C, on the other hand, polycrystals tended to be similar to <111> crystals, especially when the creep rates were not very high. As mentioned above, however, fine-grained specimens showed a notable deviation from this behavior. According to Fig. 46(b) in its presented form, one might even conclude that polycrystals become

more creep-resistant than <111> crystals at low stresses. If the creep rates were also normalized with respect to G, however, this conclusion would be untenable.

As reported in Table V, all undoped single crystals, showed the same activation energy of 75 kcal/mole, whereas the doped crystal had a lower activation energy of 43 kcal/mole. It is rather significant that polycrystals were also characterized by a lower activation energy of ~53 kcal/mole, regardless of n; the same activation energy was measured by Dorn's technique where n = 1. According to this technique, the activation energy for the tertiary stage (as shown in Fig. 31 for a coarse-grained specimen) was essentially identical with the values obtained in the same specimen before the tertiary stage occurred. Furthermore, these results showed a good agreement with the conventional activation energy determined from the steady creep rate vs. stress plot for the test temperature used.

IV. DISCUSSION

A. Single Crystals

Understanding of slip in single crystals is fundamental to the studies of polycrystalline deformation by dislocation motion. In the following, the difference between primary and secondary slip and the effect of Ni doping will be considered.

1. Primary vs. Secondary Slip

The behavior of <100> or <110> crystals corresponds to the primary slip, i.e., slip {110} planes whereas that of <111> crystals corresponds to the secondary slip, i.e., slip on {100} planes. It can be predicted on the basis of structural considerations that the dislocations would always be less mobile on {100} planes than on {110} planes. The greater flow stress for a <111> crystal than a <100> crystal observed throughout the whole range of strain rates and temperatures studied is thus consistent with the prediction.

However, such plastic anisotropy decreased with decreasing strain rates in accord with a decrease with increasing temperatures. This result is equivalent to saying that the flow stress of <111> crystals is more sensitive to strain rates than the flow stress of <100> crystals. The difference in strain rate sensitivity (SRS) is most pronounced at small strains. As an extreme case, the yield stress of stress-strain tested <100> crystals is essentially constant regardless of strain rate (and temperature). The SRS of flow stress at a given strain increases as the strain is increased. The difference in the SRS between <100> and <111> crystals is thus reduced

when steady flow stresses are considered; however, the former crystal still exhibited a smaller SRS than the latter. In terms of the stress-dependence of steady creep rates (or in inverse of the SRS), the corresponding values of <100> and <111> crystals are 4.0 and 2.7, respectively. These respective values are quite comparable to 4.1 and 3.1 observed for LiF single crystals crept at higher homologous temperatures.[24]

The stress dependence of ~4 for <100> crystals suggests that Weertman's climb model[11] is applicable where the rate-controlling process is dislocation climb to overcome the barrier. According to the model, the activation energy for steady creep corresponds to diffusion. The apparent activation energy estimated from the temperature-dependence of steady creep rates is ~75 kcal/mole. The value is significantly smaller than 110 kcal/mole for intrinsic lattice diffusion of oxygen and somewhat greater than ~60 kcal/mole for pipe or extrinsic diffusion of oxygen (Table VIII). It seems likely that the observed value represents a weighted average between predominant contribution from pipe diffusion and less prounced contribution from intrinsic diffusion.

Since dislocation glide on {100} planes is accompanied by electrostatic faulting, it may be reasonable to associate the greater creep resistance and the stress dependence of ~3 for <111> crystals with the Peierls mechanism. Weertman[42] has proposed a model for such a mechanism predicting stress-dependence of the same magnitude as observed here. In his model, however, the rate-controlling mechanism

is the thermally-activated overcoming of the Peierls barrier and hence the activation energy is not due to diffusion. Whereas the activation energy for <111> crystal is of the same magnitude as for <100> crystals and thus can be identified with that for diffusion. Therefore, the present result is not in full accord with the model, while it agrees with the earlier result on <111> LiF single crystals in that the observed activation energy compares facorably with that for diffusion.

A reaction can occur in a <111> crystal between dislocations moving on {100} planes;

$$\frac{a}{2}[100] + \frac{a}{2}[0\bar{1}\bar{1}] = \frac{a}{2}[101]$$

The resultant dislocation lies on a (101) plane for which there is no resolved shear stress. Hence, this dislocation is immobile with respect to glide. However, it can climb out of the (101) plane. Consequently, the rate of deformation will be determined by the rate of dislocation climb. The subboundaries observed in a crept specimen (Fig. 8(b)) indicate that dislocation did climb. Therefore, it is suggested that creep of <111> crystals is dependent on dislocation climb. In view of similarity in the temperature dependencies (Table V), yielding and subsequent stress-strain deformation is also likely to be controlled by dislocation climb.

It is noted that Nabarro's steady-state creep model,[43] postulating deformation by dislocation climb alone, predicts a similar stress dependence but strain rates much slower than observed values. According to Weertman's modification,[44]

$$\dot{\varepsilon} = \frac{\pi D \Omega \sigma^3}{10 b^2 G^2 kT}$$

where Ω is the atomic volume, D the diffusion coefficient, σ the applied stress, b the Burgers vector, G the shear modulus, k the Boltzmann constant, and T the temperature. Taking $D = 3.0 \times 10^{-3} e^{-\frac{62,700}{RT}}$ for pipe diffusion of oxygen as reported by Narayan and Washburn,[45] and pertinent values for other parameters, the steady state creep rate is calculated to be $1.06 \times 10^{-8} sec^{-1}$ at 1400°C and σ = 18,000 psi. This value is about two orders of magnitude lower than the experimental value of $2.26 \times 10^{-6} sec^{-1}$.

2. Effect of Ni Doping

Nickel ions are completely soluble in MgO, as may be anticipated from their size and valence in comparison with those for Mg ions. On this basis, any significant effect of doping on the dislocation glide seems unlikely. Nevertheless, Ni-doped MgO has been observed prveiously[46] to exhibit softening when stress-strain tested at high temperatures in a reducing atmosphere. The occurrence of interpenetrating slip on oblique systems was indicated by the enhanced tendency toward subgrain formation. This behavior was attributed to the accelerated climb of dislocations with the aid of extra vacancies generated by removal of oxygen. As mentioned earlier, there is a possibility that extra vacancies generated during crystal growth are present in the specimens used in the present work. Considering the similarity between the present and the previous

observations, i.e., the low flow stresses accompanied by enhanced subgrain formation and considering the high susceptibility to recovery of the doped crystal, the above possibility could not be ruled out. The hardening as a result of prior annealing or recovery for an extended period as observed in the present study can also be explained in terms of extra vacancies, the number of vacancies being decreased by such treatments.

However, it is important that the softening effect of doping did not persist at the higher temperature. It will be recalled that the stress-strain curve of the doped specimen for a strain rate of 1×10^{-5} sec^{-1} showed continuous hardening over that of the undoped specimen at 1400°C, whereas the reverse was observed at 1200°C (Fig. 21). Also, the doped crystal is more resistant to creep at 1400°C than the undoped crystal, although the opposite was the case at 1200°C (cf. Figs. 45(a) and (b)). The softening or hardening dependent on temperature can be explained if a deformation mechanism with a lower activation energy is operative. The stress exponent of 3 observed for the steady creep suggests Weertman's microcreep mechanism[42] where the dislocation glide is controlled by diffusion of the solute. The solute being Ni ions, the observed low activation energy for the doped crystal can be taken as that for diffusion of Ni ions through MgO or interdiffusion between Ni and Mg ions (Table VIII). Cannon and Sherby[47] have recently advanced a similar suggestion for the creep behavior of polycrystalline NaCl-KCl solid solutions.

As long as the cation diffusivity is enhanced by doping, dislocation climb can be expected to occur rapidly. There would be no need to invoke the extra vacancy argument. The increased climb rate will facilitate the overcoming of barriers and hence the oblique intersections. The occurrence of oblique slip is borne out by the additional observation that the absolute rates of strain hardening (h_o) corresponding to a stress-strain test at 1200°C are increased by doping (Fig. 34). Since, however, the recovery rates are also increased, the flow stresses are actually lower for the doped specimen.

It should be recognized that dislocation mobility is not necessarily reduced by the presence of dopant, whether the dislocation motion is controlled by cation diffusion either directly or indirectly via climb.

B. Polycrystals

1. Deformation by Slip

That slip or dislocation glide was a major mode of deformation under most testing doncitions employed is indicated by the correlation found between single crystals and polycrystals. Although the combination of high temperature and a low strain rate (or stress) gave rise to deformation by mass transport in fine-grained specimens, this behavior does not represent a majority of the observations and will be considered later. Thus, the experimental results described earlier can be summarized as follows.

Concerning flow stresses, the present polycrystals were not harder than a <111> single crystal, nor softer than a <100> crystal

for a given testing condition. Depending on grain size and testing condition, however, a polycrystal could be as hard as <111> crystal, or as soft as <100>. The grain size dependence of flow stress was most pronounced at yielding stages, but tended to diminish as a steady state was approached unless the achievement of a steady state was prevented by premature failure. When the steady flow did occur at 1200°C, hence with extensive (and yet nonpropagating) intergranular separations, polycrystals behaved similarly to <100> crystals in terms of steady flow stresses. However, polycrystals tended to be similar to <111> crystals at 1400°C where the extent of intergranular separation decreased. Thus, under creep testing conditions at 1400°C, polycrystals were quite comparable to <111> crystals, as long as diffusional creep was not operative.

Concerning ductilities observed during stress-strain tests, on the other hand, it was observed that polycrystals could be considerably less ductile than single crystals. Polycrystalline ductility increased with decreasing grain size. Ductility for a grain size larger than 15μm, however, was less than that of a <111> crystal at 1400°C, even when the polycrystal yielded at the same stress as the crystal. Fine-grained specimens were more ductile than a <111> crystal, following yielding at a lower stress than the latter.

Pileup of dislocations at grain boundaries in medium- and coarse-grained specimens is borne out by the observed grain size dependence of yield stresses in qualitative agreement with the Hall-Petch

relation. Because of the lower critical resolved shear stress, dislocation motion will be initiated on the primary slip plane. Since stress concentrations are generated due to subsequent pileup of these dislocations at grain boundaries, the critical resolved shear stress for the secondary slip plane can be reached locally, provided that the grain boundaries can withstand the stress concentration without losing their coherence. Indeed, evidence of the localized secondary slip along grain boundaries was obtained previously in a coarse-grained LiF deformed at room temperature.[48] Thus, yielding may occur with the help of localized secondary slip. A large ductility, however, seems unlikely in a coarse-grained material, since the interior of grains must deform with less degrees of freedom provided only by primary slip systems. Furthermore, there are indications that intergranular separations (IGS) occurred causing premature yielding in coarse-grained and medium-grained specimens as will be considered in a forthcoming section.

As mentioned above, no polycrystalline specimens tested were harder than a <111> crystal for a given testing conditions. This observation suggests that activation of the secondary slip systems, and hence all five independent slip systems, sets an upper limit to polycrystalline strengths and thus to applicability of the Hall-Petch relation, provided that no impurity-associated hardening is effective. In view of the absence of F in single crystals, however, it may be suggested that the presence of F in polycrystalline specimens did not cause any appreciable impediment to dislocation motion on secondary slip planes, in particular.

Regarding medium-grained specimens that yielded at essentially the same stress as <111> crystals, it can be stated that extensive primary slip could not occur in a polycrystalline body until secondary slip (or other accomodation mechanisms) became operative. This statement is substantiated by the data of elastic limits (Fig. 36(a)) which should correspond to the initiation of macroscopic flow. It is, therefore, apparent that primary slip on a microscopic scale could not produce sufficiently high stress concentrations for these particular grain sizes. Magnitude of the observed elastic limit also suggests that no grain boundary sliding could take place as a deformation mode independent of slip so as to casue yeilding at a stress lower than the observed level. It can be deduced further that grain boundaries remained largely coherent until the elastic limit was exceeded; if IGS occurred to any appreciable extent, then the elastic limit should have been lower than was observed, for IGS would trigger the premature yielding as will be discussed later.

As has been discribed previously, yielding in these medium-grained specimens was also characterized by a yield drop (or plateau); these events occurred shortly after the stress-strain curve deviated from the elastic region. The yield drop may seem analogous to the sigmoidal creep of the same type of specimens, both corresponding to the rapid multiplication of dislocations.[49] The drop, however, is characteristic of these polycrystals, since it was not observed in <111> single crystals. Earlier, Evans et al[50] have made a similar observation with CaF_2 polycrystals;

the yeild drop or the distinct yield point was then attributed to IGS.

This observation is also consistent with the microstructural evidence of IGS obtained in a fine-grained specimen deformed to a point where the flow stress had just started to decrease, immediately following yielding that occurred at the same stress level as for medium-grained specimens (Fig. 13(a)). Hence, it is suggested that the yield drop of the medium-grained specimens may also be accounted for by IGS.

Corresponding to the drop, the IGS of concern must have occurred rather suddenly and only after yielding at the same stress level as a <111> crystal. Hence, it is to be distinguished from the IGS that occurred at early stages in coarse-grained specimens without exhibiting a distinct yeild point. Recalling the earlier discussion on single crystal behavior, primary slip can proceed at a considerably greater rate than secondary slip if both slip systems are activated simultaneously at a given stress. Consequently, such plastic anisotropy should play a substantial role in causing the IGS and hence the distinct yield point. Thus, it cannot be over-emphasized that IGS may still occur despite the fulfillment of the von Mises requirement. In this connection, it is also noteworthy that medium-grained specimens are less ductile than fine-grained specimens.

2. Diffusion Contribution

It is clear that diffusion should play an increasingly important role as the deformation temperature is increased. Among other roles, stress-directed diffusion can directly produce strains as it occurs in the diffusional creep. The diffusional creep was indicated in fine-grained (<15μm) specimens crept under low stresses (lower than 7000 psi) at 1400°C. The steady creep rates were characterized by a linear stress-dependence (Fig. 46(b)) and reduced creep resistance with respect to that of <100> crystal. The corresponding activation energy was 56 kcal/mole which was comparable to that of either extrinsic or grain boundary diffusion (Table VIII). Subsequently, three models predicting a viscous behavior were applied to the specimen with a grain size of 15μm crept under 3000 psi at 1400°C. According to Nabarro[1] and Herring[2], diffusion across the grains results in deformation, while diffusion along the grain boundaries is postulated by Coble.[3] Recently, Ashby and Verrall[51] put forward a superplasticity model where strains are produced by grain boundary sliding accomodated by diffusion along the grain boundaries as well as across the grains. As shown in Appendix III, Coble's mechanism seems to be operative in the present case. However, the superplastic mechanism connot be ruled out completely in view of the highly ductile behavior of the fine-grained specimens.

In either case, the observed activation energy would correspond to that for grain boundary diffusion (presumably of oxygen).

As can be noted from the literature data (Table IX), Coble creep with truly linear stress-dependence was not observed in F-free MgO. This evidence points to the fact that grain boundary diffusion was enhanced by the presence of F within the grain boundary zone; the electroneutrality requirement would dictate the production of extra cation vacacies due to the presence of F ions. Since the diffusional creep of Li-containing MgO[66] did not indicate the operation of the Coble mechanism, it can be deduced that it is F and not Li which accentuates the grain boundary diffusion.

Diffusion within the grains becomes important under the conditions where dislocation creep is predominant, as the rate of climb of edge dislocations within the grains is controlled by a diffusion process. The fact that dislocation motion was involved in creep at high stresses is indicated by the formation of dislocation subboundaries in the crept specimens (e.g., Fig. 18) as well as the large stress-dependence (greater than 3). Dislocation climb as a rate-limiting process is suggested from the activation energy of 53 kcal/mole, which is of the same order of magnitude as that of grain boundary, pipe or extrinsic diffusion reported in the literature (Table VIII). Grain boundary diffusion, however, is unlikely in this case, since the steady creep rate for a given stress is independent of the grain size at high stresses (Fig. 46). In view of the sizable difference in the activation energy between single crystals and polycrystals, it seems that extrinsic diffusion is operative due to F. This conclusion would then imply that a sufficient amount of F is present within the grains as well as at the grain boundaries to cause the extrinsic behavior.

When deformation occurs by dislocation motion, the interaction between dislocations could cause strain-hardening. At elevated temperatures, however, strain-hardening can be effectively counteracted by concurrent recovery which involves reduction in the dislocation density or rearrangement of dislocations. Thus, the participation of dislocation climb in the high-temperature deformation could facilitate the process of recovery, while enabling the blocked disloations to overcome the barriers as well; the latter process has been incorporated in Weertman's creep model.[11] These factors would tend to attenuate the severity of dislocation pileup which might lead to crack nucleation. On this basis, one might be able to correlate the ductility with the recovery rates. It has been subsequently found that the ductility is greater for the fine-grained specimens which are also more susceptible to recovery as compared with the medium-grained specimens. It is also noteworthy that a fine-grained specimen yielded at the same stress as a <111> crystal when stress-strain tested at the highest strain rate employed. While this fact would be indicative of the operation of all five independent slip system, no significant ductility was exhibited. These observations corroborate the occurrence of dynamic recovery and its importance in ductile deformation.

From the accomodation viewpoint, it is important to recognize the role of dislocation climb. Since Nabarro[43] has shown that dislocation climb alone can produce strains, Groves and Kelly[67] have recently pointed out that dislocation climb, by itself or in

conjunction with glide, can provide the degree of freedom required for a general change of shape. In the case of a cubic crystal such as MgO, either six independent climb systems corresponding to six <110> vectors or four independent climb systems plus two independent, non-orthogonal primary slip systems are needed to produce such an effect.

The actual occurrence of this accomodation mode was indicated by fine-grained polycrystals. When stress-strain tested, these specimens yielded at stresses lower than the stress required to extensively activate the secondary slip, i.e., the yield stress for a <111> crystal. Nevertheless, a full accomodation must have been achieved at the grain boundaries since the specimens remained transparent through the yielding stages.

Previously, Copley and Pask[68] have suggested that high applied stresses may be not necessary if the grain boundaries were sufficiently strong to withstand the stress concentration that can locally activate the secondary slip. If this were the case, however, the larger the grain size, the longer will be the slip band and hence the higher the stress concentration. Thus, medium-grained specimen should have yielded at even lower stresses than fine-grained specimens. The opposite effect has been observed from grain sizes less than 15μm. Therefore, the observed effect can be attributed to the accomodation involving diffusion process such as dislocation climb; the diffusion contribution would be enhanced in the fine-grained materials because of the shorter diffusion path. This conclusion

is also consistent with the observation that the yield stress increased with increasing strain rate or decreasing temperature, i.e., with decreased diffusion contribution.

The simultaneous operation of glide and climb for accomodation is to be distinguished from the mechanism of grain boundary sliding (GBS). The latter phenomenon has been proposed to occur by alternating glide and climb along the grain boundary.[69] Hence, the observed GBS (Fig. 17) is merely a concurrent process. That GBS does not constitute an accomodation mechanism has been previously pointed out.[70]

3. Intergranular Separation

The complete or partial spearation at the grain boundaries was observed in all polycrystalline specimens tested, in many cases immediately following yielding. It was also noted, however, that the extent of the complete intergranular separation (IGS) was limited to a single grain facet, suggesting its stability against subsequent propagation as a crack. Under such conditions, the IGS may be considered as an accomodation mechanism in view that it was observed prior to fracture, i.e., the accelerated loss of load-carrying capacity. Namely, the IGS would allow not only stress concentrations to be dissipated but also the barrier of grain boundary itself to be removed. This effect would be equivalent to the relaxation of the von Mises requirement. As suggested by the microscopic evidence, grain boundary sliding along the facet adjacent to the separated one could be facilitated

thereby, resulting in a continuous widening of the intergranular gap. The process of lateral widening will give rise to a longitudinal shrinkage of the compressive specimen. Thus, the IGS can also contribute directly to the deformation accompanied, however, by a corresponding increase in the specimen volume. For tensile specimens of matels, Widmer and Grant[71] observed that the axial opening due to IGS could account for 10 to 50% of the total strain. A qualitatively similar observation is illustrated in Fig. 19.

Such roles of IGS as described above might explain the stress-strain behavior of the coarse-grained specimens. They showed apparent yielding at stresses lower than that necessary to activate the secondary slip in <111> single crystal. Since the IGS was observed shortly after yielding, it is not likely that the low yield stresses were due to strongly bonded grain boundaries. The strong grain boundaries would withstand a high stress concentration to locally activate the secondary slip so that yielding could occur at a low externally applied stress. The latter was proposed previously by Copley and Pask[68] to be the case for their specimen of a comparable grain size which exhibited a low yield stress in association with large ductility. The relatively insignificant ductilites encountered in the present case, therefore, support the other conclusion that apparent yielding may occur due to the IGS at a low stress level. The observed decrease in the yield stress with increasing strain rate lends further support, since the increase in strain rate would enhance the likihood of IGS by increasing the critical

resolved shear stress for the secondary slip. The precipitous decrease in the yield stress with increasing grain size and hence the increased deviation from the Hall-Petch type of relationship (Fig. 36(b)) is also indicative of the increased susceptibility to IGS. This is consistent with the estimated large amount of F per unit area of grain boundary (Fig. 2), i.e., a rapid decrease in the strength of intergranular bonding.

There are further indications that a difference in mechanical behavior can be encountered for the same grain size as a function of the cohesive strength of the grain boundaries: a) Particulary weak intergranular cohesion for the cloudy specimen (annealed in air for 170 h at 1400°C), as indicated by the grain boundary features or IGS (Fig. 1), gave rise to low flow stresses and ductility (Figs. 36 through 38) when compared with the specimen annealed at a higher temperature without the loss of transparency. b) Little further grain growth occurred when the annealing time (in the Pt at 1400°C) was increased from 70 to 110h. Therefore, the lower yield stress of the former specimen (Fig. 36(b)) must be accounted for by the greater retention of F, or the weaker grain boundaries. c) Provided that the observed yield drop was caused by IGS, the magnitude of the drop may be a measure of the grain boundary strength for the same grain size and testing conditions. As shown in Table III, the drop was more pronunced for the lower annealing temperature (1400°C for 170h vs. 1500°C for 110h), or for the greater amount of residual F and hence, the weaker grain boundaries. Similarly, annealing for a shorter time

resulted in a larger drop (12h in air vs. 110h in Pt). This observation is also consistent with the fact that the former specimen deformed at lower stresses than the latter (Fig. 24(a)).

As long as the IGS facilitated deformation, one might expect decreased flow stresses at all stages. Hence, the negative deviation of the steady-state flow stresses for polycrystals from those for <111> single crystals may be attributed to the IGS-induced weakening. The more extensive the IGS, the greater will be the deviation. Therefore, the deviation will increase with increasing strain rates. This was probably reflected in the high stress-dependence of 4.4 at high strain rates, as suggested for ZrO_2[8] and Al_2O_3[10] in earlier studies.

It must be pointed out, however, that IGS does not facilitate deformation if the strain rate is too high or too low. If the strain rate is high, the diffusion-controlled process of grain boundary sliding and hence the widening of intergranular gaps cannot occur rapidly. Under such conditions, the IGS can only lead to a premature failure. If the strain rate is low, on the other hand, the accomodation by slip on five independent systems becomes easy due to the reduced plastic anisotropy. The IGS now occurs in the form of cavities which are not very effective in relaxing the von Mises requirement.

C. Correlations

1. Correlation between Stress-Strain and Creep Tests

Stress-strain tests differ from creep tests in the boundary testing condition and the strain rates involved. Whereas the applied stress or load is maintained constant under creep condition, it is allowed to increase during a stress-strain test so that deformation can proceed at a constant rate of straining or stressing. The difference in the boundary condition, however, becomes immaterial at steady states, because the corresponding flow stress is constant for a given strain rate and hence the stress-strain and creep tests are identical. Secondly, the strain rates involved in creep tests are usually much lower than those for stress-strain tests.

It was noted that either of these differences could be associated with different mechanisms of deformation operative, depending on the specimen type. Thus, in the case of <100> and N<100> crystals, while little temperature- (and strain-rate-) dependence was observed for yielding in stress-strain tests, a strong temperature (and stress or strain-rate) dependence was exhibited during initial stages of creep. This would indicate that thermally-activated deformation is a necessity under creep conditions. It is, however, interesting to note that the stress-dependency of initial (or maximum) creep rates for <100> crystals is still greater than that for <111> crystals. This behavior is in accord with the extreme stress-sensitivity of strain rates (or, equivalently, the lack of strain-rate-sensitivity of yield stresses) indicated in stress-strain tests of <100> crystals

as compared with <111> crystals.

Similarly, the occurrence of diffusional creep observed in as-received polycrystal specimens at a high temperature and low stresses (or strain rates) is consistent with the stress-strain behavior. It will be recalled that the low yield stresses and high strain-rate-sensitivity of this specimen type could be accounted for in terms of increased diffsuion contribution.

It must be cautioned, however, that the increased diffusion contribution could allow coarser-grained (e.g. 15μm vs 4μm for the as-received condition) polycrystals to exhibit a similar behavior, i.e., the diffusional creep if the strain rate is sufficiently low. This would be in contrast with the stress-strain behavior corresponding to a higher strain rate, i.e., the high yield stresses for the same specimen type in comparison with the as-received specimen. The grain size effect on the flow stresses during stress-strain test, however, diminished at a steady state.

Also, while somewhat persistent effects of prior annealing were noted on stress-strain curves of single crystals at 1200°C, such effects on steady creep were not observed. Therefore, it can be seen that steady creep behavior cannot be predicted from the information on the early stages of stress-strain curves.

2. Correlation between Deformation and Recovery

High temperature deformation is often characterized by the fact that the rate of observed strain-hardening is decreased and a steady state tends to be approached with continued straining.

This fact is indicative of the occurrence of dynamic recovery. It is widely accepted that the increased creep resistance of two-phase materials derives from the capability of stabilizing deformation structure, i.e., the resistance of recovery. Ishida and McLean[72] have shown that an increase in the creep resistance by alloying was accompanied by a corresponding increase in the recovery resistance. Hence it may be suggested that the deformation resistance is determined by dislocation structure which, in turn, is affected by the recovery process. Dislocations may decrease in their density or rearrange themselves during recovery so as to reduce the structural resistance to gliding dislocations. High recovery rates would then reflect a high glide mobility. On this basis, a correlation was sought between flow stresses and recovery rates pertaining to stress-strain tests.

Concerning the correlation between flow stress and recovery rate, several observations could be cited. a) From a given stress-strain curve, the shape of the curve reflected the corresponding change in the recovery rate. For instance, for the stress-strain curev as shown in Fig. 44, it can be seen that the initial decrease in the flow stress was accompanied by increasing recovery rates and the subsequent strain-hardening by decreasing recovery rates. The stress-strain curve shown in Fig. 21(a) for a <100> single crystal tested at $\dot{\varepsilon}\sim 1\times 10^{-5}\,sec^{-1}$ at 1200°C exhibited three stages. These stages could be matched with three subdivisions of the corresponding recovery plot (Fig. 43). Namely, the initial and the final stages of the stress-strain curve corresponded to the

regions of the plot where the recovery rate increased with the stress to the fourth power. The intermediate stage characterized by the steepest slope corresponded to the middle region where the recovery rate did not increase as rapidly. b) A similar correlation can be made when the stress-strain curves for similar specimen types are compared. At 1200°C and $\dot{\varepsilon} \sim 1 \times 10^{-5} sec^{-1}$, the doped <100> crystal strain-hardened less rapidly than the undoped <100> crystal (Fig. 21(a)) in accord with the higher recovery rates for the former (Fig. 43). A <111> crystal shows a general elevation of the stress-strain curve as a result of prior annealing (Fig. 22(c). The elevation, however, is accompanied by the decreased susceptibility to recovery (Fig. 41). The increased flow stresses for medium-grained polycrystals (annealed in Pt) over those for fine-grained (as received) polycrystals (Figs. 24(a) and (b)) are consistent with the lower recovery rates for the former specimens (Fig. 42(a) and (b)).

Although the above examples demonstrate a close relation between the deformation resistance and the recovery rate, the correlation is not applicable between dissimilar specimen types. For instance, <111> crystals are considerably harder than <100> crystals, and yet the former specimens recover more rapidly than the latter (c.f. Fig. 41 and Figs. 39 and 43). This apparent anomaly can, however, be explained by the extremely rapid strain-hardening (Fig. 34) that accompanies that high recovery rate of <111> crystals.

So far as the recovery has a counteracting effect on the strain-hardening, it might be expected that the dislocation pileups leading to crack nucleation are thereby attenuated. Therefore, the possible correlation was examined between recovery rates and ductilities. The polycrystalline ductility increases as the grain size is decreased. This is in agreement with the observation that a fine-grained specimen is more resistant to the loss of transparency and recovers more readily than a medium-grained specimen. It is also consistent with the fact that ducility increases with increasing temperature and decreasing strain rate. Such correlation between recovery rate and ductility tends to emphasize the importance of microcracking (intergranular separation in this case) in determining the load-carrying capacity in terms of the strain, even though visible macrocracks may not occur. It should be pointed out, however, that a similar correlation cannot be extended to specimens of a different type. Namely, a medium-grained polycrystal recovers more rapidly than a <100> crystal, although the former is less ductile. Again, such disparity can be attributed phenomenologically to the rapid strain hardening associated with the former type.

If the correlation is limited to the polycrystals, the faster recovery of fine-grained specimens can be correlated with the larger primary creep strains (Figs. 32(a) and (b)) as compared with coarse-grained specimens. This observation is consistent with the result that the primary strain increases with increasing temperature or stress, since the recovery rate increases accordingly.

Such behavior can be understood if one considers that the primary period corresponds to a net strain-hardening; recovery will tend to delay the achievement of the steady state by counteracting strain-hardening.

V. SUMMARY AND CONCLUSIONS

1. Plastic anisotropy between {110} and {100} slip plenes was reduced not only with increasing temperature but also with decreasing strain rate. It was considered that the anisotropy was associated with the stress drop immediately following yielding and limited ductility as observed in medium-grained specimens stress-strain tested at 1200°C. In these specimens,yeilding occurred at essentially the same stress as a <111> crystal, thus suggesting simultaneous activation of slip on both planes. It was also noted that no polycrystals tested were harder than a <111> crystal under given testing condition.

2. There are at least two accomodation modes operative in polycrystalline MgO in addition to the mode involving slip on all five independent slip systems, i.e. on both {110} and {100} planes:

a) One mode is primary slip plus dislocation climb as suggested by Groves and Kelly.[67] This mode occurred in fine-grained (<15μm) specimens characterized by a high but strain rate sensitive ductility in comparison with coarse-grained specimens. Thus, except for the highest strain rate used, these specimens yielded at a lower stress than medium-grained specimens, deviating from the Hall-Petch relation. The susceptibility to diffusion contribution in this type of specimen was also demonstrated by high recovery rates during stress-strain tests and Coble creep exhibited at 1400°C and $\dot{\varepsilon} < 6\times10^{-7}\,sec^{-1}$.

b) Another mode is intergranular separation limited to a single grain facet that relaxes the von Mises requirement while contributing directly to the observed strain. Except for coarse-grained specimens, steady flow and a considerable compressive ductility during stress-strain test as well as creep was not prevented thereby. The increased stress-dependency of steady strain rates in a high strain rate region or at a low temperature, however, was attributed to the weakening caused by intergranular separation. In coarse-grained specimens, there were indications that apparent yielding occurred followed by a premature loss of load-carrying capacity due to intergranular separation. Cavitation that occurred at a high temperature or low strain rates did not, however, appear to have a direct influence on accomodation nor on failure.

3. While the grain size was a mjaor material parameter determining the yield stress and the ductility, little grain size dependence was observed for the steady flow stress as long as no diffusional creep mechanism was operative. Also, variability of the mechanical properties was noted for a given grain size as a function of prior annealing, and was attributed to the variable strengths of intergranular cohesion as affected by F concentration at the grain boundaries.

4. Fluorine was also considered responsible for the extrinsic and the grain boundary diffusion indicated in the polycrystalline specimens studied. Similarly, it was shown that the mechanical behavior of a single crystal could be affected by a soluble dopant such as Ni. In this case, a change in deformation mechanism resulted

from doping, involving interdiffusion between cations.

5. Dynamic recovery was closely associated with high temperature deformation, as suggested by the correlation between the recovery rate and the stress-strain curve, the primary creep strain and the ductility.

6. Comparison of steady creep resistance on the basis of yield stresses was basically valid between <100> and <111> crystals whereas it was not among the polycrystals studied. Comparison between single crystals and polycrystals was only valid for certain grain size and testing conditions.

ACKNOWLEDGMENTS

My sincere thanks are due to Professor J. A. Pask for his patient guidance throughout the course of this work. Thanks are extended to Ms. Lorine Hesleph for typing the manuscript, John Flambard and Bob Stevens for line drawings, to Don Whittaker, Walt Toutolmin, Mahlon Pryor, Wilt Lawrence and Jack Wodei for their technical assistance with experimentation. I would also like to thank Professors E. Parker and I. Finnie for reading the manuscript. This work was supported by the U.S. Energy Research and Development Administration.

APPENDIX I

THICKNESS OF GRAIN BOUNDARY "FILM" OF FLUORINE

The thickness of the film on each side of grain boundary is given by $\frac{v}{2S}$ where v is the volume of the film per unit volume of the sample, and S the total area of grain boundaries per unit volume.

For a grain size of GS (in μm), the average chord length of the grains is $\frac{GS}{1.27}$, as determined by lineal intercept method. The magnitude of S is then given by

$$2/\frac{GS\times10^{-4}}{1.27} = 2.54\times10^{4}/GS(cm^2/cm^3)$$

By taking the values for atomic weight of 19.0 and the ionic radius of 1.36Å for a F ion, the density of the film consisting solely of F ions that are arranged in simple cubic packing is calculated as

$$\frac{19.0\times1}{(2.72\times10^{-8})^3\times6.023\times10^{23}} = 1.57\ g/cm^3$$

The F content in the bulk of F (in ppm) corresponds essentially to $F\times10^{-6}$ g or $\frac{F\times10^{-6}}{1.57}$ cm^3 of F per g or $\frac{1}{3.57}$ cm^3 of MgO. Hence the magnitude of v is given by

$$\frac{F\times10^{-6}}{1.57} / \frac{1}{3.57} = 2.28\times10^{-6}\ F\ cm^3 \text{ of fluorine/cm}^3 \text{ of MgO.}$$

Therefore, the "film" thickness, as an indicator for the amount of F concentrated at grain boundaries, is given by

$$\frac{v}{2S} = \frac{2.28\times10^{-6}\ F}{2\times2.54\times10^{4}/G} = 4.49\times10^{-11}\ (F)\cdot\ (GS),\ \text{cm}$$

$$= 4.49\times10^{-3}\ (F)\cdot(GS),\ \text{Å}$$

$$= \frac{4.49\times10^{-3}\ (F)(GS)}{2.72}$$

$$= 1.65\times10^{-3}\ (F)\cdot(GS),\ \text{atomic layers.}$$

The residual amounts of F in the bulk after annealing for 12 and 40h in air at 1500°C have not been measured. Instead, they were estimated assuming that the fluorine content decreased linearly with time. Thus

$$F = 415 - 3.16t\ \text{ppm}$$

where t is the annealing time in hours.

According to this assumed relation, the F content after 4 h of annealing is calculated to be 402 ppm as compared with the measured value of 390 ppm. There, the assumption of linear time dependency may be considered not too unreasonable.

APPENDIX II

PREDICTED STEADY CREEP RATES ($\dot{\varepsilon}$)

1. Nabarro-Herring Creep

$$\dot{\varepsilon}_{NH} = \frac{13.3\Omega D\sigma}{d^2 kT}$$

where Ω is the atomic volume, D the lattice diffusion coefficient, σ the applied stress, d the drain size, k the Boltzmann constant, T the absolute temperature. Taking $\Omega = 1.88\times10^{-23}\,cm^3$. σ = 3000 psi, d = μm, T = 1673°K, and $D = 2.5\times10^{-6}\, e^{-\frac{62400}{RT}} = 1.75\times10^{-14}\ cm^2/sec$ for extrinsic lattice diffusion of oxygen as reported by Oishi and Kingery,[30] $\dot{\varepsilon}_{NH}$ is calculated to be $1.76\times10^{-9}\,sec^{-1}$. This predicted value is 1/77 of the observed value of $1.35\times10^{-7}\,sec^{-1}$.

2. Coble Creep

$$\dot{\varepsilon}_c = \frac{47.7\ D_b w}{d^2 kT}$$

where D_b is the coefficient of grain boundary diffusion, w the width of the boundary and other parameters have the same meaning and values as above. The magnitude of D_b w was estimated from the oxygen data obtained at higher temperatures by McKenzie et al.[52] for their as-received MgO bicrystals,

$$D_b\ w = 24\times10^{-10} D^{1/2}\,cm^3/sec$$

at 1670°C (or 1943°K).

If it is assumed that the grain boundary width is independent of temperature as suggested by Wuensch and Vasilos and that the activation energy for grain boundary diffusion (Q_b) is half of that for lattice diffusion (Q), as noted for FCC metals by James and Leak,[53] then

$$D_b\, w = 24\times10^{-10} D^{1/2} cm^3/sec$$

at 1400°C (or 1673°K). It, however, $Q_b > Q/2$, then the proportionality constant will decrease, as indicated in the data by McKansie et al.[52] Taking $D = 2.5\times10^{-6}\, e^{-\frac{62,400}{RT}} = 1.75\times10^{-14} cm^2/sec$ for extrinsic lattice diffusion of oxygen as above,

$$\frac{D_b w}{d} = 2.12\times10^{-3} cm^2/sec$$

Therefore, the upper limit of $\dot{\varepsilon}_c$ is calculated to be $7.43\times10^{-8} sec^{-1}$ which is 1/1.8 of the actual value.

3. Ashby-Verrall Creep

$$\dot{\varepsilon}_{AV} = \frac{100\Omega}{d^2 kT} \left(D+3.3\,\frac{D_d w}{d}\right) \left(\sigma-0.72\,\frac{\Gamma_d}{d}\right)$$

When Γ_b is the grain boundary free energy and others have the same meaning and values as above. Since the magnitude of Γ_b is in the order of 10^3 erg/cm^2, the second term in the second parenthesis is negligible compared with the applied stress. Also, the magnitude of D is negligible in comparison with the second term in

the first parenthesis, if D is taken as the value for extrinsic lattice diffusion of oxygen. Subsequently, $\dot{\varepsilon}_{AV}$ is calculated to be $5.24\times10^{-7}\,sec^{-1}$. This value is 3.9 times the experimental value.

REFERENCES

1. F. R. N. Nabarro, Deformation of Crystals by the Motion of Single Ions, Rept. of a Conf. on Strenght of Solids 75-90, The Physical Society, London (1948).

2. C. Herring, Diffusional Viscosity of a Polycrystalline Solid, J. Appl. Phys. 21, 437-445 (1950).

3. R. L. Coble, A Model for Boundary Diffusion Controlled Creep of Polycrystalline Materials, J. Apply. Phys. 34, 1679-1682 (1963).

4. von Mises, Mechanik der Plastischen Formänderung von Kristallen, Z. Angew. Math. Mech. 8, 161-185 (1928).

5. C. O. Hulse, S. M. Copley and J. A. Pask, Effect of Crystal Orientation on Plastic Deformation of MgO, J. Am. Ceram. Soc. 46, 317-323 (1963).

6. W. M. Armstrong, W. R. Irvin and R. H. Martinson, Creep Deformation of Stoichiometric UO_2, J. Nucl. Mat. 7, 133-141 (1962).

7. M. S. Seltzer, A. H. Clauer and B. A. Wilcox, The Stress Dependence for High Temperature Creep of Polycrystalline UO_2, J. Nucl. Mat. 34, 351-353 (1970).

8. P. E. Evans, Creep in Yttria-and Scandia-Stabilized ZrO_2, J. Am. Ceram. Soc. 53, 609-613 (1970).

9. T. Sugita and J. A. Pask, Creep of Doped Polycrystalline Al_2O_3, J. Am. Ceram. Soc. 53, 609-613 (1970).

10. A. Crosby and P. E. Evans, Creep in Pure and Two Phase Nickel-Doped Alumina, J. Mat. Sci. 8, 1573-1580 (1973).

11. J. Weertman, Steady-state Creep through Dislocation Climb, J. Appl. Phys. 28, 362-364 (1957).

12. M. H. Leipold and E. R. Blosser, The Role of Composition in Ultrafine-grain Ceramics, Ultrafine-Grain Ceramics, ed. by J. J. Burke et al., 99-107, Syracuse Univ. Press (1970).

13. R. B. Day and R. J. Stokes, Mechanical Behavior of Polycrystalline MgO at High Temperature, J. Am. Ceram. Soc. 49, 345-354 (1966).

14. C. O. Hulse and S. M. Copley, High-Temperature Compressive Compressive Deformation Equipment, Am. Ceram. Soc. Bull. 45, 530-534 (1966).

15. S. R. MacEwen, O. A. Kupics and B. Ramaswami, An Investigation of an Incremental Unloading Technique for Estimating Internal Stresses, Scripta Met. 3, 441-448 (1969).

16. H. I-Lei Huang, O. D. Sherby and J. E. Dorn, Activation Energy for High Temperature Creep of High Purity Aluminum, Trans. AIME 206, 1385-1388 (1956).

17. D. R. Cropper and J. A. Pask, Effect of Plastic Instability on Compressive Deformation, Am. Ceram. Soc. Bull. 48, 555-558 (1969).

18. H. C. Chang and N. J. Grant, Observations of Creep of the Grain Boundary in High Purity Aluminum, Trans. AIME 194, 619 (1952).

19. A. G. Evans, D. Gilling and R. W. Davidge, The Temperature-

Dependence of the Strength of Polycrystalline MgO, J. Mat. Sci. 5, 187-197 (1970).

20. R. W. Davidge and P. L. Pratt, Plastic Deformation and Work-Hardening in NaCl, Phys. Stat. Sol. 6, 759-776 (1964).

21. T. V. Cherian, P. Pietrokowsky and J. E. Dorn, Some Observations on the Recovery of Cold Worked Aluminum, Trans. AIME 185, 948-956 (1949).

22. D. H. Chung and W. G. Lawrence, Relation of Single-Crystal Elastic Constants to Polycrystalline Isotropic Elastic Moduli of MgO: II, Temperature Dependence, J. Am. Ceram. Soc. 47, 448-455 (1964).

23. J. L. Lytton, C. L. Meyers and T. E. Tietz, The Effect of Elastic and Plastic Strain on the Tensile Flow Stress Recovery of Aluminum, Trans. AIME 224, 1250-1258 (1962).

24. D. R. Cropper and J. A. Pask, Creep of LiF Single Crystals at Elevated Temperatures, Phil. Mag. 27, 1105-1124 (1973).

25. J. Narayan and J. Washburn, Self Diffusion in MgO, Acta Met. 21, 533-538 (1973).

26. M. O. Davies, Transport Phenomena in Pure and Doped MgO, J. Chem. Phys. 38, 2047-2055 (1963).

27. L. H. Rovner, Diffusion of Oxygen in MgO, Cornell Univ. Ithaca, N. Y., Dep of Engineering Physics, Technical Report TR-10 (March 1966).

28. G. W. Groves and A. Kelly, Prismatic Dislocation Loops in Cold-Warked and Annealed MgO Crystals, J. Appl. Phys. 34, 3104-3107 (1963).

29. J. Narayan and J. Washburn, Pipe Diffusion in MgO, Crystal Lattice Defects 3, 91-98 (1972).

30. Y. Oishi and W. D. Kingery, Oxygen Diffusion in Perclase Crystals, J. Chem. Phys. 33, 905-906 (1960).

31. H. Hashimoto, M. Hama and S. Shirasaki, Preferential Diffusion of Oxygen along Grain Boundaries in Polycrystalline MgO, J. Appl. Phys. 43. 4828-4829 (1972).

32. C. M. Kapadia and M. H. Leipold, Grain Growth in Pure Dense MgO, J. Am. Ceram. Soc 57, 41-42 (1974).

33. R. A. Brown, Sintering in Very Pure MgO and MgO Containing Vandium, Am. Ceram. Soc. Bull. 44, 483-487 (1965).

34. R. Lindner and G. D. Parfitt, Diffusion of Radioactive Magnesium in MgO Crystals, J. Chem. Phys. 26, 182-185 (1957).

35. B. C. Harding and D. M. Price, Cation Self-diffusion in MgO up to 2350°C, Phil. Mag. 26, 253-260 (1972).

36. T. K. Gupta, Sintering of MgO: Densification and Grain Growth, J. Mat. Sci. 6, 25-32 (1971).

37. S. P. Mitoff, Electronic and Ionic Conductivity in MgO, J. Chem. Phys. 36, 1383 (1962).

38. P. F. Eastman and I. B. Cutler, Effect of Water Vapor on Initial Sintering of Magnesia, J. Am. Ceram. Soc. 49, 526-530 (1966).

39. B. J. Wuensch and T. Vasilos, Diffusion of Transition Metal Ions in Single-Crystal MgO, J. Chem. Phys. 36, 2917-2922 (1962).

40. S. L. Blank and J. A. Pask, Diffusion of Iron and Nickel In MgO Single Crystals, J. Am. Ceram. Soc. 52, 669-675 (1969).

41. B. J. Wuensch and T. Vasilos, Grain-boundary Diffusion in MgO, J. Am. Ceram. Soc. 47, 63-68 (1964).

42. J. Weertman, Steady-State Creep of Crystals, J. Appl. Phys. 28, 1185-1189 (1957).

43. F. R. Nabarro, Steady-State Diffusional Creep, Phil. Mag. 16, 231-237 (1967).

44. J. Weertman, Dislocation Climb Theory of Steady-State Creep, Trans. Am. Soc. Met. 61, 681-694 (1968).

45. J. Narayan and J. Washburn, Pipe Diffusion in MgO, Crystal Lattice Defects, 3, 91-98 (1972).

46. R. B. Day and R. J. Stokes, Plastic Softening of MgO at High Temperatures by NiO Addition:, J. Am. Ceram. Soc. 50, 445-448 (1967).

47. W. G. Cannon and O. D. Sherby, High-Temperature Creep of NaCl-KCl Solid Solution Alloys , J. Am. Ceram. Soc. 53, 346-349 (1970).

48. W. D. Scott and J. A. Pask, Deformation and Fracture of Polycrystalline LiF, J. Am. Ceram. Soc. 46, 284-293 (1963).

49. W. G. Johnston, Yield Points and Delay Times in Single Crystals, J. Appl. Phys. 33, 2716-2730 (1962).

50. A. G. Evans, C. Roy and P. L. Pratt, The Role of Grain Boundaries in the Plastic Deformation of Calcium Fluoride, Porc. Brit. Ceram. Soc. 6, 173-188 (1966).

51. M. F. Ashby and R. A. Verrall, Diffusion-Accomodated Flow and Superplasticity, Acta Met. 21, 149-163 (1973).

52. D. R. McKenzie, A. W. Searcy, J. B. Holt and R. H. Condit, Oxygen Grain-Boundary Diffusion in MgO, J. Am. Ceram. Soc. 54, 188-190 (1971).

53. D. W. James and G. M. Leak, Grain Boundary Diffusion of Iron Cobalt and Nickel in Alpha-iron and of Iron in Gamma-iron, Phil. Mag. 12 491-503 (1965).

54. J. H. Hensler and G. V. Cullen, Stress, Temperature, and Strain Rate in Creep of MgO, J. Am. Ceram. Soc. 51, 557-559 (1968).

55. J. M. Birch and B. Wilshire, The Effect of Stress Changes during Creep of Single- and Polycrystalline MgO, Phil. Mag. 30, 1023-1031 (1974).

56. W. E. Snowden and J. A. Pask, High-Temperature Deformation of Polycrystalline MgO, Phil. Mag. 29, 441-455 (1974).

57. J. R. Kreglo and W. J. Smoothers, Mechanism of Creep in MgO Brick, J. Am. Ceram. Soc. 50, 457-460(1967).

58. J. F. Wygant, Elastic and Flow Properties of Dense, Pure Oxide Refractories, J. Am. Ceram. Soc. 34, 374-380 (1951).

59. H. Tagai and T. Zisner, High-Temperature Creep of Polycrystalline Magnesia: I, Effect of Simultaneous Grain Growth, J. Am. Ceram. Soc. 51, 303-310 (1968).

60. E. M. Passmore, R. H. Duff and T. Vasilos, Creep of Dense, Polycrystalline MgO, J. Am. Ceram. Soc. 49, 594-600 (1966).

61. T. Vasiloc, J. B. Mitchell and R. M. Springgs, Creep of Polycrystalline Magnesia, J. Am. Ceram. Soc. 47, 203-204 (1964).

62. V. S. Bakunov, E. S. Lukin and D. N. Polyboyarinov, Tr. Mosk. Khim-Teckhnol. Inst. 50, 216 (1966).

63. J. B. Bilde-Sörensen, Dislocation Structures in Cree-Deformed Polycrystalline MgO, J. Am. Ceram. Soc. 55, 606-610(1972).

64. M. Hurm and B. Escaig, Propriétés Mécaniques et Structurales en Fluage Très Haute Température de Magnésie Polycristalline Dopée, J. de Phys. 34 Colloque C9m Supplément, 347-358 (1973).

65. T. G. Langdon and J. A. Pask, The Mechanism of Creep in Polycrystalline MgO, Acta Met. 18, 505-510(1970).

66. E. Yasuda, M. Ootsuka, S. Kimura and H. Tagai, Compression Creep of Polycrystalline Magnesia at High Temperature, Bull. Tokyo Inst. Tech. 108, 113-121 (1972).

67. G. W. Groves and A. Kelly, Change of Shape Due to Dislocation Climb, Phil. Mag. 19, 977-986 (1969).

68. S. M. Copley and J. A. Pask, Deformation of Polycrystalline MgO at Elevated Temperatures, J. Am. Ceram. Soc. 48, 636-642 (1965).

69. Y. Ishida and M. Henderson-Brown, Dislocations in Grain Boundaries and Grain Boundary Sliding, Acta Met. 15, 857-860 (1967).

70. U. F. Kocks, The Relation Between Polycrystal Deformation and Single-Crystal Deformation, Met. Trans. 1, 1121-1143(1970).

71. R. Widmer and N. J. Grant, The Creep Rupture Properties of 80 Ni-20Cr Alloys, Trans, AIME: J. Basic Eng. Ser. D, 82, 829-838 (1960).

72. Y. Ishida and D. McLean, Effect of Nitrogen and Manganese on Recovery Rate and Friction Stress during Creep of Iron, J. Iron and Steel Inst. 205, 88-93 (1967).

Table I. Composition of MgO Specimens

(A) Spectrographic Analysis

Constituent*	Specimen Type (wt%) Undoped Single Crystal	Ni-doped Single Crystal	As-received Polycrystal
Mg	Principal constituent in each type		
Li	Less than 0.1% in each, not detected		
Ni	0.001	0.8	0.001
Ca	.1	.015	.003
Fe	.01	.02	.007
Si	.01	.001	.002
Al	.004	.003	.002
Ti	.003	.001	--
Co	--	.003	--
Cr	.001	.006	--
Cu	.001	.001	.001
Total	.130	.850	.016

*Constituents reported as oxides of the elements indicated except for Li which is not included in the total. Analysis performed by American Spectrographic Laboratories, Inc., San Francisco, Calif.

Table I. Composition of MgO Specimens

(B) Neutron Activation Analysis of Polycrystalline Specimens

Specimen Type	F (ppm)*
As-received	415
Annealed 4h in air at 1500°C	390
Annealed 110h in Pt at 1500°C	133
Annealed 110h in air at 1500°C	ND≤67†

*Analysis performed by Dr. L. E. Kovar at General Activation Analysis, Inc., San Diego, Calif.

†ND = not detected. Upper limits (≤) are based on three standard deviations from counting statistics.

Table II. Shear Moduli (G, x 10^6 psi) of MgO Specimens

Specimen Type	25°C	1200°C	1400°C
Single Crystal			
<100>	17.74	11.76	(10.68)*
<110>			
N <100>			
<111>	22.44	(19.76)*	(19.28)*
Polycrystal			
As-received	18.91	(14.22)*	(13.37)*
Annealed			

*Extrapolated from low temperatures.[22]

TABLE III. Magnitude of Yield Drop

(Test Temperature = 1200°C)

Specimen Type	Strain-Rate (sec^{-1})	Elastic Limit (psi)	Upper Yield Point-Lower Yield Point=Magnitude of Drop (psi)
Annealed 170h in Pt at 1400°C	1×10^{-5}	25600	27400 = 25400 = 2000
	3×10^{-4}	25000	26000 - 21700 = 4300
Annealed 12h in air at 1400°C	1×10^{-5}	22900	25800 - 24800 = 1000
	1×10^{-4}	22100	26100 - 25800 = 300
Annealed 110h in Pt at 1500°C	1×10^{-5}	28400	29400 - 29300 = 100
Annealed 450h in Pt at 1400°C	1×10^{-5}	25300	28400 - 28400 = 0^{1}
	5×10^{-5}	24500	28800 - 28800 = 0^{2}

Note: 1. Sharp yeild

2. Yield plateau

Table IV. Recovery-Hardening

Test Temperature (°C)	Strain Rate (sec^{-1})	Prior Heat Treatement	Recovery Period (h)	$(\sigma_{max}-\sigma_o)^*$ (psi)
1200	3×10^{-5}	As-received	2 1/2	4100
1400	3×10^{-5}	Annealed 4h in air at 1400°C	2 1/2	2600
1400	3×10^{-5}	Annealed 12h in air at 1500°C	2 1/2	900
1400	1×10^{-5}	Annealed 4h in air at 1400°C	1	1700
1400	1×10^{-5}	Annealed 110h in Pt at 1500°C	1	0

*σ_{max} = maximum stress upon reloading after recovery.

σ_o = steady state stress before unloading for recovery.

Table V. Activation Energy (Q, kcal/mole) and Stress Dependency (n)

Specimen Type	Steady Creep		Static Recovery		Yielding	
	Q	n	Q	n	Q	n
Single Crystal						
<100>	73.9	4.0	41.8[3] 79.7[4]	4.0 4.0	86.2[6] 0[7]	5.9 ∞
N<100>	43.2	3.0	43.0	3.0	56.3[6] 0[7]	3.0 ∞
<110>	75.3	3.0	--	--	--	--
<111>	75.0	2.7	52.8 87.9[5]	5.6 5.6	70.0[1,6] 73.2[2]	3.0 6.2
Polycrystal						
As-received	54.4[1] 50.6[2]	3.0 4.4	---[1] 46.6[2]	3.0 5.0	45.7[1,6] 40.6[2]	1.9 6.2
Annealed	56.1* 54.4[1] 50.6[2]	1.0 3.0 4.4	56.2	4.0	51.2[1,6] 50.6[2]	3.0 6.2

Note:
* Determined by Dorn's technique
1 Low-stress region
2 High-stress region
3 Early stages ($\dot{\varepsilon} \sim 1 \times 10^{-5}$ sec^{-1})
4 Later stages (")
5 Annealed prior to deformation
6 Creep data (initial or maximum creep rate)
7 Stress-strain data

Table VI. Fracture Stress and Strain
(Single crystals)

Specimen Type	Test Temperature (°C)	Strain Rate (sec^{-1})	Fracture Stress (psi)	Fracture Strain (%)
<100>	1200	1×10^{-5}	28,200	>40
		3×10^{-4}	15,100*	9
	1400	1×10^{-5}	10,400	>36
		3×10^{-4}	29,000	>51
N<100>	1200	1×10^{-5}	16,800	>59
		3×10^{-4}	26,100*	37
	1400	1×10^{-5}	14,600	>48
		3×10^{-4}	28,800	>60
<110>	1200	1×10^{-5}	38,300	8
		3×10^{-4}	44,800	5
	1400	1×10^{-5}	23,500	29
		3×10^{-4}	36,200	8
<111>	1200	1×10^{-5}	50,100	11
		3×10^{-4}	66,600	5
	1400	1×10^{-5}	25,900	37
		3×10^{-4}	46,700	11

NOTE: *Stress corresponding to the first cracking.

Table VII. Effect of Recovery Stress on Recovery Rate

Specimen Type	Test Temp. (°C)	Strain Rate (sec^{-1})	Deformation Stress (psi)	Recovery Stress (psi)	Recovery Period (min)	Recovery Rate (psi/sec)
Single Crystal						
<100>	1200	1×10^{-5}	12,400	~*10,800	5	0.69
				<**12,400		0.39
		5×10^{-5}	15,200	~†0	5	1.74
				~12,700		1.80
	1400	1×10^{-4}	9,400	~0	1	8.23
				~6,400		7.55
N<100>	1200	1×10^{-5}	12,600	~11,000	5	1.58
				<12,600		1.05
		3×10^{-4}	19,200	~0	5	6.87
				~12,500		4.55
				<19,200		2.80
	1400	1×10^{-4}	12,700	~0	5	6.20
				~ 9,300		5.88
				<12,700		4.91
<110>	1400	5×10^{-5}	26,800	~0	5	20.8
				~17,500		25.9
<111>	1200	1×10^{-5}	36,600	~26,800	10	19.0
				<36,600		7.94
		1×10^{-4}	40,700	~0	5	19.9
				~28,100		15.6

Note: † Unloaded to a preload level (1000 psi)
* Slightly less than
** Being relaxed from

Table. VIII. Activation Energy (Q) for Diffusion in MgO (Literature Data)

Diffusing Species	Rate Process	Specimen Type	Temperature	Q (kcal/mole)	Diffsuion Mechanism	Investigators
Oxygen	Shrinkage of isolated dislocation loop	Single crystal	1100-1430	110	intrinsic	Narayan and Washburn (1973)[25]
Oxygen	Electrical conduction	Polycrystal	1100-1300 1000-1100	120 62	intrinisic extrinsic	Davies (1963)[36]
Oxygen	Tracer diffusion	Polycrystal	1000	82	---	Rovner (1966)[27]
--	Growth of dislocation loops	Single Crystal	1240-1430	76	---	Groves and Kelly (1963)[28]
Oxygen	Breakup of dislocation dipoles	Single crystal	930-1370	61-63	pipe	Narayan and Washburn (1972)[29]
Oxygen	Gas/solid exchange	Powder	1300-1750	62	extrinsic	Oishi and Kingery (1960)[30]
Oxgyen	Gas/solid exchange	Powder (grain-size of 15 μm)	1100-1400	60	grain-boundary	Hashimoto et al. (1972)[31]
Oxygen	Grain growth	Polycrystal	1300-1650	66	grain-boundary	Kapadia and Leipold[32] (1974)
--	Initial sintering	Powder	1300-1500	27	grain-boundary	Brown (1965)[33]

Table VIII. Activation Energy (Q) for Diffusion in MgO (Literature Data) (Continued)

Diffusing Species	Rate Process	Specimen Type	Temperature	Q (kcal/mole)	Diffusion Mechanism	Investigators
Magnesium	Tracer diffusion	Single crystal	1400-1600	79	intrinsic	Lindner and Parfitt (1957)[34]
Magnesium	Electrical Conduction	Polycrystal	1000-1350 770-1000	81 22	intrinsic extrinsic	Davies (1963)[26]
Magnesium	Trancer diffusion	single crystal	1910-2350 1540-1800 1100-1450	80 36 74	intrinsic extrinsic precipitation-influenced	Harding and Price (1972)[35]
Magnesium	Grain growth	Polycrystal (porous)	1450-1650	76	intrinsic	Gupta (1971)[36]
Magnesium	Electrical conduction	Single crystal	1000-1500	50	---	Mitoff (1962)[37]
Magnesium	Initial sintering	Powder	800-1110	48	Grain boundary	Eastman and Culter (1964)[38]
Nickel	Impurity diffusion	Single crystal	1000-1850	48	---	Wuensch and Vasilos (1962)[39]
Nickel	Interdiffusion	Single crystal	1200-1400	43	---	Blank and Pask (1969)[40]
Nickel	Penetration along grain boundary	Polycrystal	1400-1900	23-46	Grain-boundary	Wuensch and Vasilos (1964)[41]

Table IX. Activation Energy (Q) and Stress-Dependency (n) for Creep of MgO (Literature Data)

A. Li/F - Free Polycrystals (Continued)

Specimen Characteristics	Stress (psi)	Temperature (C°)	Q (kcal/mole)	n	Proposed Mechanism	Investigators
Porosity = 0.5% GS = 2 μm	1000-5000 (Four-point Bending)	1110-1530	96*	1.0	Nabarro-Herring controlled by intrinsic diffusion of magnesium.	Passmore et al. (1966)[60]
Porosity = 0.5% GS = 5.5-20 μm	1000-5000 (Four-point Bending)	1110-1530	54*	1.5	Nabarro-Herring controlled by extrinsic diffusion of oxygen or cable controlled by grain-boundary diffusion.	Passmore et al. (1966)[60]
Porosity ~0% GS = 2 μm	1600-2800 (Four-point Binding)	1180-1260	74*	1	Nabarro-Herring controlled by intrinsic diffusion of magnesium.	Vasilos et al. (1964)[61]
Porosity = 3% GS = 50 μm	----- (Four-point Bending)	1650-1800	89	--	-----	Bakunov et al. (1966)[62]

*Determined by Dorn's technique

**Initial GS (final GS = 20 - 40 μm)

Table IX. Activation Energy (Q) and Stress-Dependency (n) for Creep of MgO (Literature Data)

A. Li/F - Free Polycrystals

Specimen Characteristics	Stress (psi)	Temperature (C°)	Q (kcal/mole)	n	Proposed Mechanism	Investigators
Porosity = 2% GS = 13-68μm	1000-6500 (Compression)	1200-1500	111	2.6	Accomodation of grain boundary sliding at triple points	Hensler and Cullen (1968)[54]
Porosity = 5% GS = 12 μm	10,000	1323	107*	3	Growth of three-dimensional dislocation network controlled by intrinsic diffusion of oxygen.	Birch and Wilshire (1974)[55]
Porosity = 1% GS = 17 μm	11,000-20,000 (Compression	1200	110*	7	Climb of edge dislocations controlled by intrinsic diffusion of oxygen.	Snowden and Pask (1974)[56]
Porosity = high (Refractory)	---- (Compression)	1205-1425	62	4.5	Dislocation mechanism.	Kreglo and Smothers (1967)[57]
Porosity = 2% GS = 10 μm	1200-3600 (Torsion)	1100-1300	46	3.5	----	Wygant (1951)[58]
Porosity = 1.5-3% GS < 20**μm	---- (Three-point Bending)	1200-1500	104	1	Nabarro-Herring controlled by intrinsic diffusion of magesium (or oxygen).	Tagai and Zisner (1968)[59]

Table IX. Activation Energy (Q) and Stress-Dependency (n) for Creep of MgO (Literature Data)

B. LiF - Added Polycrystals

Specimen Characteristics	Stress (psi)	Temperature (C°)	Q (kcal/mole)	n	Proposed Mechanism	Investigators
LiF <2%+ Porosity 0.2% GS = 100-190 μm	3500-7800	1300-1460	76	3.2	Growth of three-dimensional dislocation network controlled by extrinsic diffusion of oxygen.	Bilde-Sorensen (1972)[63]
Li <360 ppm+ Porosity = 0.1% GS = 13-150 μm	2000-17000 (Compression)	12000-1700	60	3.4	Climb of edge dislocations controlled by pipe diffusion of oxygen.	Burn and Escaig (1973)[64]
LiF <3%+ Porosity 0.2% GS = 12-52 μm	5,000-20,000	1200	51*	3.3	Climb of edge dislocations controlled by extrinsic diffusion of oxygen.	Langdon and Pask (1970)[65]
Li_2O <0.2%+ Porosity 0.2% GS = 42 μm	70-500 (Compression)	1500-1620	90	1	Nabarro-Herring controlled by intrinsic diffusion of magnesium.	Yasuda et al. (1972)[66]

+ Amount added prior to hot-pressing.

* Determined by Dorn's technique

FIGURE CAPTIONS

Fig. 1. Two sections of grain boundary features present in cloudy polycrystals after annealing 170h in air at 1400°C.

Fig. 2. Grain-size-dependence of the amount of F associated with unit area of grain boundary ("film thickness").

Fig. 3. Grain growth behavior during annealing prior to testing.

Fig. 4. Laue back-reflection X-ray photographs of undeformed polycrystals (a) in the as-received condition (b) after annealing 12h in air at 1500°C (grain size = 4 and 23μm, respectively).

Fig. 5. <100> crystal crept to 20% at 1200°C, (left-hand side was ground off after test). Compression axis is vertical.

Fig. 6. Laue X-ray patterns for the specimen shown in Fig. 5: (a) from a flat surface, and (b) from a curved surface. Compression axes vertical.

Fig. 7. (a) Fine-grained polysrystal (annealed 4h in air at 1500°C) stress-strain tested to 31% at 1200°C and $\dot{\varepsilon} \sim 1 \times 10^{-5}\ sec^{-1}$.
(b) As-received polycrystal crept to 40% at 1400°C.
(c) As-received polycrystal crept to 45% at 1400°C; this specimen was deformed 12% more than the specimen shown in (b) at low stresses ($\leq$6000 psi). Compression axes vertical.

Fig. 8. A (i00) plane of <111> crystals crept (a) to 26% at 1200°C, and (b) to 69% at 1400°C. Compression axes not shown.

Fig. 9. N<100> crystal stress-strain tested at 58% at 1200°C under $\dot{\varepsilon}\sim 1\times10^{-5}\,sec^{-1}$. Compression axis vertical.

Fig. 10. <100> crystals deformed at 1400°C (a) stress-strain tested to 62% and $\dot{\varepsilon}\sim 1\times10^{-5}\,sec^{-1}$, (b) crept to 52% at σ = 8000 psi. Compression axes vertical.

Fig. 11. N<1 0> crystals crept at 1400°C and σ = 8000 psi (a) by 13% (after prior deformation of 29%); (b) by 31% (after prior deformation of 43%). Compression axes vertical.

Fig. 12. A (110) plane of (a) <110> crystal crept to 26% at 1200°C, and (b) <111> crystal crept to 33% at 1200°C. Compression axis indicated by the arrows facing each other.

Fig. 13. Fine-grained polycrystals (annealed 4h in air at 1500°C): (a) Stress-strain tested to 1.5% at 1200°C and $\varepsilon\sim 1\times10^{-5}\,sec^{-1}$, (b) stress-strain tested to 31% (beyond fracture strain) at 1200°C $\varepsilon\sim 1\times10^{-5}\,sec^{-1}$, (c) crept to 14% at 1200°C, (d) stress-strain tested to 53% at 1400°C and $\varepsilon\sim 1\times10^{-5}\,sec^{-1}$, (e) crept of 5% at 1400°C, (f) crept to 48% at 1400°C ($\dot{\varepsilon}<1\times10^{-6}\,sec^{-1}$). Compression axes vertical.

Fig. 14. Two different areas in as-received polycrystal crept to 99% (beyond the fracture strain) at 1400°C. Compression axes vertical.

Fig. 15. Medium-grained polycrystals (annealed 110h in Pt at 1500°C): (a) Stress-strain tested to 11% (behond fracture strain) at 1200°C and $\dot{\varepsilon}\sim 5\times10^{-5}\,sec^{-1}$, (b) crept to 46% (beyond fracture strain) at 1200°C, (c) strain-strain tested to 19% (~ fracture strain) at 1400°C and $\dot{\varepsilon}\sim 1\times10^{-5}\,sec^{-1}$, (d) crept to 92%

(beyond fracture strain) at 1400°C. Compression axes vertical.

Fig. 16. (A) Coarse-grained polycrystal (annealed 40h in air at 1500°C) crept to 4% at 1400°C, (b), (c) and (d) Three different areas in a coarse-grained polycrystal (annealed 600h in air at 1400°C) crept to 29% at 1400°c. Compression axes vertical.

Fig. 17. Scanning electron micrographs of unpolished surface for (a) as-received polycrystal stress-strain tested to 16% at 1400°C and $\dot{\varepsilon}\sim 1\times 10^{-5}\,sec^{-1}$, and (b) fine-grained polycrystal (annealed 4h in air at 1500°C), stress-strain tested to 22% at 1200°C and $\dot{\varepsilon}\sim 1\times 10^{-5}\,sec^{-1}$. Compression axes vertical.

Fig. 18. Two different areas in a medium-grained polycrystal (annealed 150h in Pt at 1500°C) stress-strain tested to 5% (beyond fracture strain) at 1200°C and $\dot{\varepsilon}\sim 1\times 10^{-5}\,sec^{-1}$. Marker scratch shown as transverse line in (b) (Optical micrographs of unpolished surface). Compression axes parallel to a longer edge of the protograph.

Fig. 19. Coarse-grained polycrystal (annealed 170h in air at 1400°C) stress-strain tested to 4% (beyond fracture strain) at 1200°C and $\dot{\varepsilon}\sim 5\times 10^{-5}\,sec^{-1}$. Compression axis vertical.

Fig. 20. Medium-grained polycrystal (annealed 100h in Pt at 1500°C) crept to 92% (beyond fracture strain) at 1400°C. Compression axis vertical.

Fig. 21. Stress-strain curves of <100> and N<100> crystals, as a function of the strain-rate at (a) 1200°C, and (b) 1400°C. Open circles correspond to 0.2% offset yield stresses.

Fig. 22. Effect of prior annealing treatment on the stress-strain curves for (a) <100> crystal deformed at 1200°C, (b) N<100> crystal deformed at 1200°C, (c) <111> crystals deformed at 1200°C and 1400°C ($\dot{\varepsilon}$~1×10-^{5}sec^{-1}). Open circles correspond to 0.2% offset yield stresses.

Fig. 23. Stress-strain curves for <110> crystal as compared with <100> crystal. Open and solid circles correspond to 0.2% offset yield stresses.

Fig. 24. Stress-strain curves for polycrystals as a function of grain size when deformed at (a) 1200°C, and (b) 1400°C. Open and solid circles correspond to 0.2% offset yield stresses.

Fig. 25. Stress-strain curves for polycrystals as compared with a <111> crystals at 1200°C and 1400°C ($\dot{\varepsilon}$~3×10^{-4}sec^{-1}). Open and solid circles correspond to 0.2% offset yield stresses.

Fig. 26. Stress-strain curves for polycrystals with several grain sizes at 1200°C ($\dot{\varepsilon}$~5×10^{-5}sec^{-1}). Open circles correspond to 0.2% offset yield stresses.

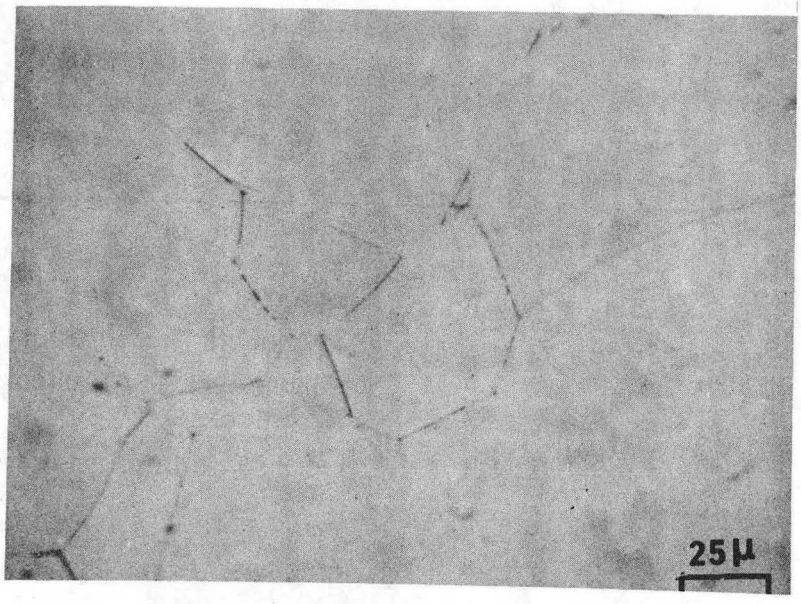

(a)

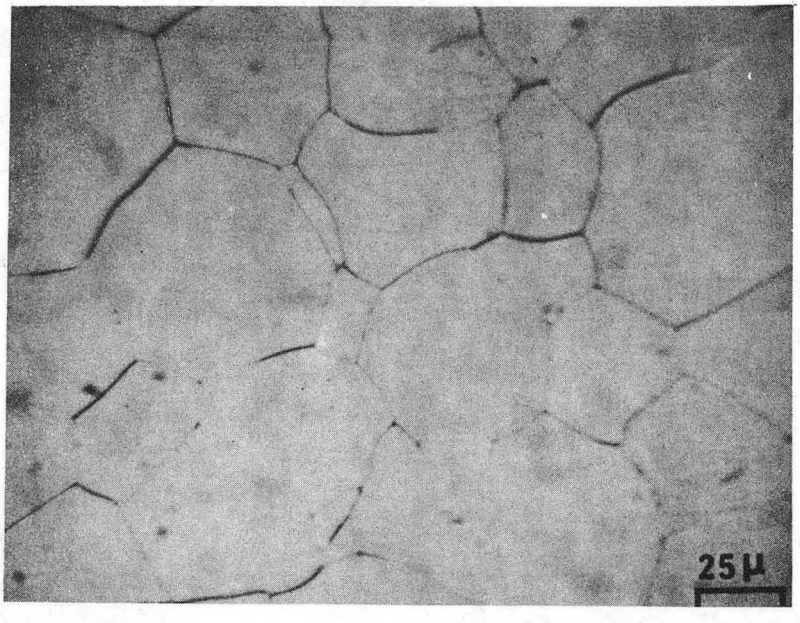

(b)

XBB 756-4445

Fig. 1.

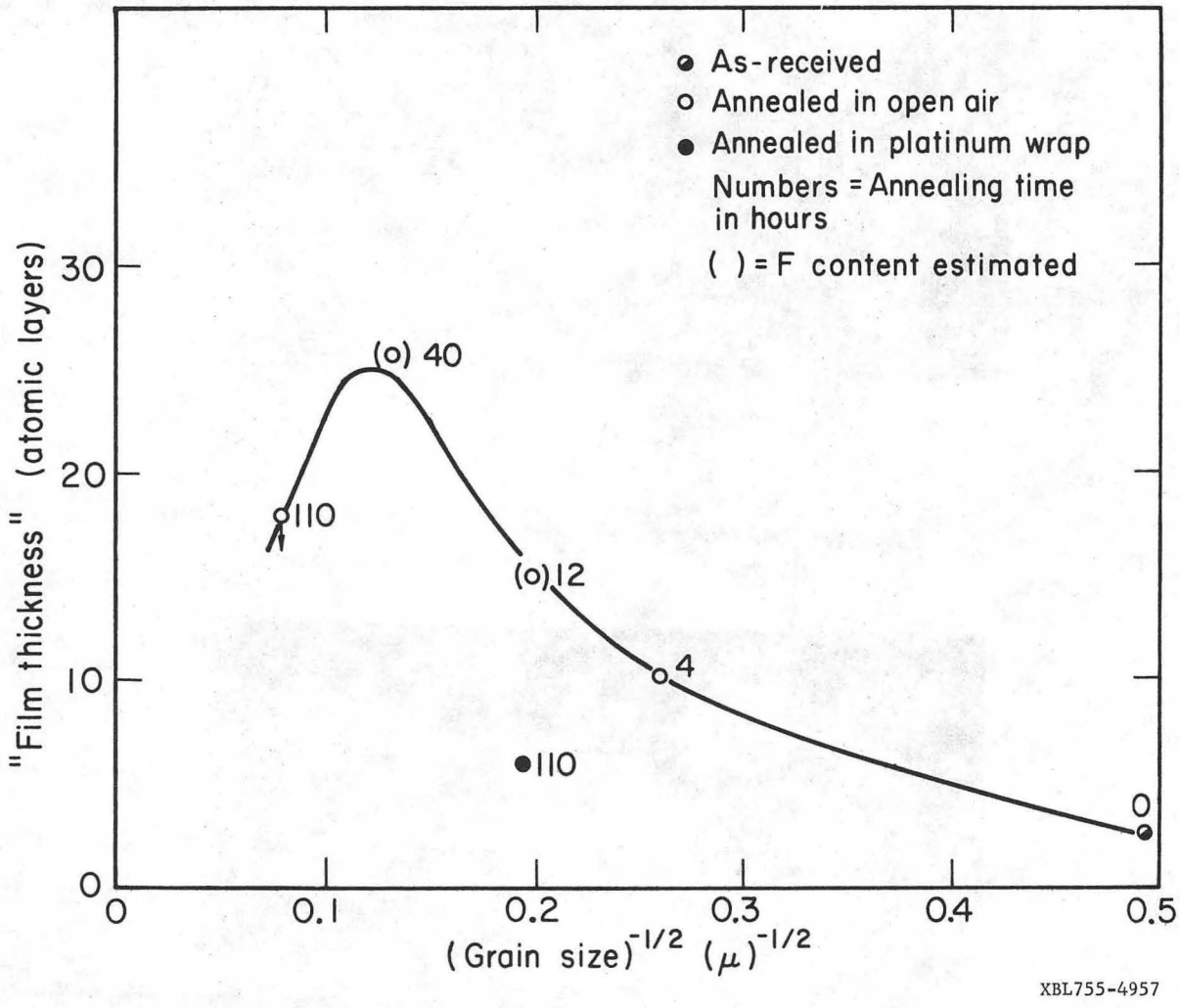
As-received
Annealed in open air
Annealed in platinum wrap
Numbers = Annealing time in hours
( ) = F content estimated
(o) 40
110
(o) 12
4
110
0
"Film thickness" (atomic layers)
0
10
20
30
0
0.1
0.2
0.3
0.4
0.5
(Grain size)$^{-1/2}$ (μ)$^{-1/2}$
XBL755-4957

Fig. 2.

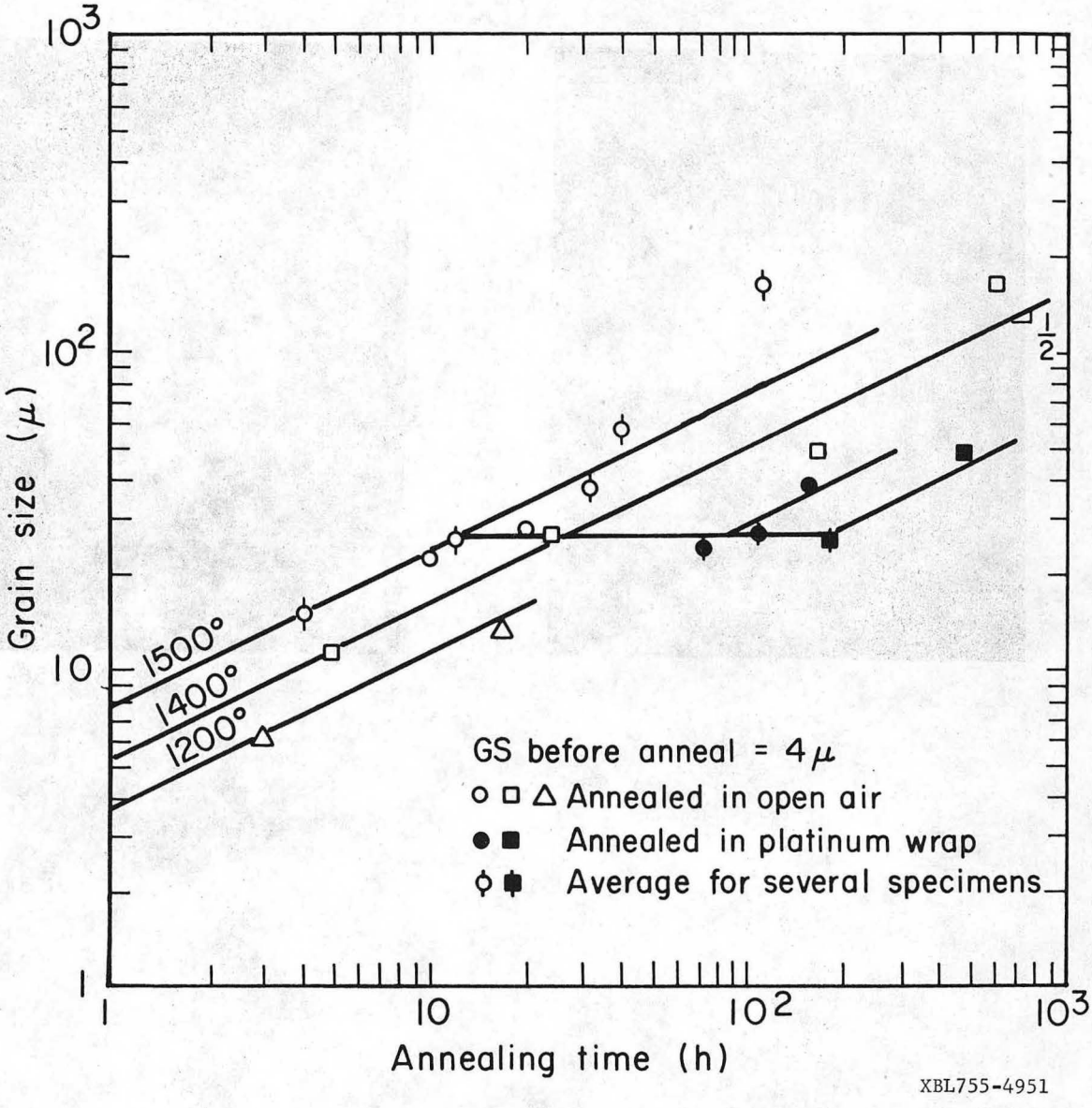

Fig. 3.

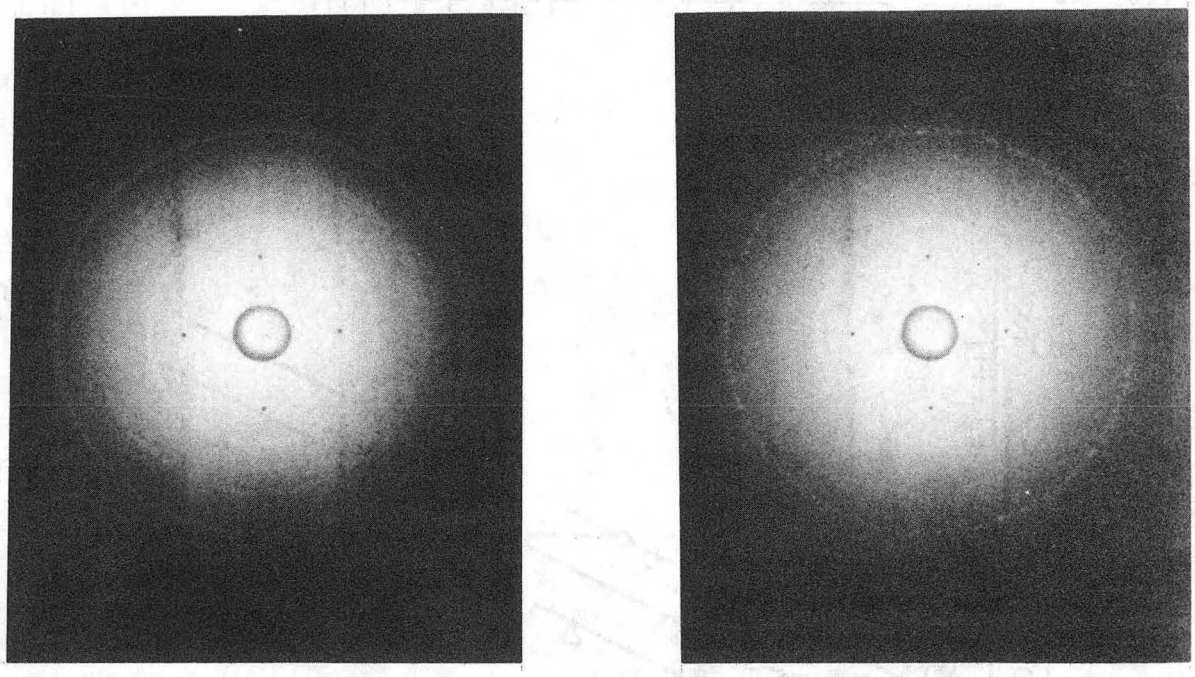

XBB 756-4447

(a) (b)

Fig. 4.

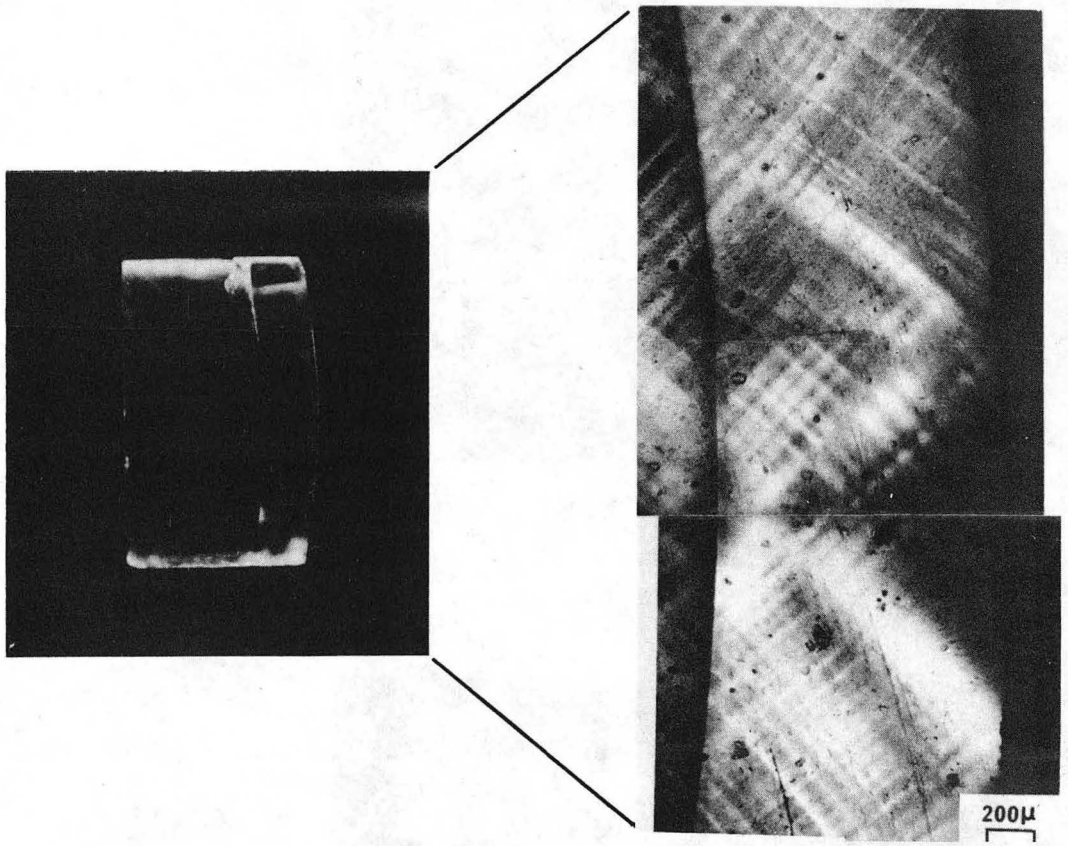

XBB 756-4978

Fig. 5.

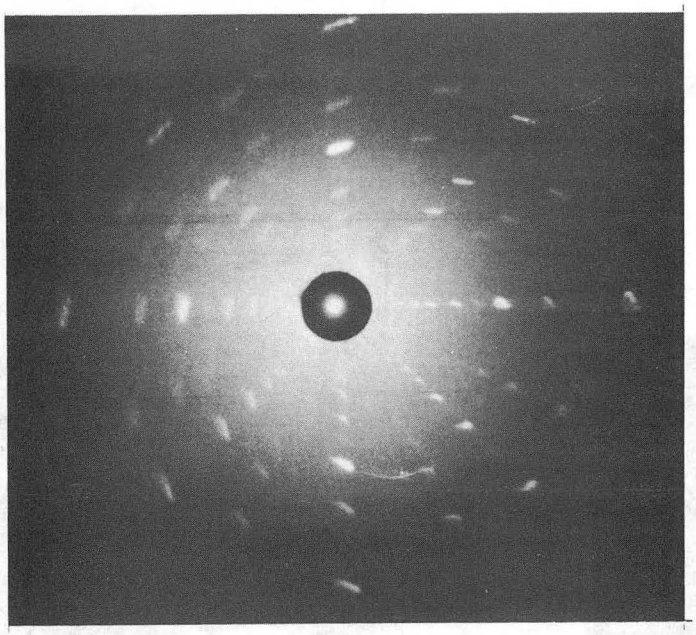

(a)

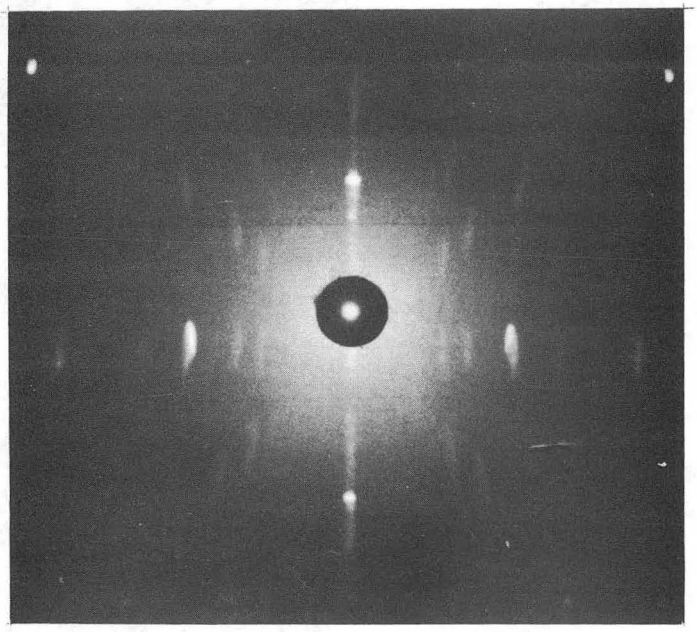

XBB 757-5202

(b)

Fig. 6.

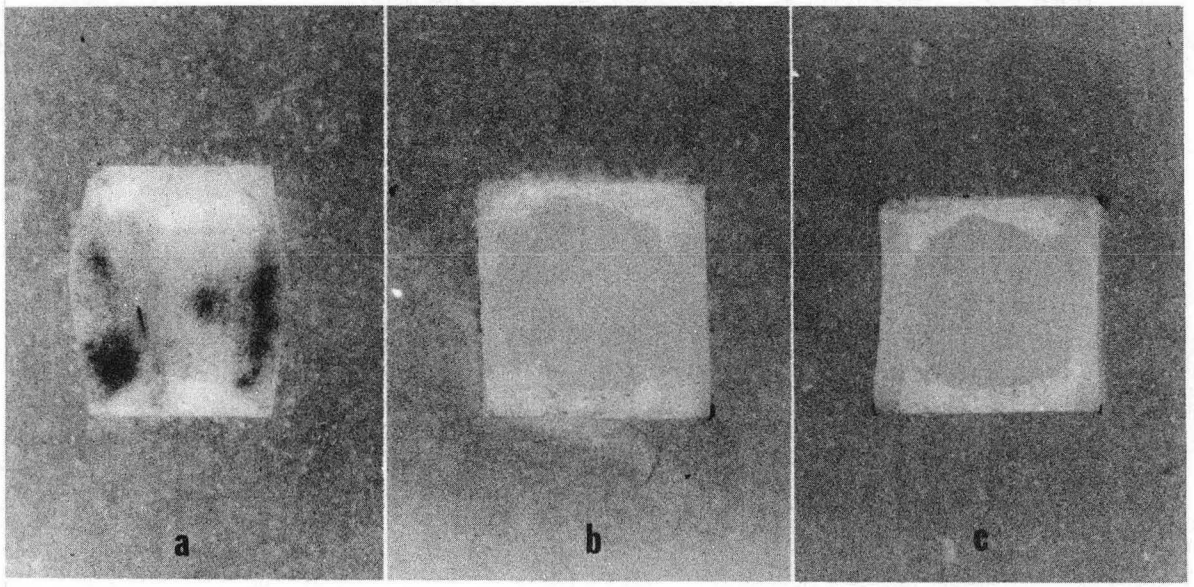

XBB 756-4446

Fig. 7.

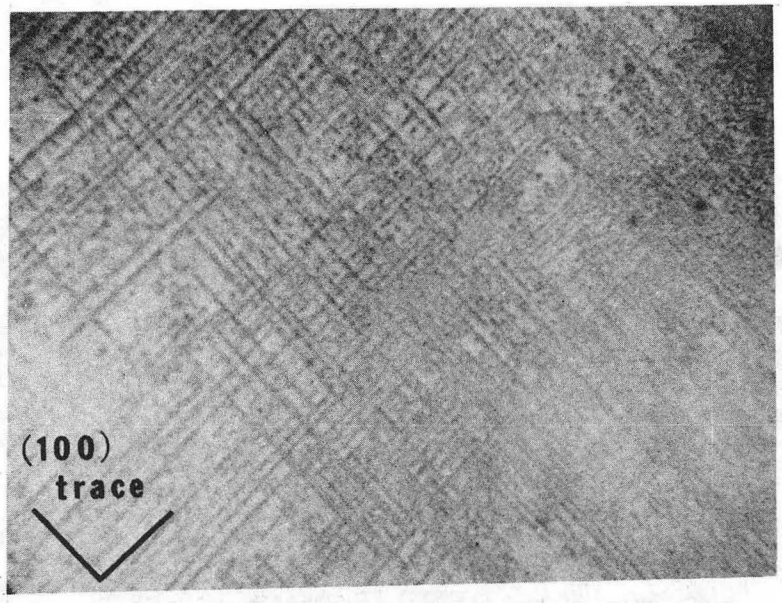

(a)

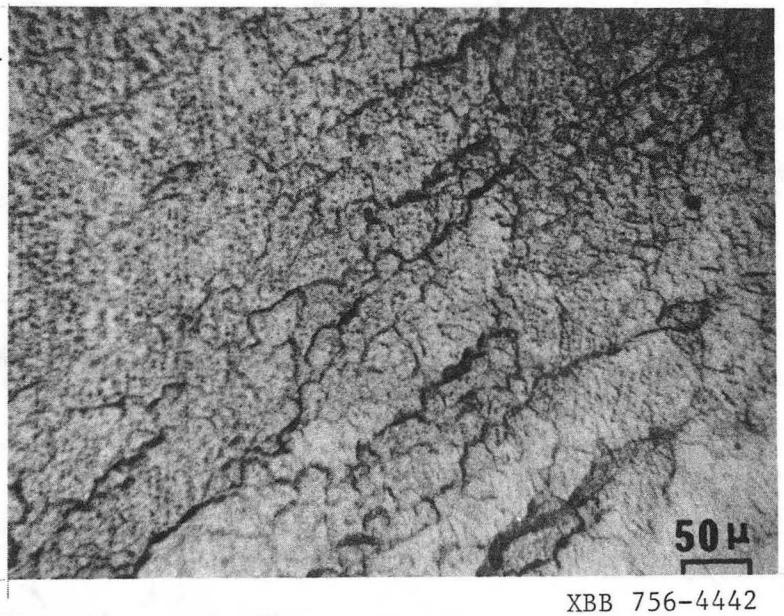

XBB 756-4442

(b)

Fig. 8.

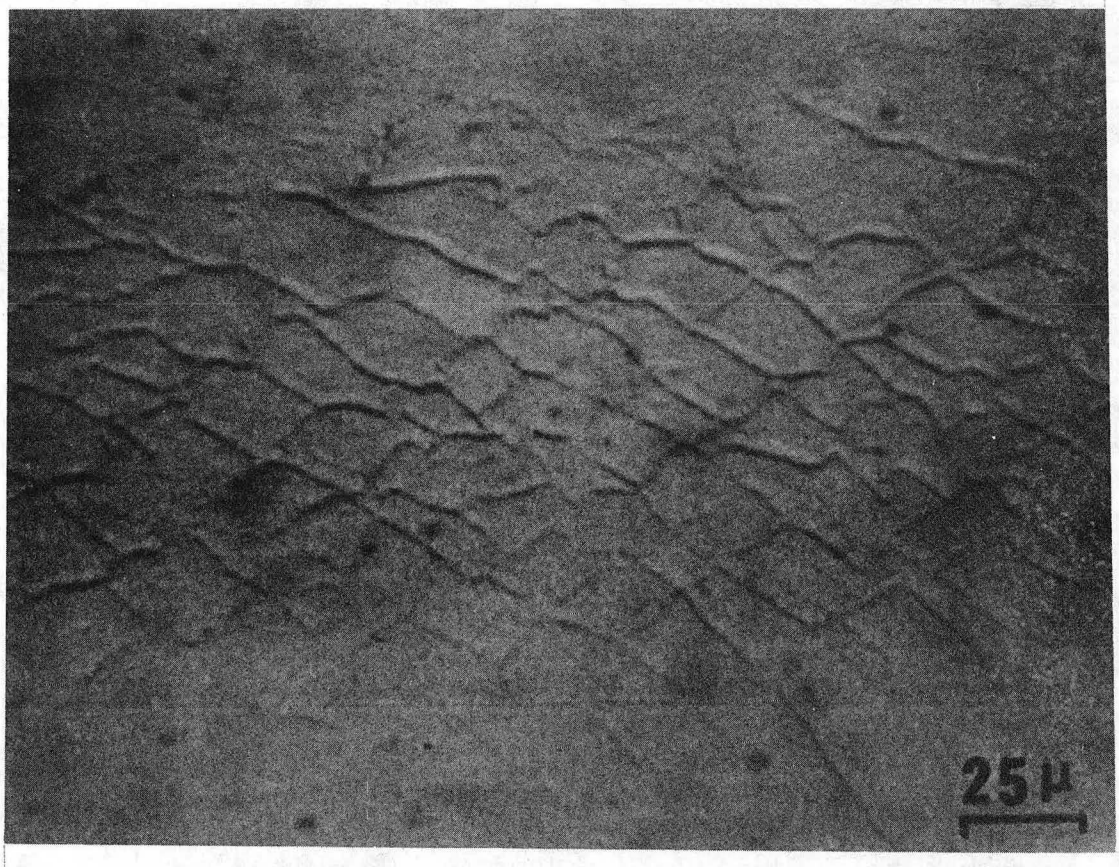

XBB 756-4430

Fig. 9.

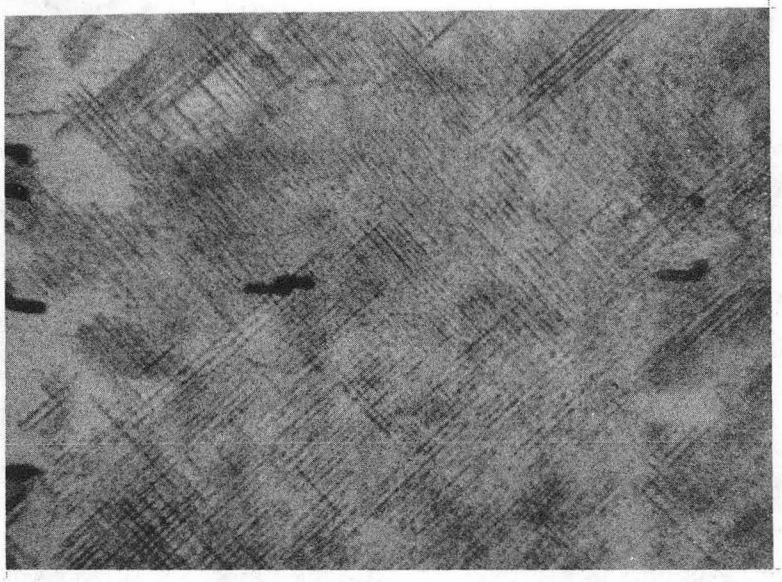

(a)

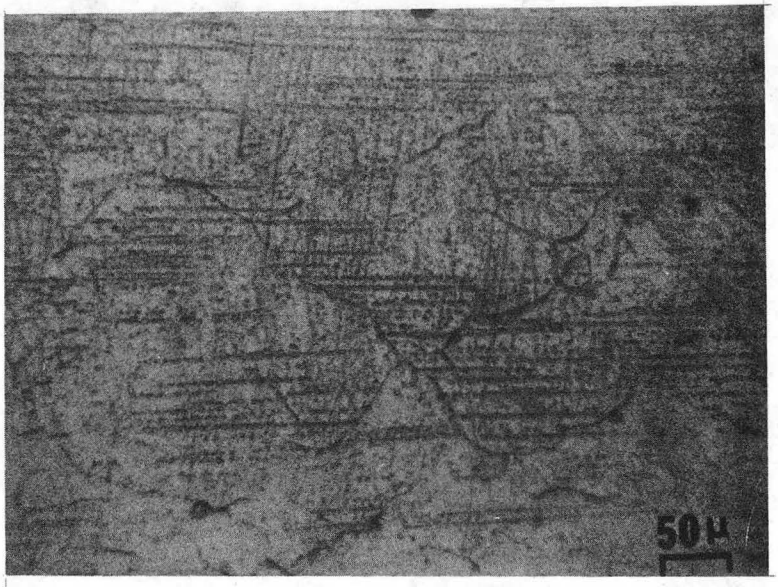

XBB 756-4444

(b)

Fig. 10.

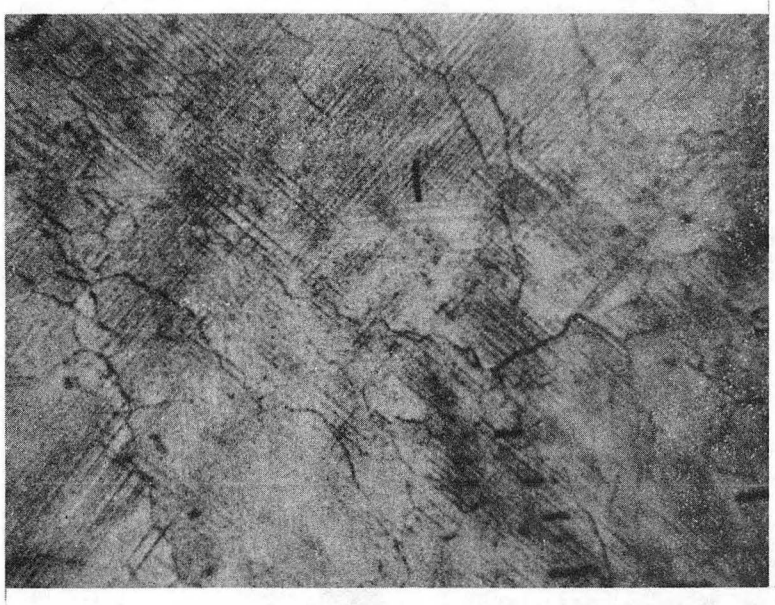

(a)

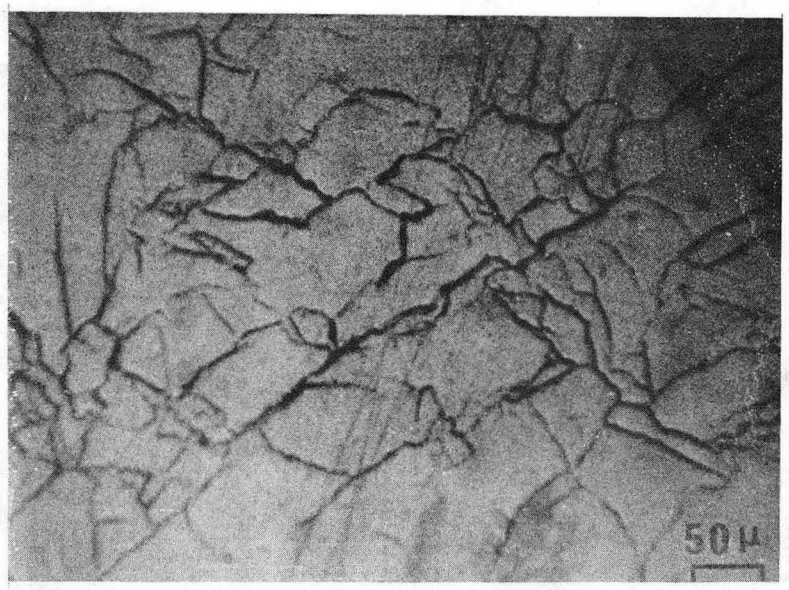

XBB 756-4443

(b)

Fig. 11.

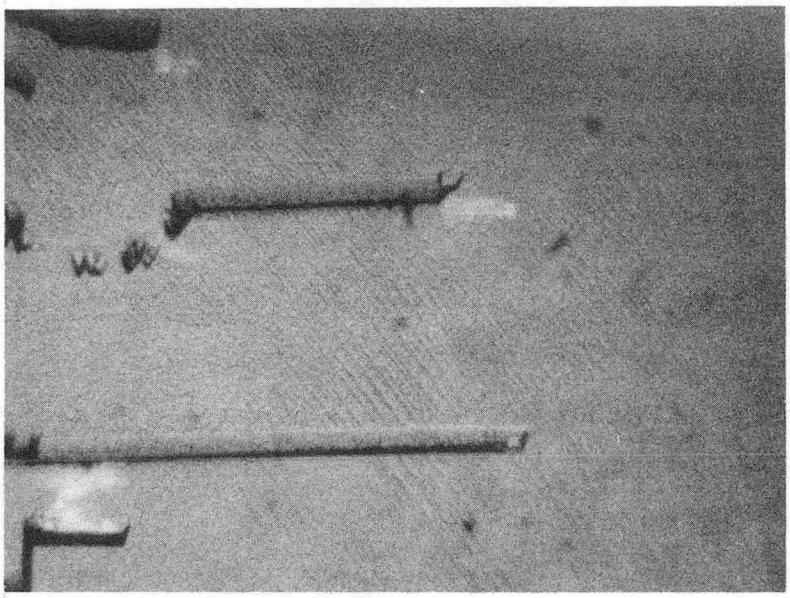

(a)

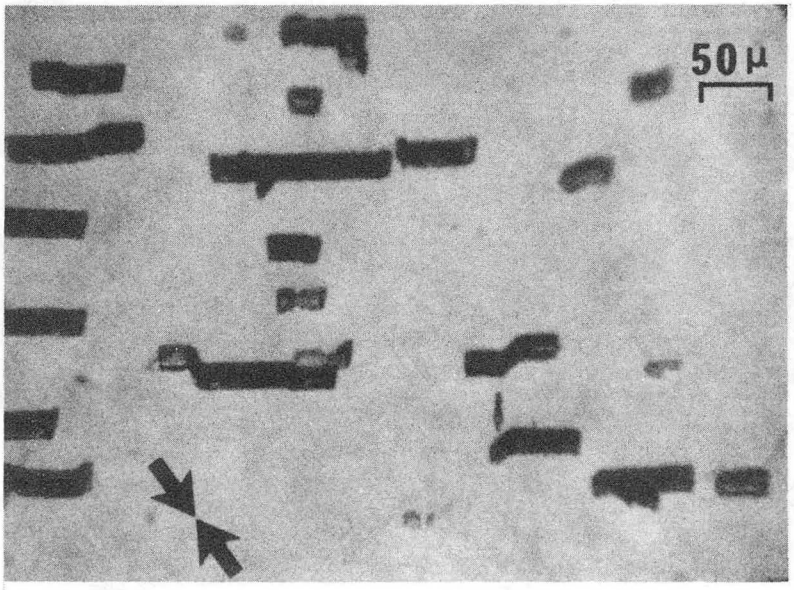

XBB 756-4441

(b)

Fig. 12.

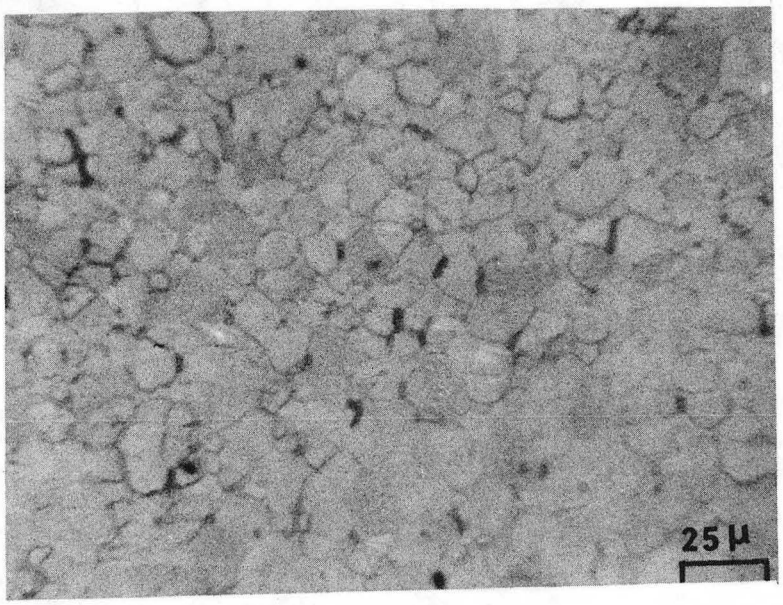

(a)

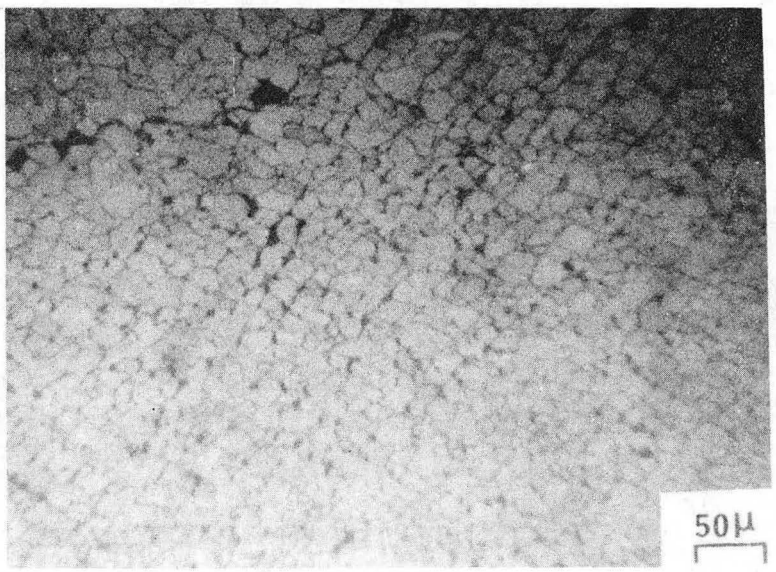

XBB 756-4438

(b)

Fig. 13.

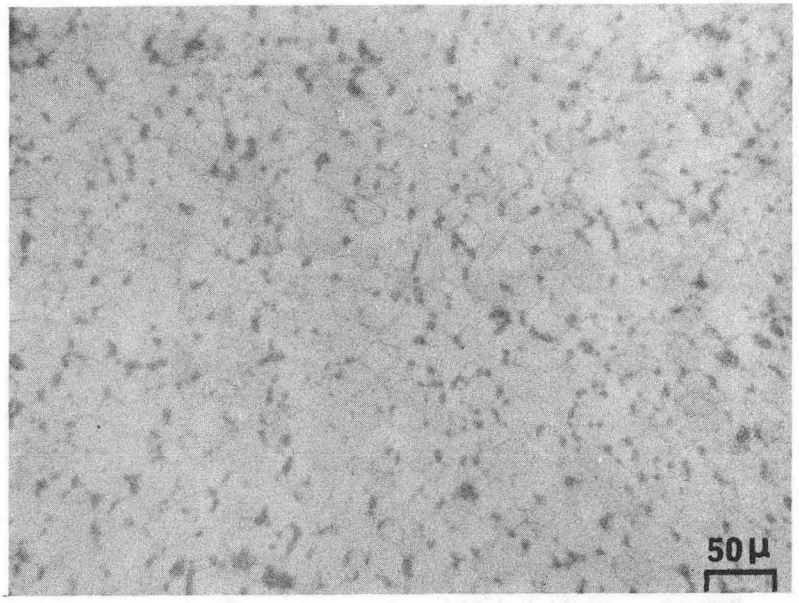

(c)

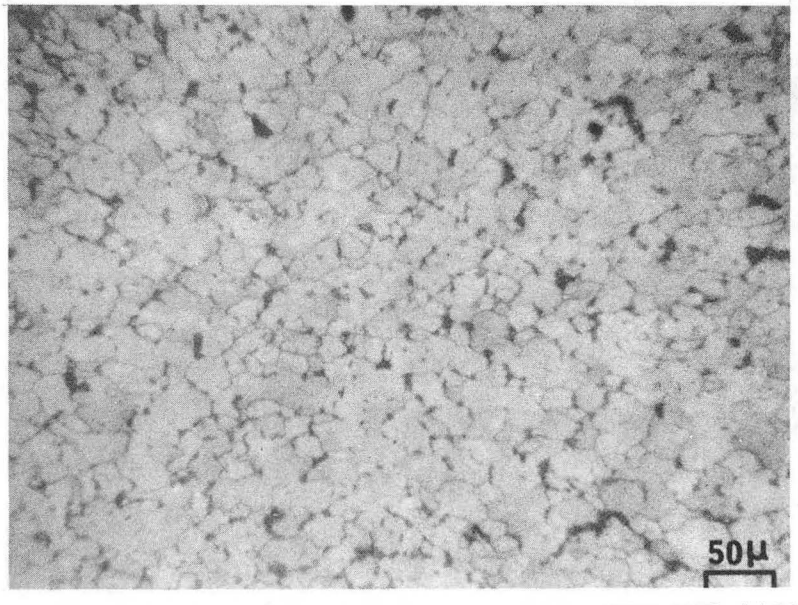

XBB 756-4439

(d)

Fig. 13.

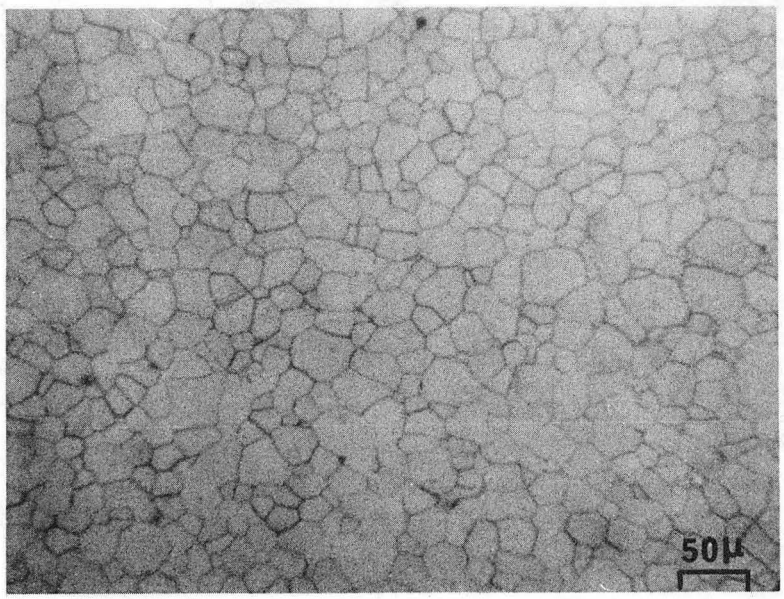

(e)

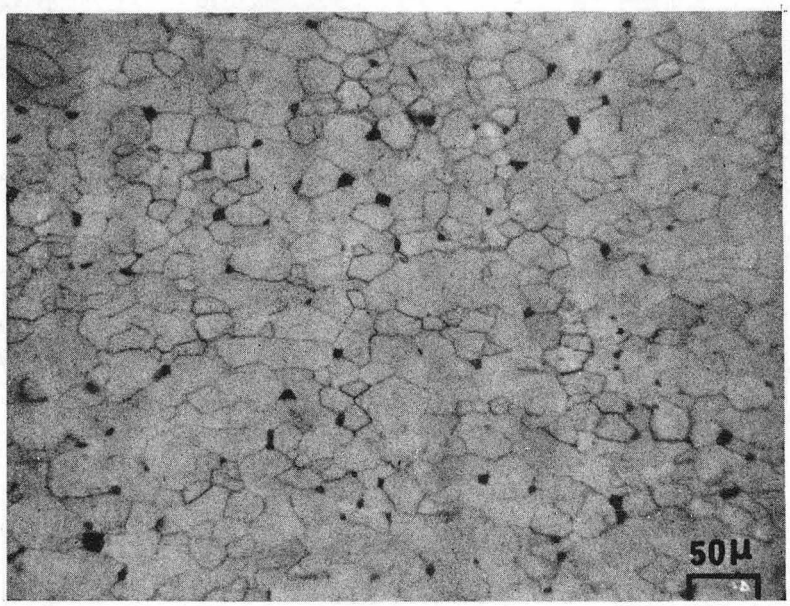

XBB 756-4440

(f)

Fig. 13.

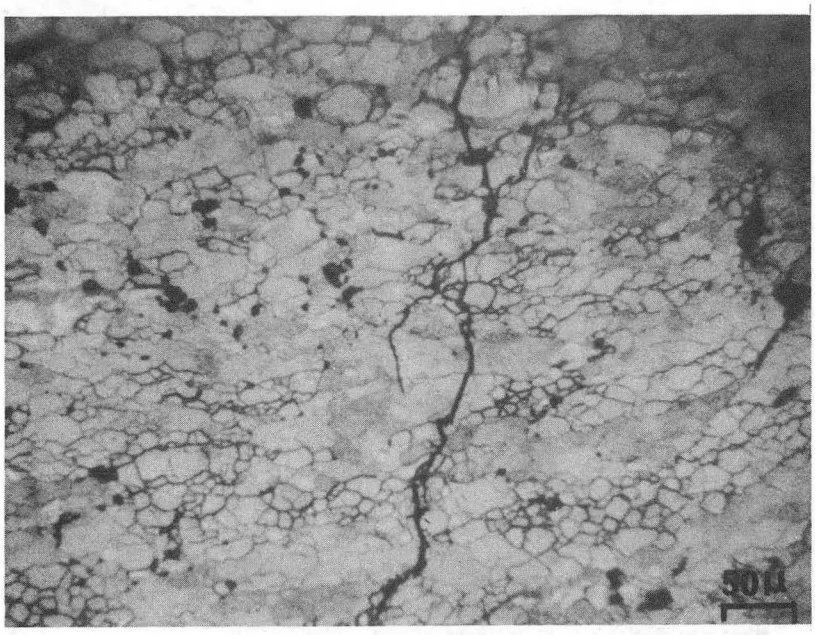

(a)

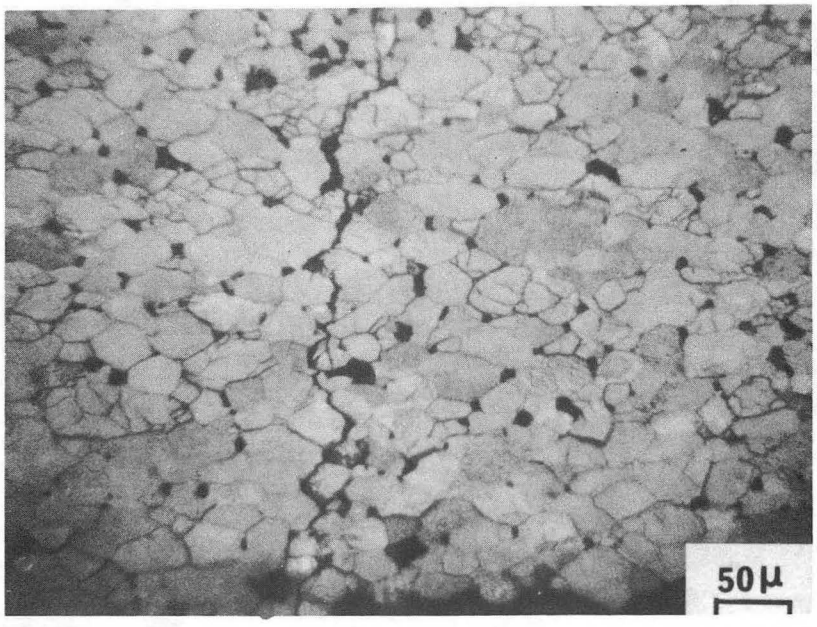

XBB 756-4428A

(b)

Fig. 14.

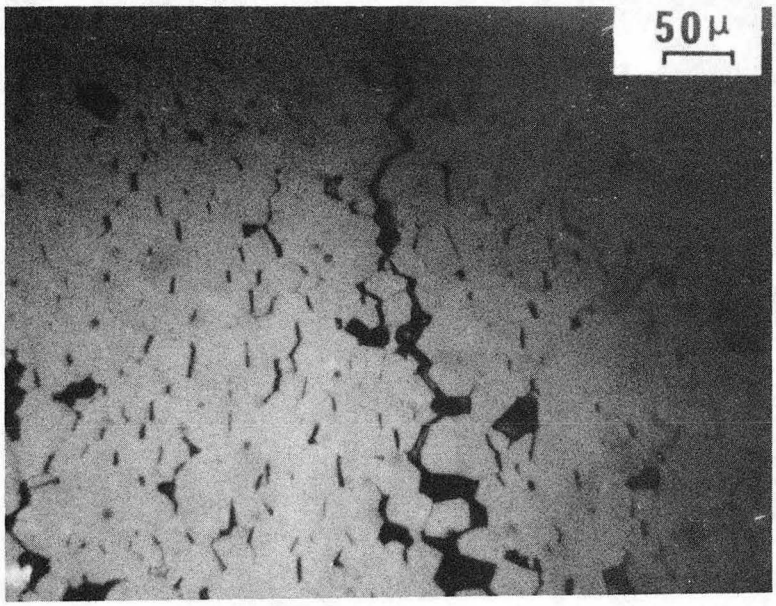

(a)

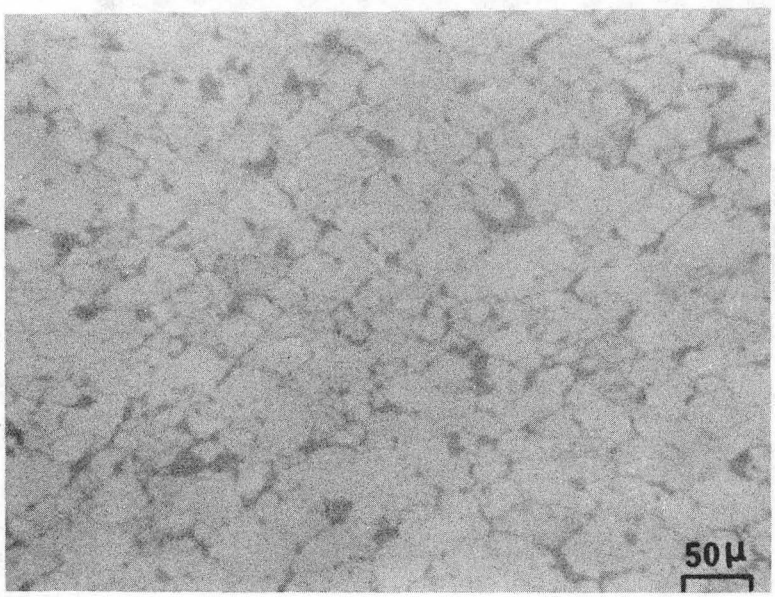

XBB 756-4434

(b)

Fig. 15.

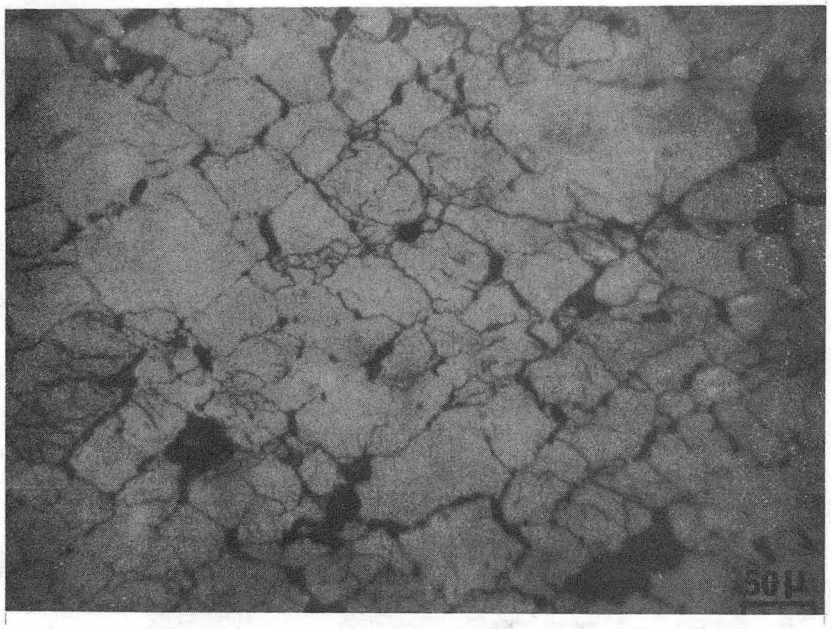

(c)

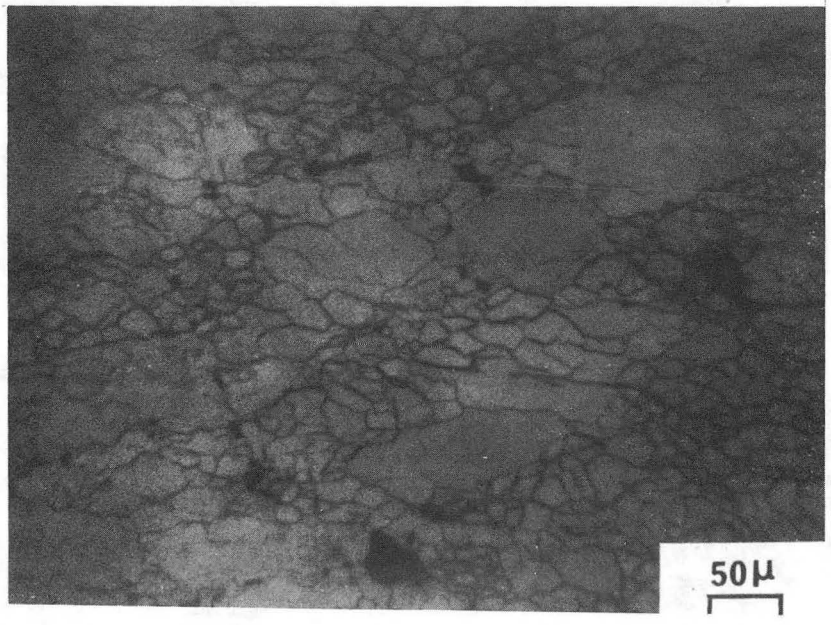

XBB 756-4982

(d)

Fig. 15.

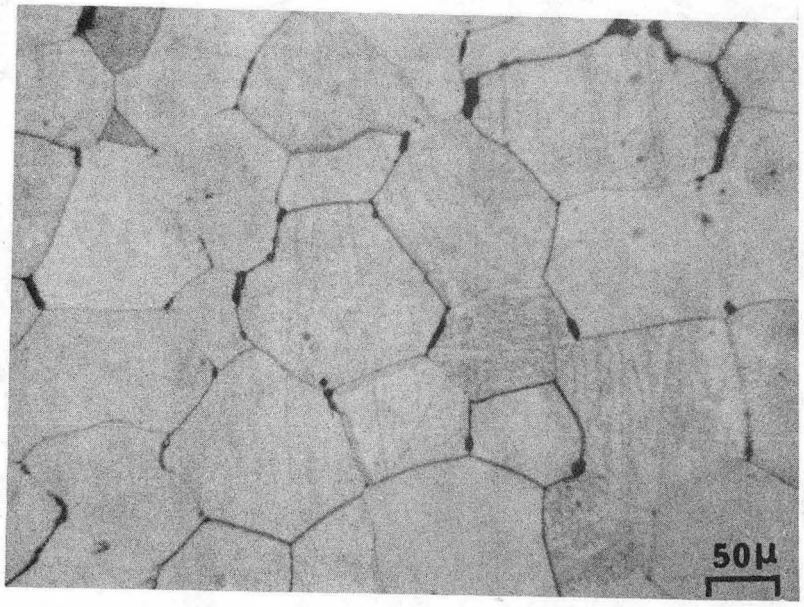

(a)

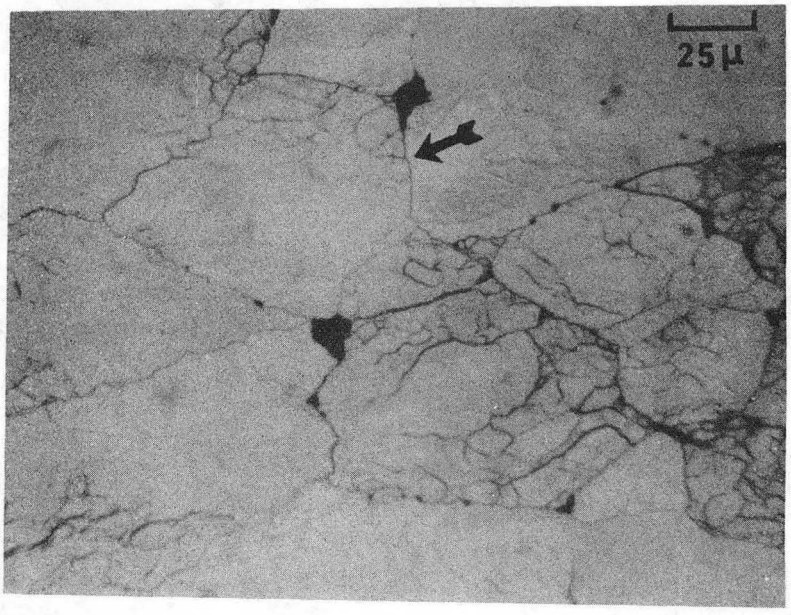

XBB 756-4432

(b)

Fig. 16.

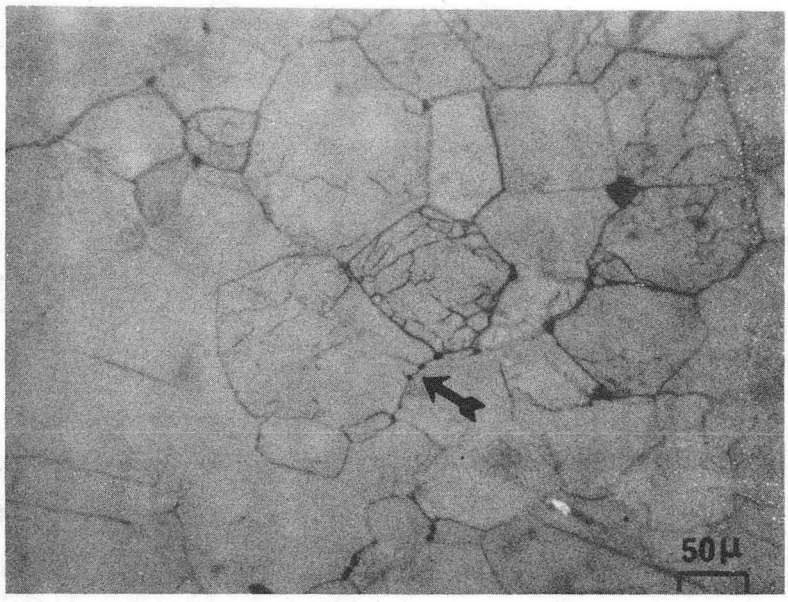

(c)

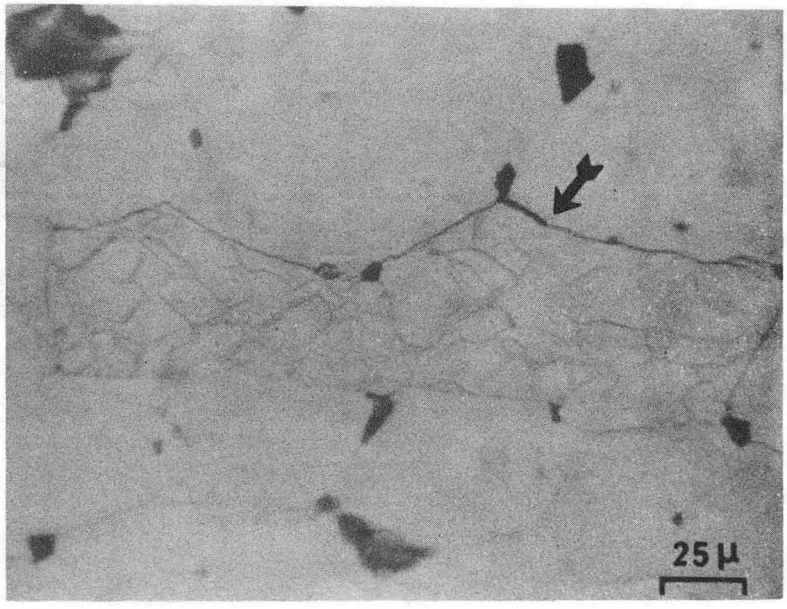

XBB 756-4433

(d)

Fig. 16.

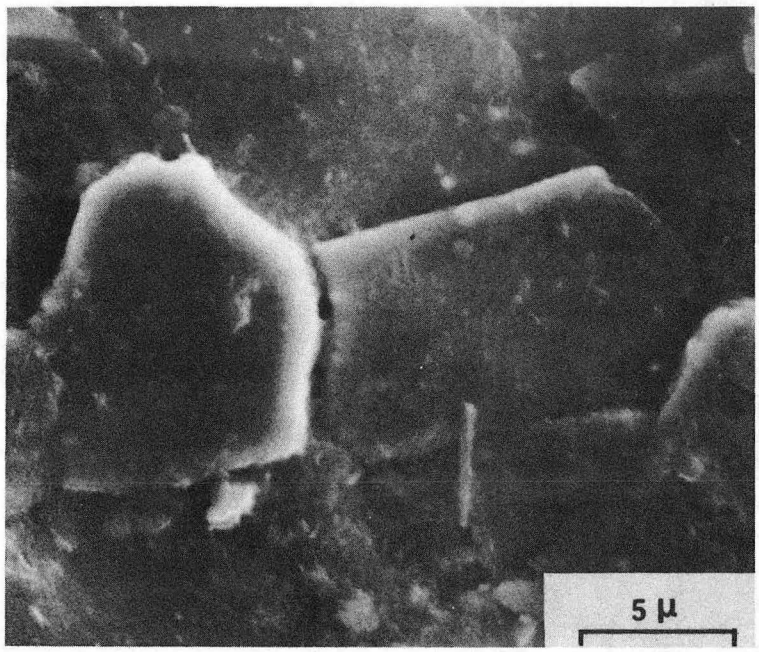

(a)

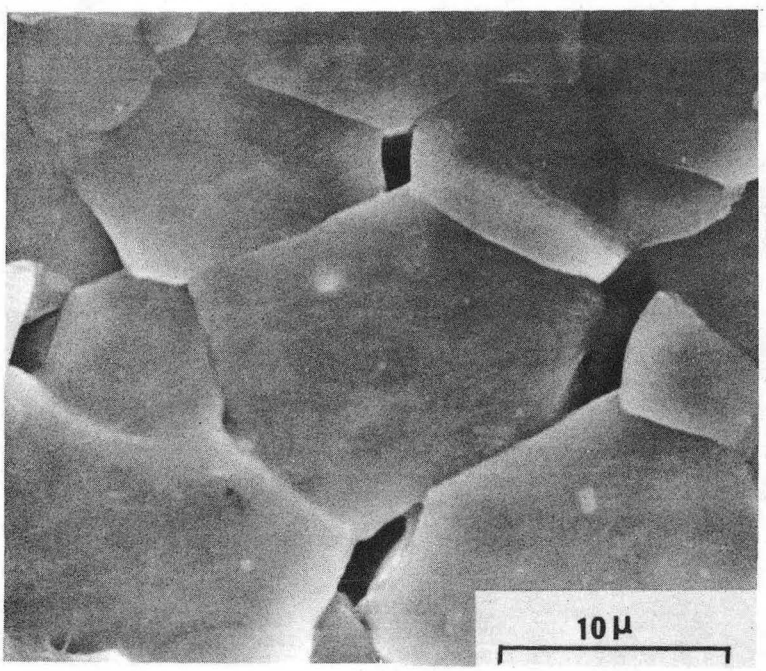

XBB 756-4981

(b)

Fig. 17.

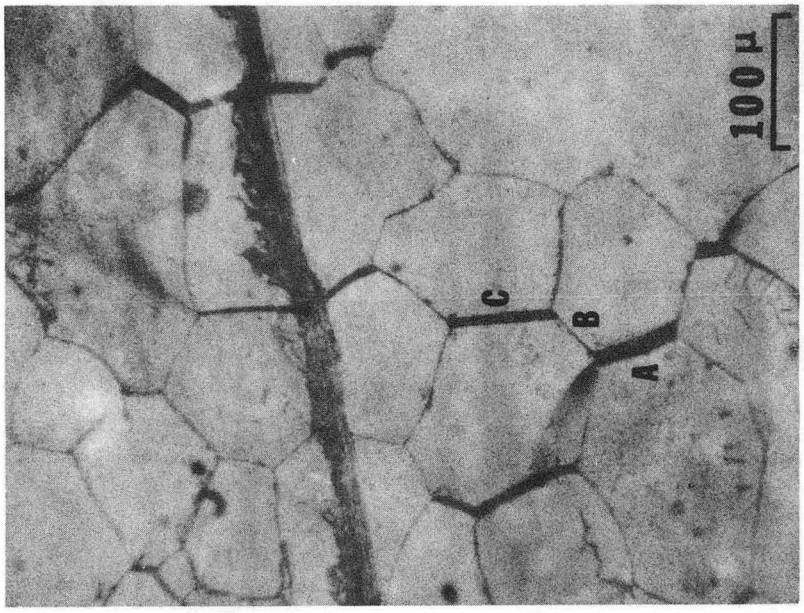

XBB 756-4436

(b)

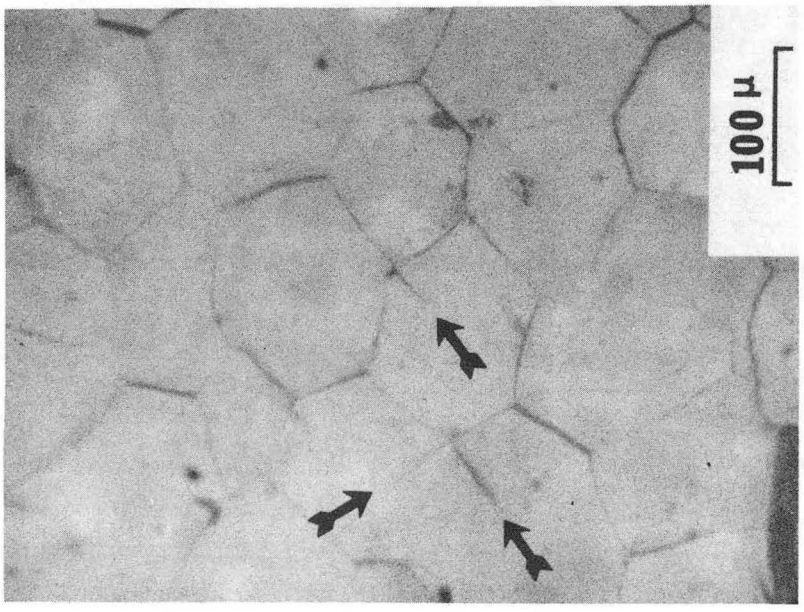

(a)

Fig. 18.

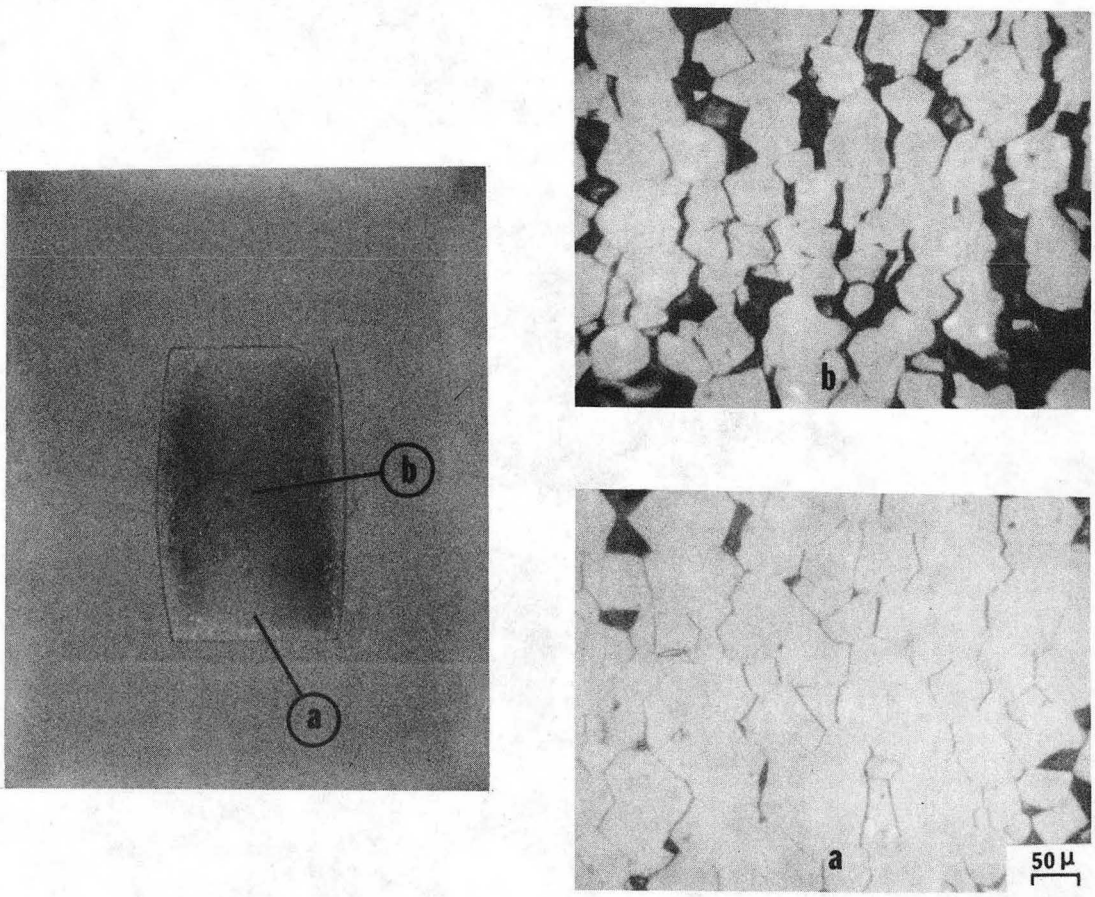

XBB 756-4984

Fig. 19.

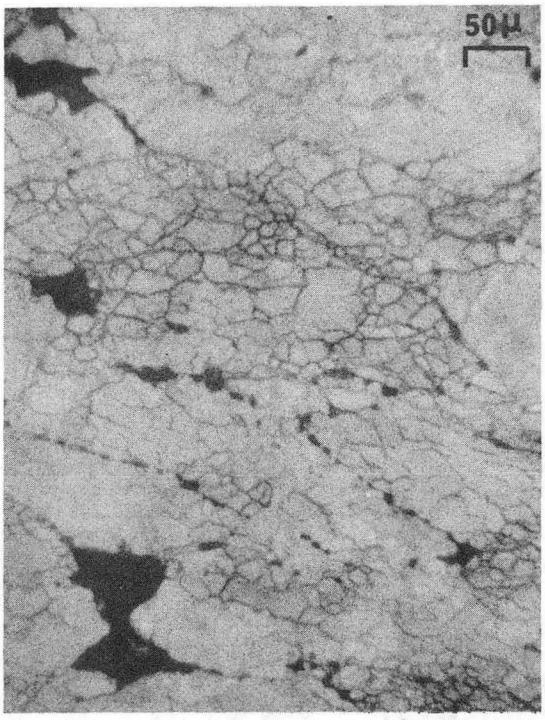

(a)

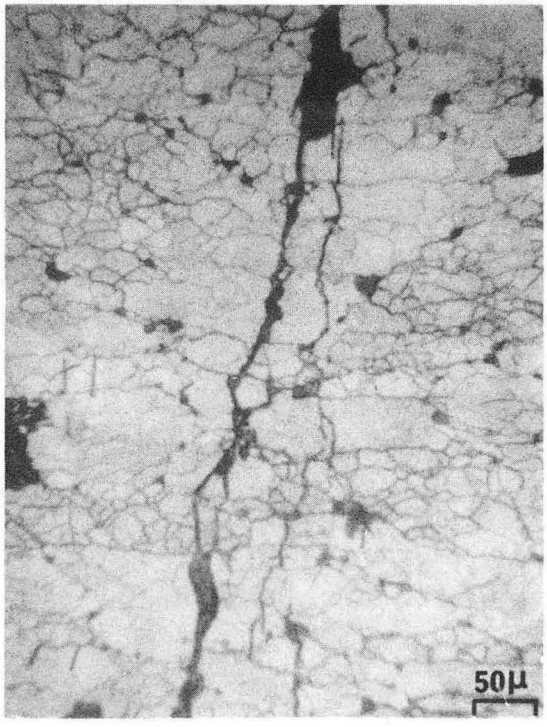

XBB 756-4983

(b)

Fig. 20.

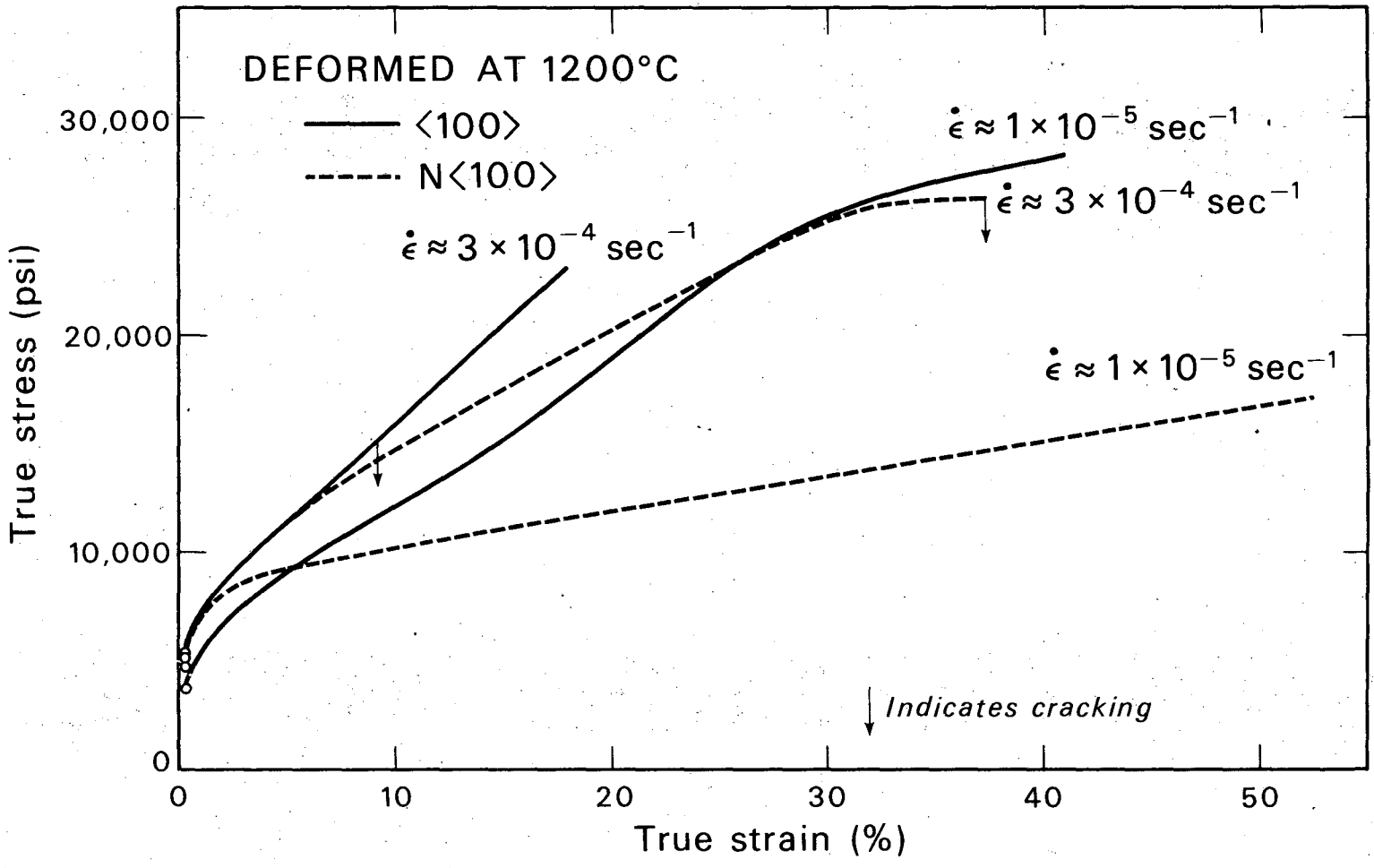

XBL 753-4746

Fig. 21(a)

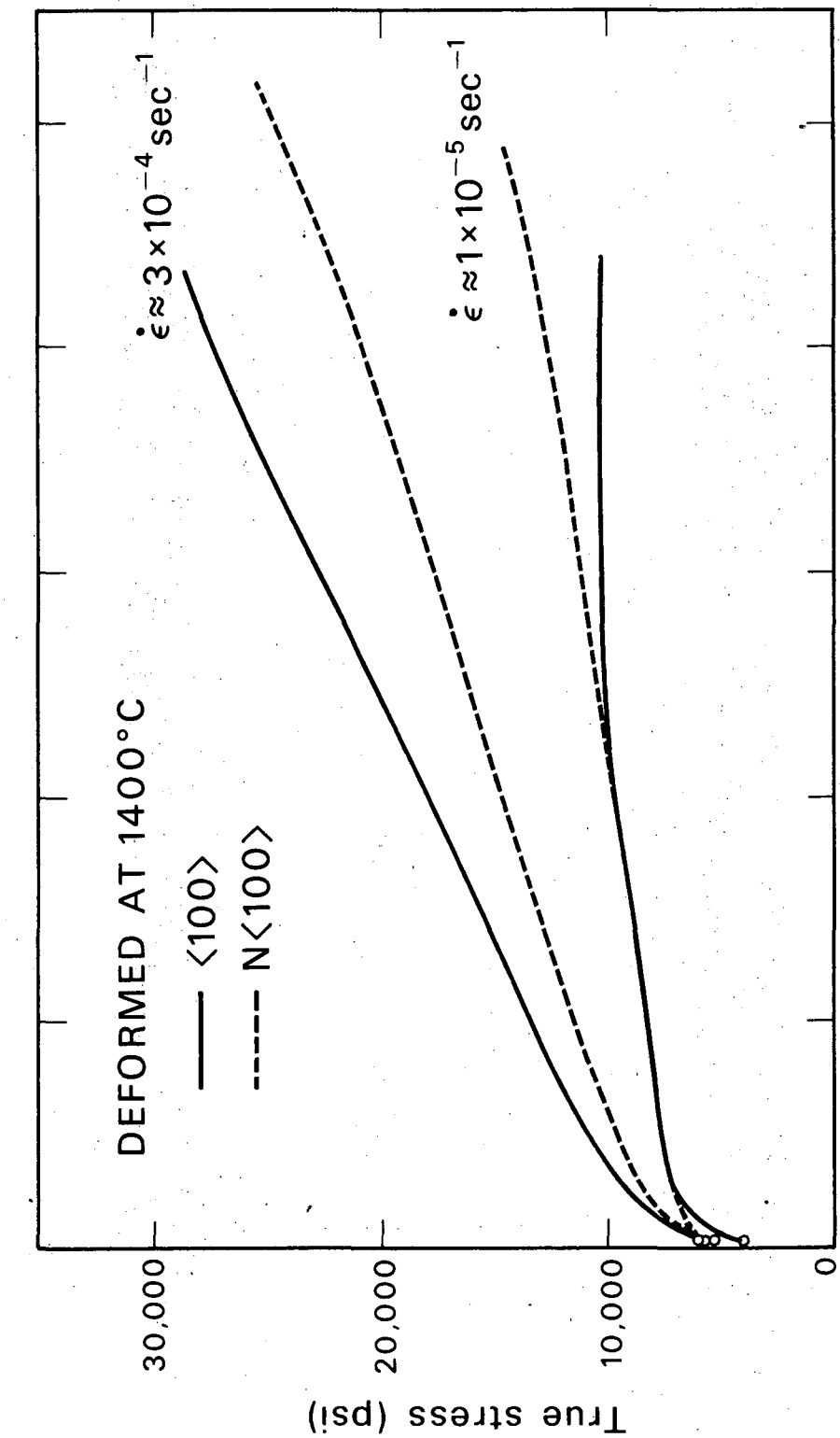

XBL 753-4745

Fig. 21(b)

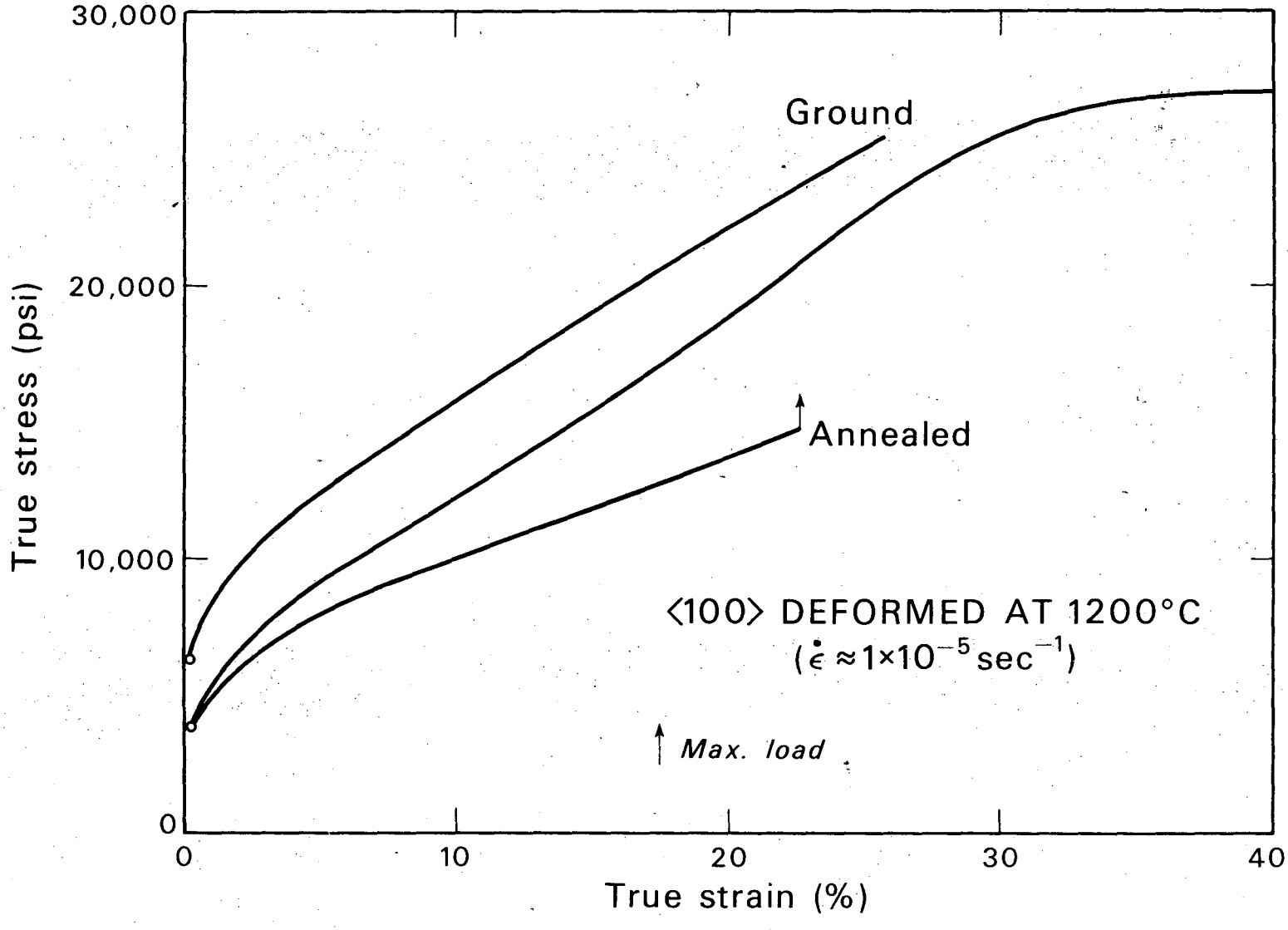

XBL 753-4743

Fig. 22(a)

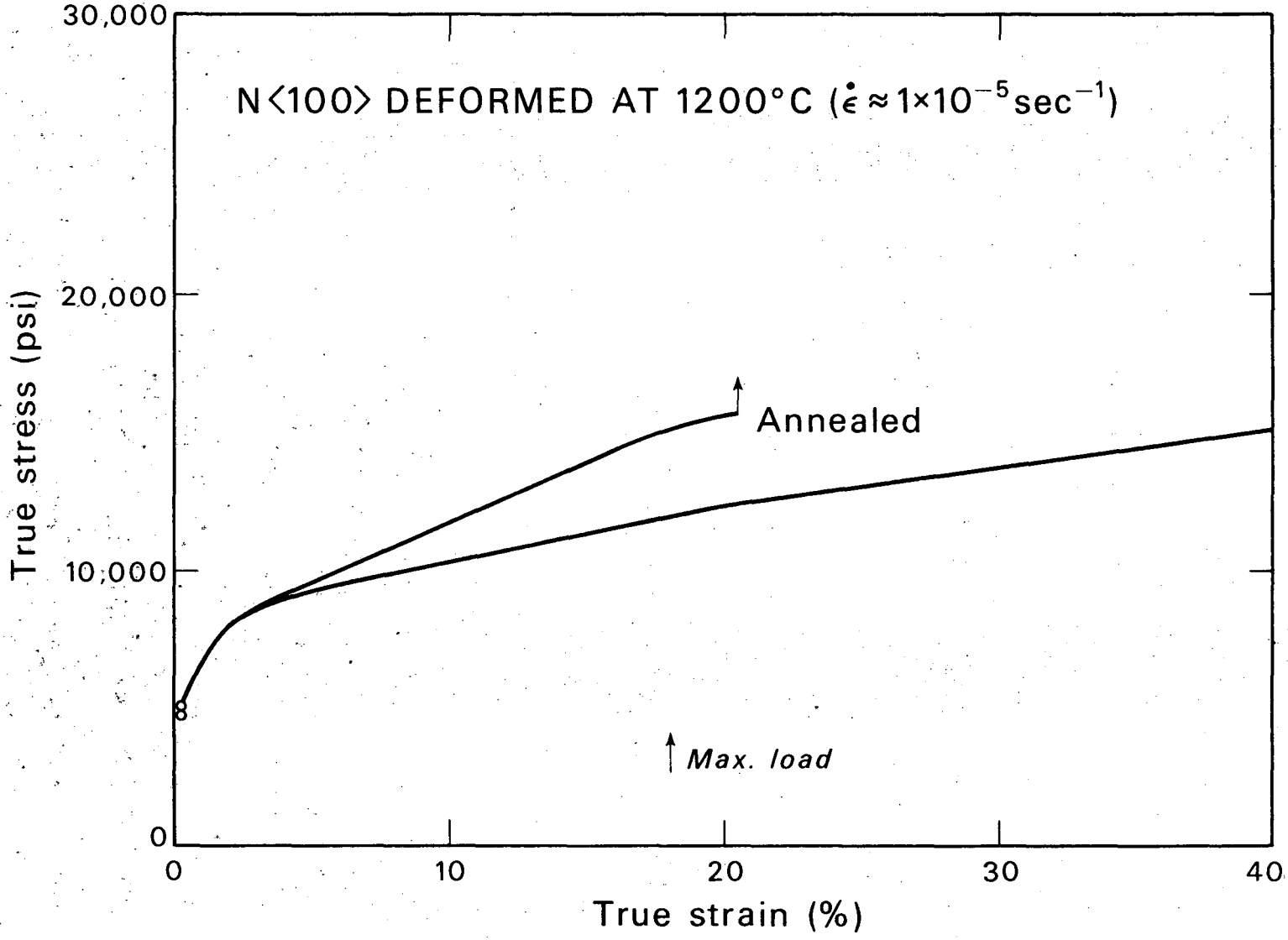

XBL 753-4744

Fig. 22(b)

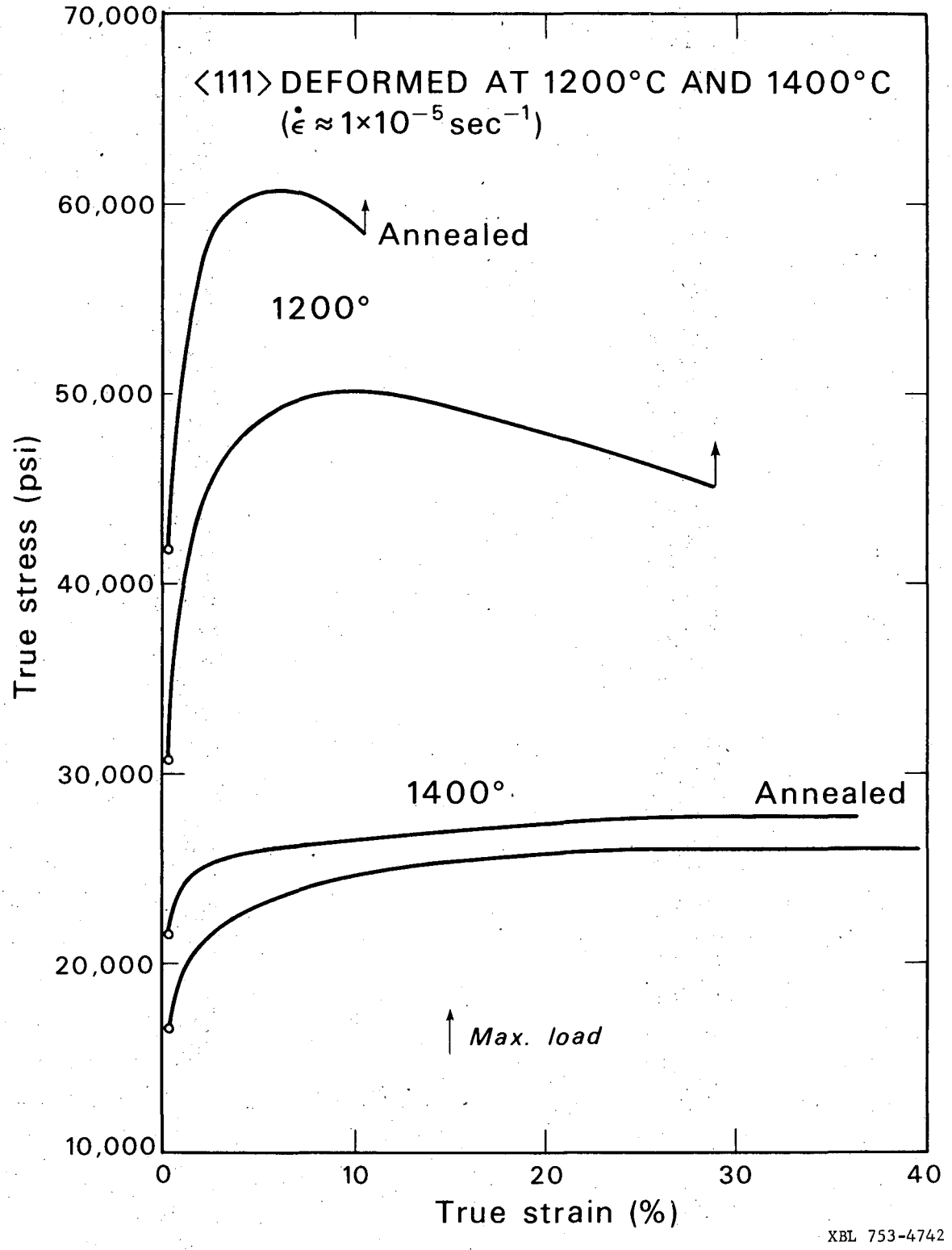

Fig. 22(c)

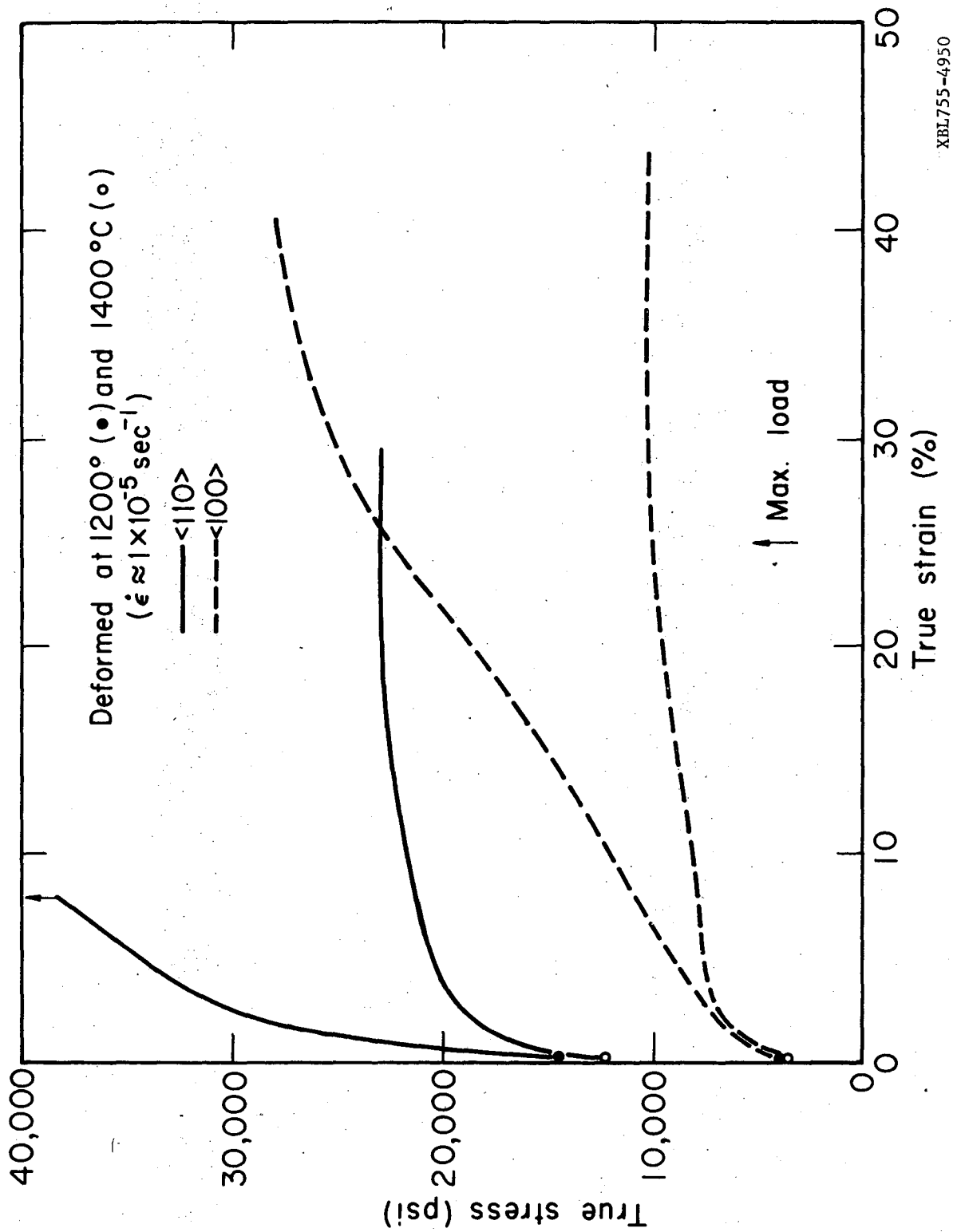
Deformed at 1200° (•) and 1400°C (○)
($\dot{\epsilon} \approx 1 \times 10^{-5}$ sec^{-1})
<110>
<100>
Max. load
True stress (psi)
40,000
30,000
20,000
10,000
0
0
10
20
30
40
50
True strain (%)
XBL755-4950

Fig. 23.

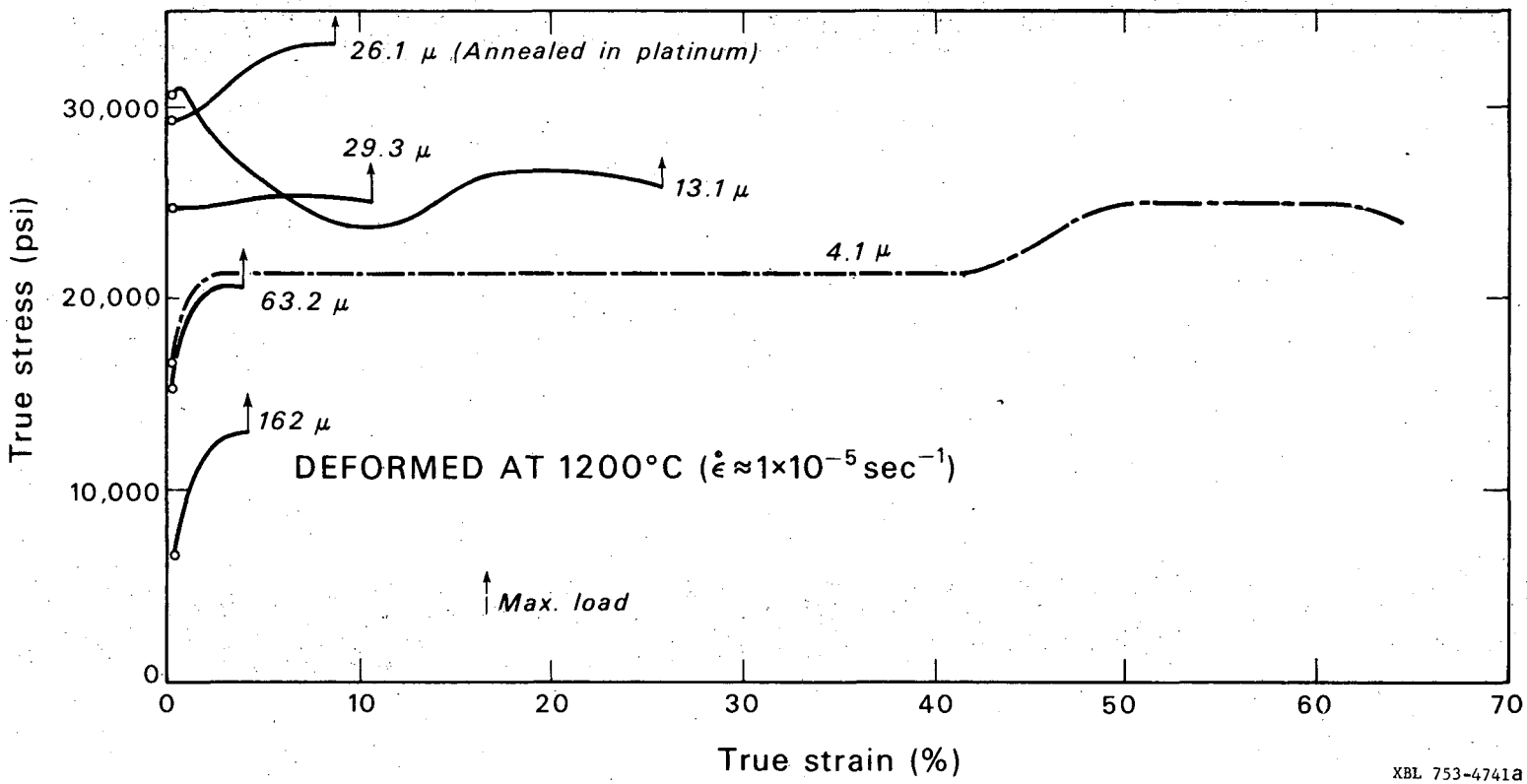
26.1 μ (Annealed in platinum)
29.3 μ
13.1 μ
4.1 μ
63.2 μ
162 μ
DEFORMED AT 1200°C ($\dot{\epsilon} \approx 1 \times 10^{-5}$ sec^{-1})
Max. load
True stress (psi)
30,000
20,000
10,000
0
0
10
20
30
40
50
60
70
True strain (%)
XBL 753-4741a

Fig. 24(a)

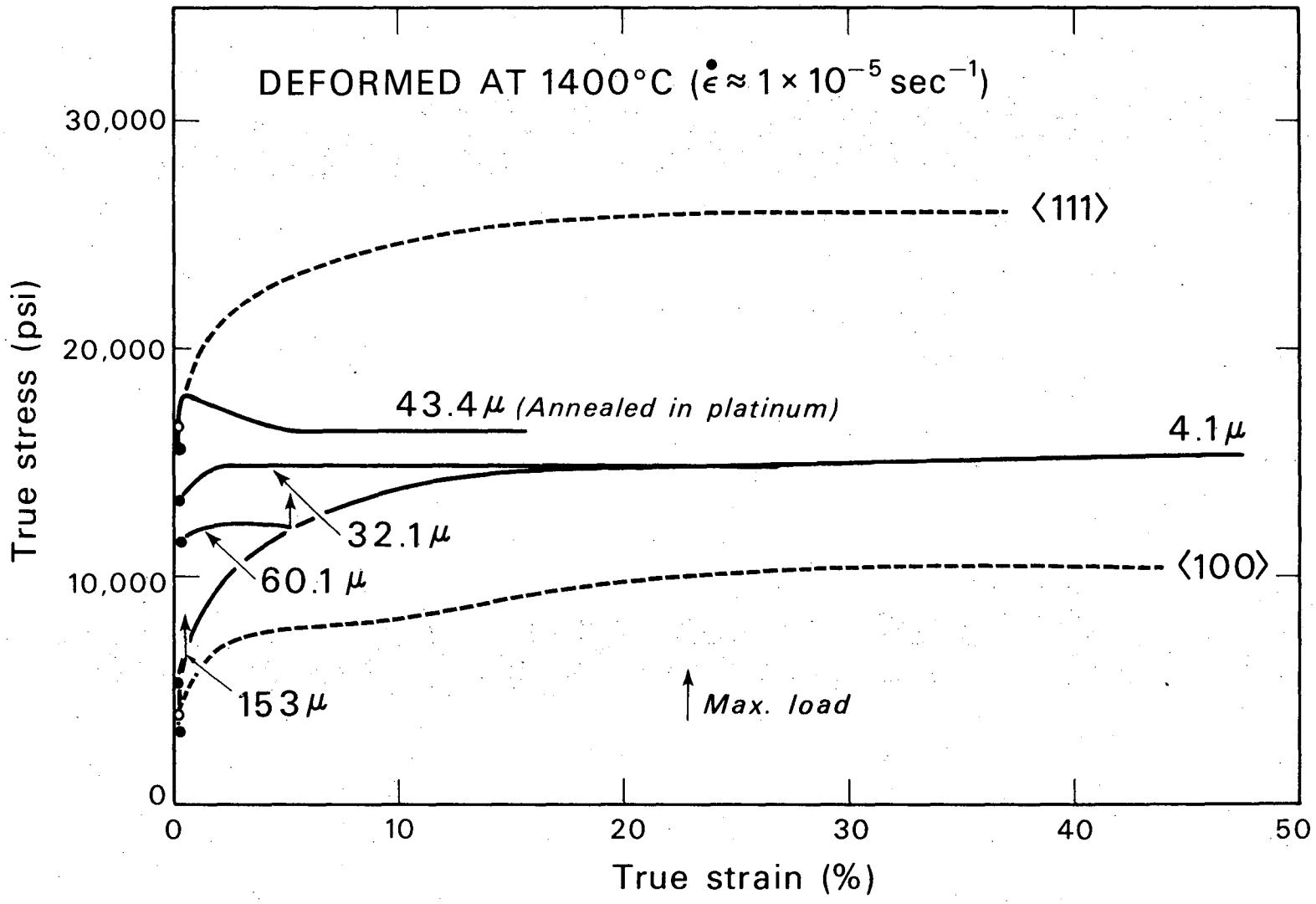

XBL 753-4739

Fig. 24(b)

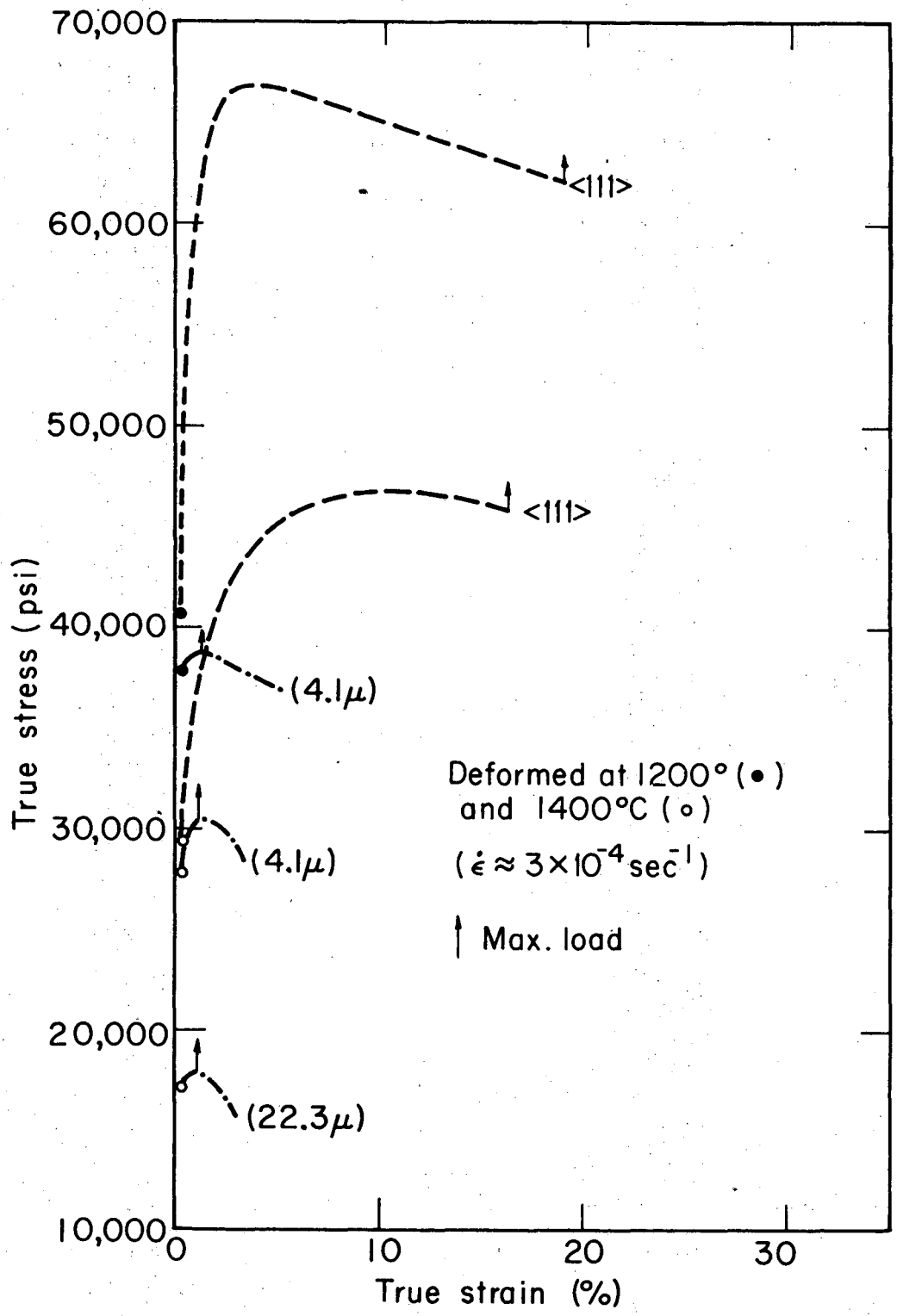
70,000
60,000
50,000
40,000
30,000
20,000
10,000
True stress (psi)
0
10
20
30
True strain (%)
<111>
<111>
(4.1μ)
(4.1μ)
(22.3μ)
Deformed at 1200° (•)
and 1400°C (○)
(ε̇ ≈ 3×10⁻⁴ sec⁻¹)
Max. load
XBL755-4952

Fig. 25.

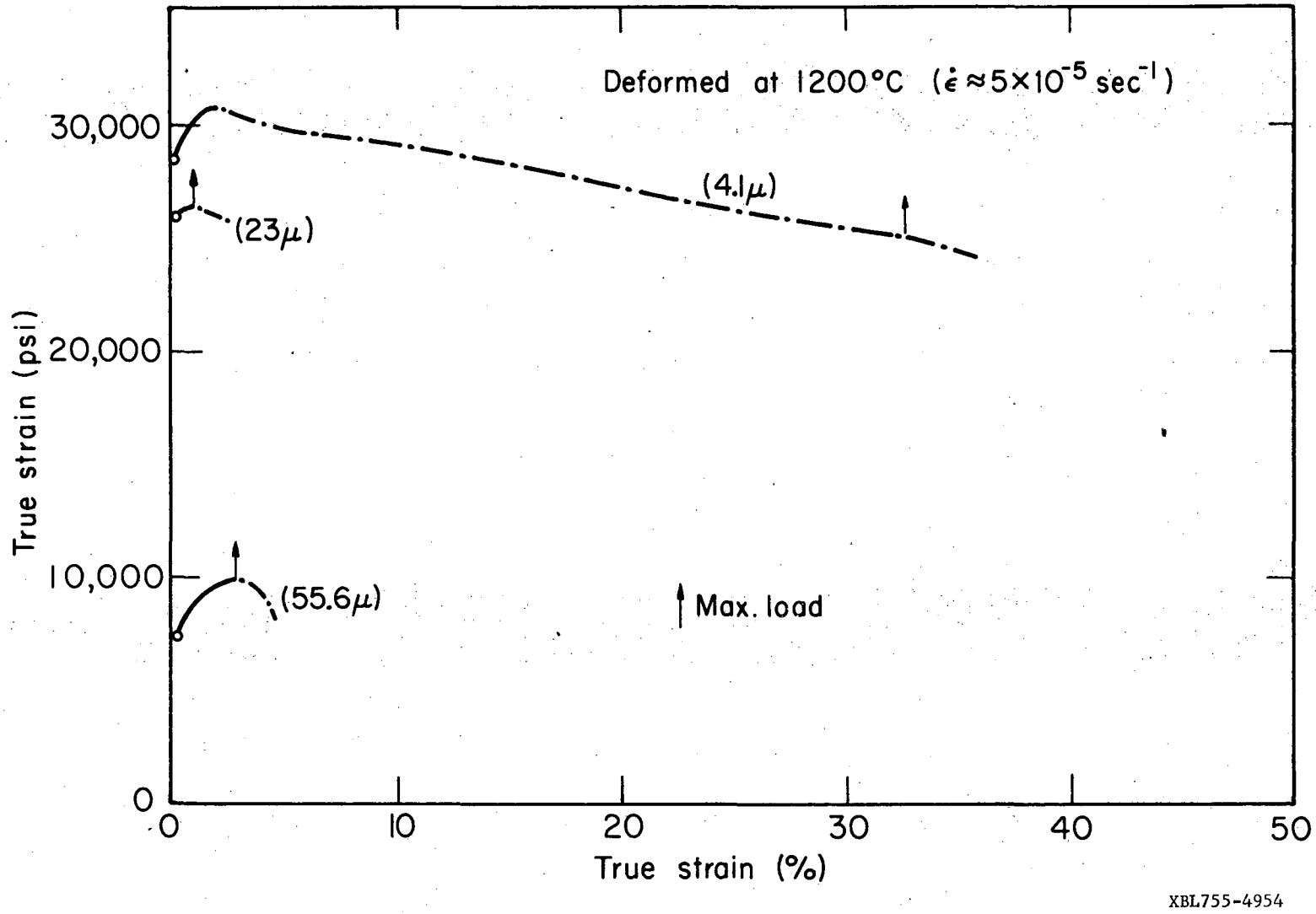
Deformed at 1200°C ($\dot{\epsilon} \approx 5 \times 10^{-5}$ sec^{-1})
30,000
20,000
10,000
0
True strain (psi)
(4.1μ)
(23μ)
(55.6μ)
Max. load
0
10
20
30
40
50
True strain (%)
XBL755-4954

Fig. 26.

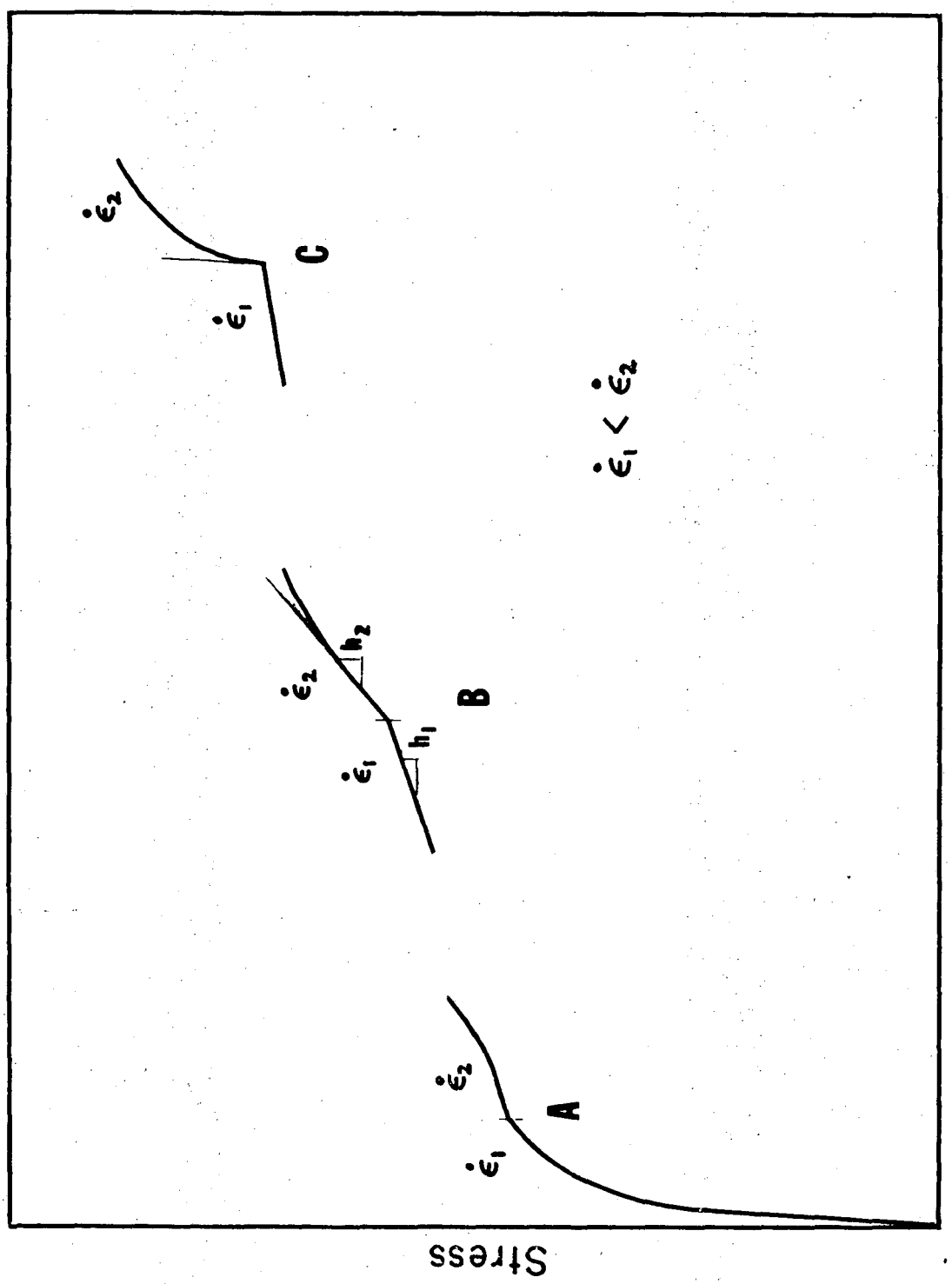

XBL 757-1791

Fig. 27.

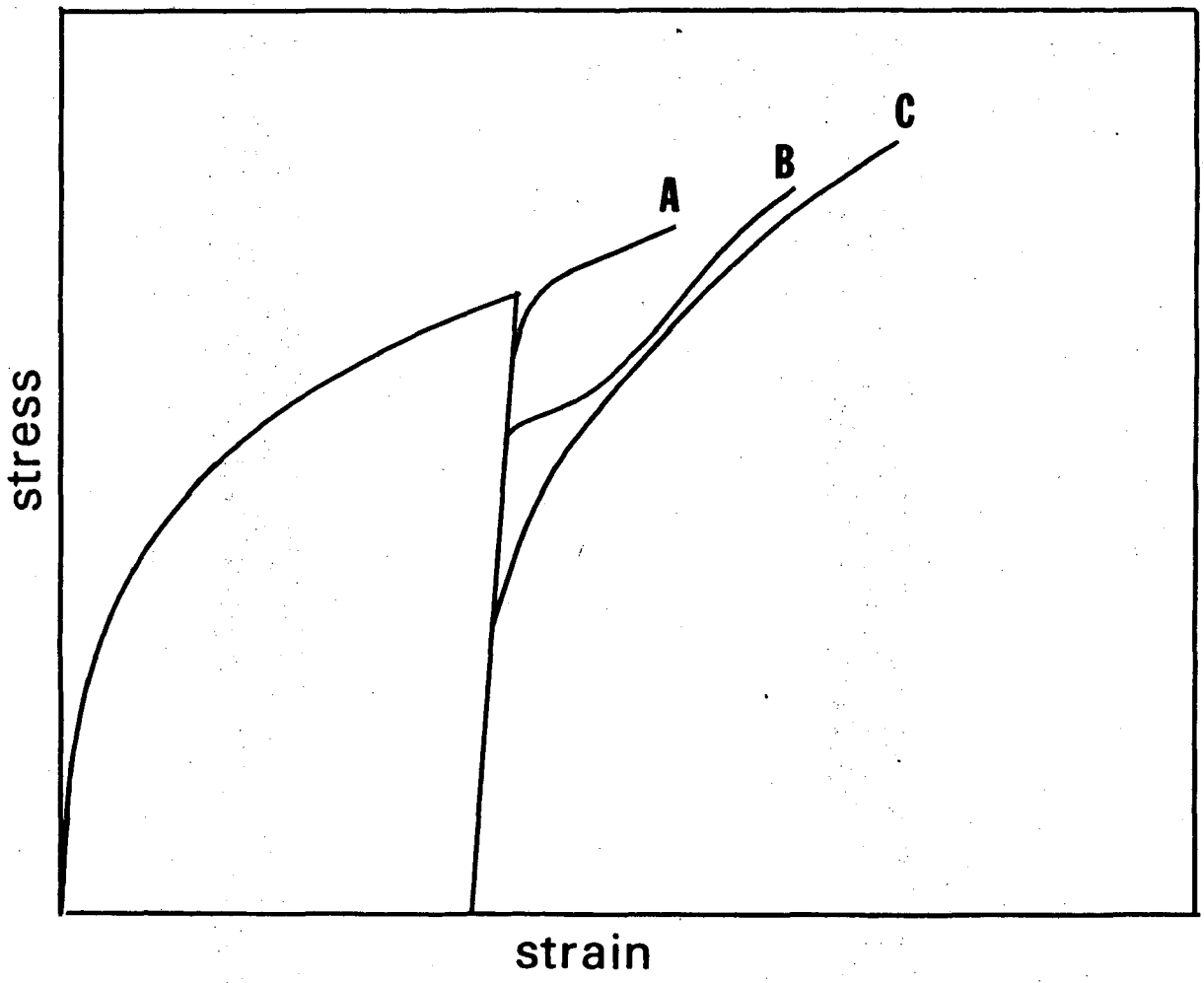

XBL 757-1769

Fig. 28.

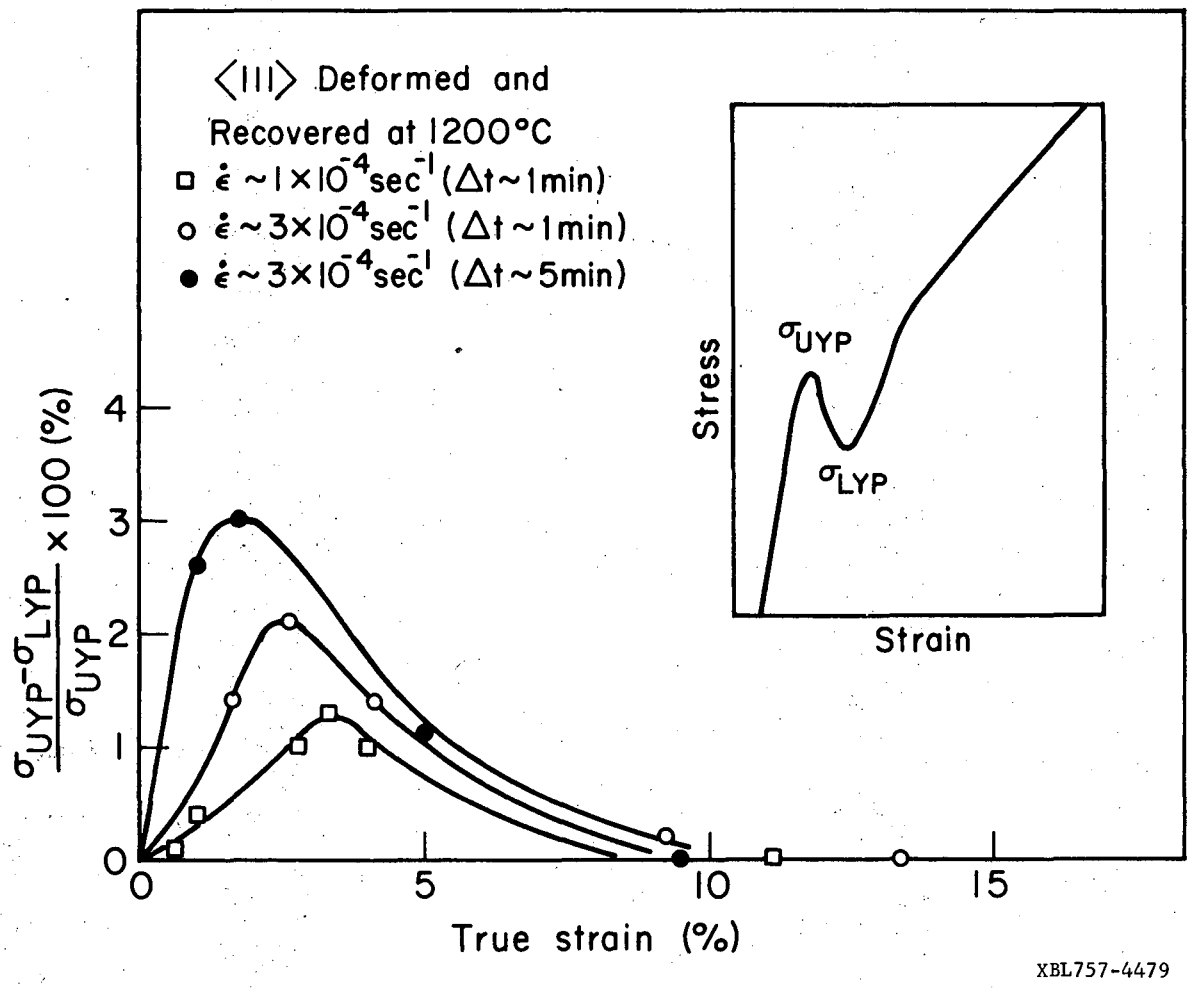
⟨111⟩ Deformed and
Recovered at 1200°C
□ ε̇ ~ 1×10⁻⁴sec⁻¹ (Δt~1min)
○ ε̇ ~ 3×10⁻⁴sec⁻¹ (Δt~1min)
● ε̇ ~ 3×10⁻⁴sec⁻¹ (Δt~5min)
σUYP
σLYP
Stress
Strain
(σUYP−σLYP)/σUYP × 100 (%)
0
1
2
3
4
0
5
10
15
True strain (%)
XBL757-4479

Fig. 29.

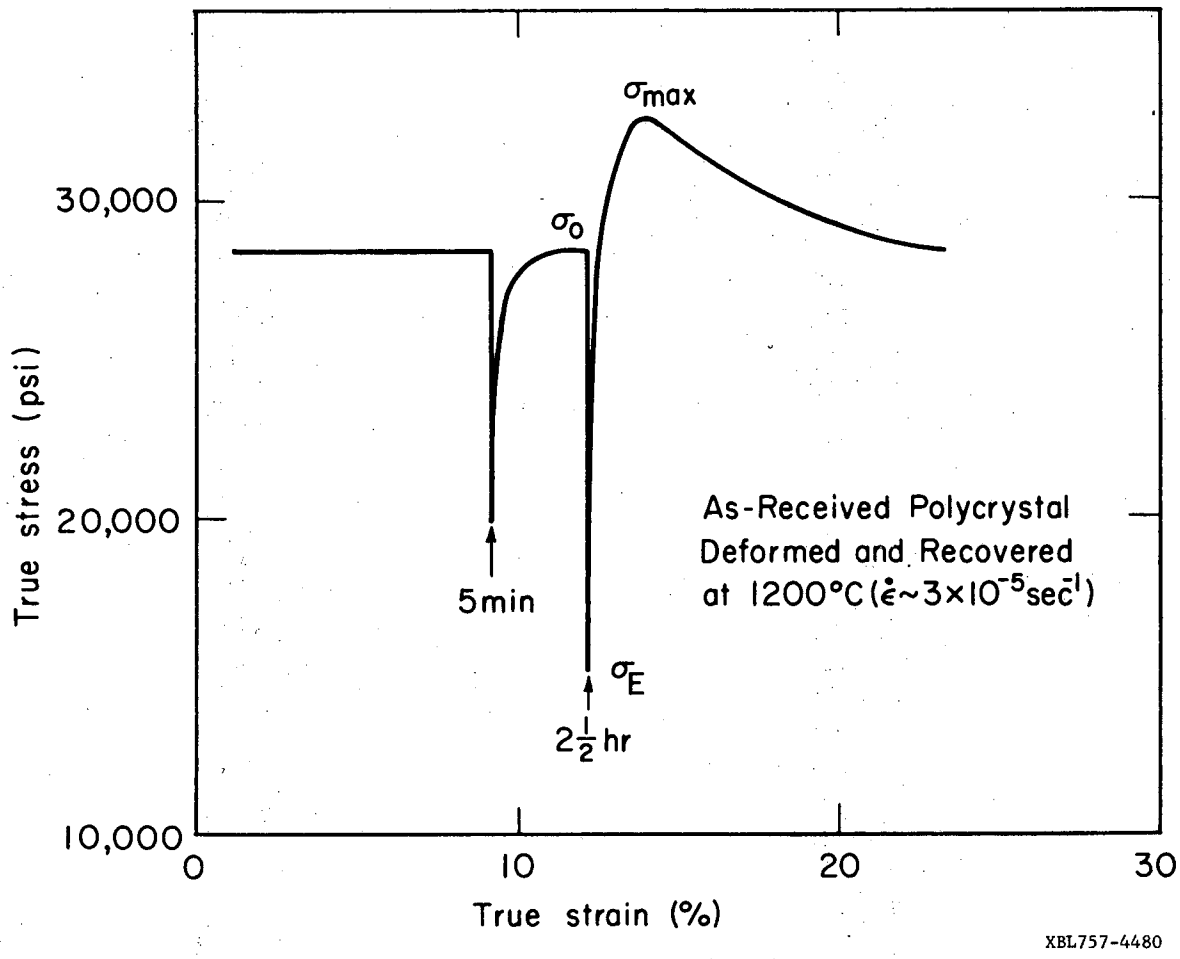
σ_{max}
σ_0
σ_E
30,000
20,000
10,000
True stress (psi)
0
10
20
30
True strain (%)
5min
$2\frac{1}{2}$ hr
As-Received Polycrystal
Deformed and Recovered
at 1200°C ($\dot{\epsilon}$~3×10^{-5}sec^{-1})
XBL757-4480

Fig. 30.

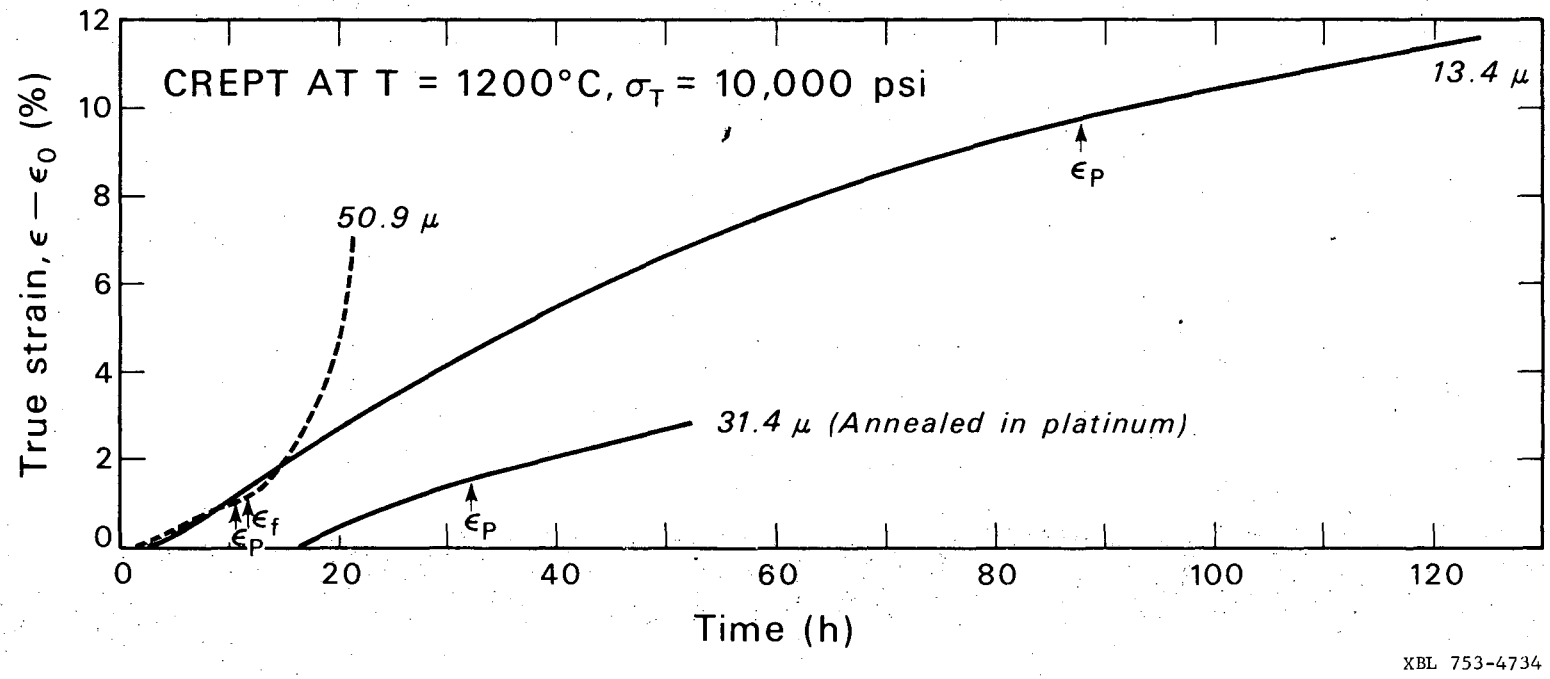

XBL 753-4734

Fig. 31.

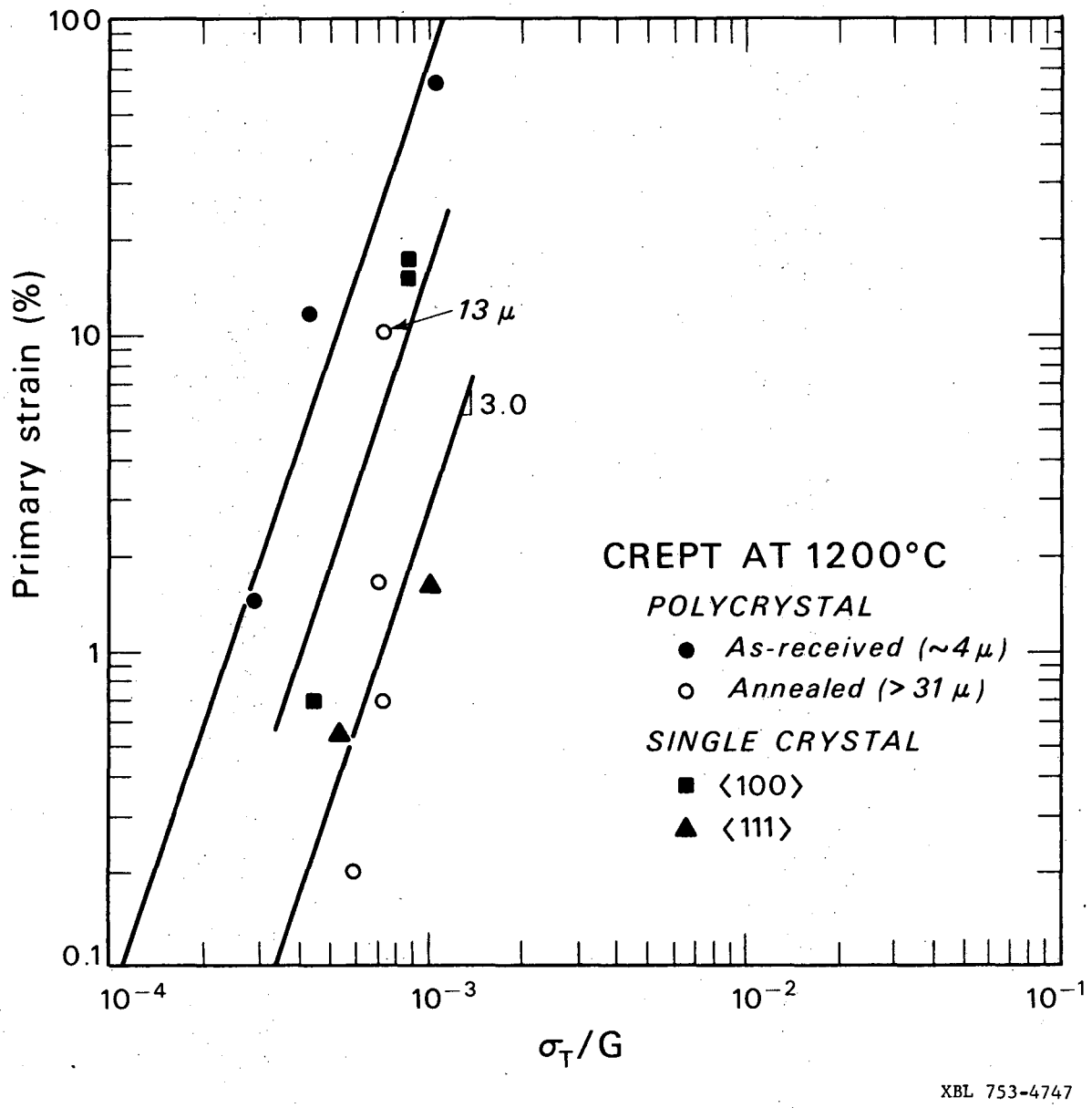
100
10
1
0.1
Primary strain (%)
13 μ
3.0
CREPT AT 1200°C
POLYCRYSTAL
As-received (~4 μ)
Annealed (> 31 μ)
SINGLE CRYSTAL
⟨100⟩
⟨111⟩
10⁻⁴
10⁻³
10⁻²
10⁻¹
σT/G
XBL 753-4747

Fig. 32(a)

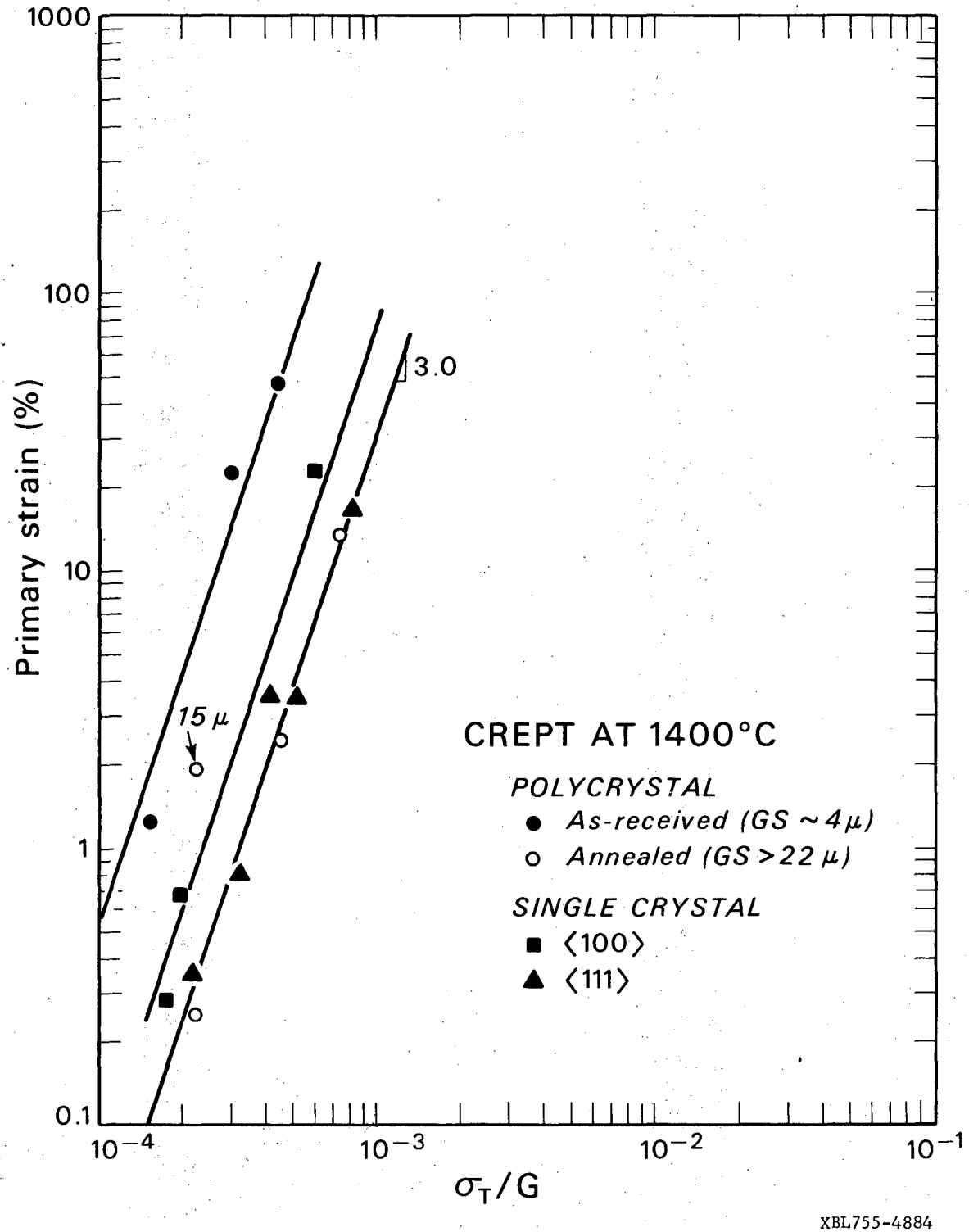

Fig. 32(b)

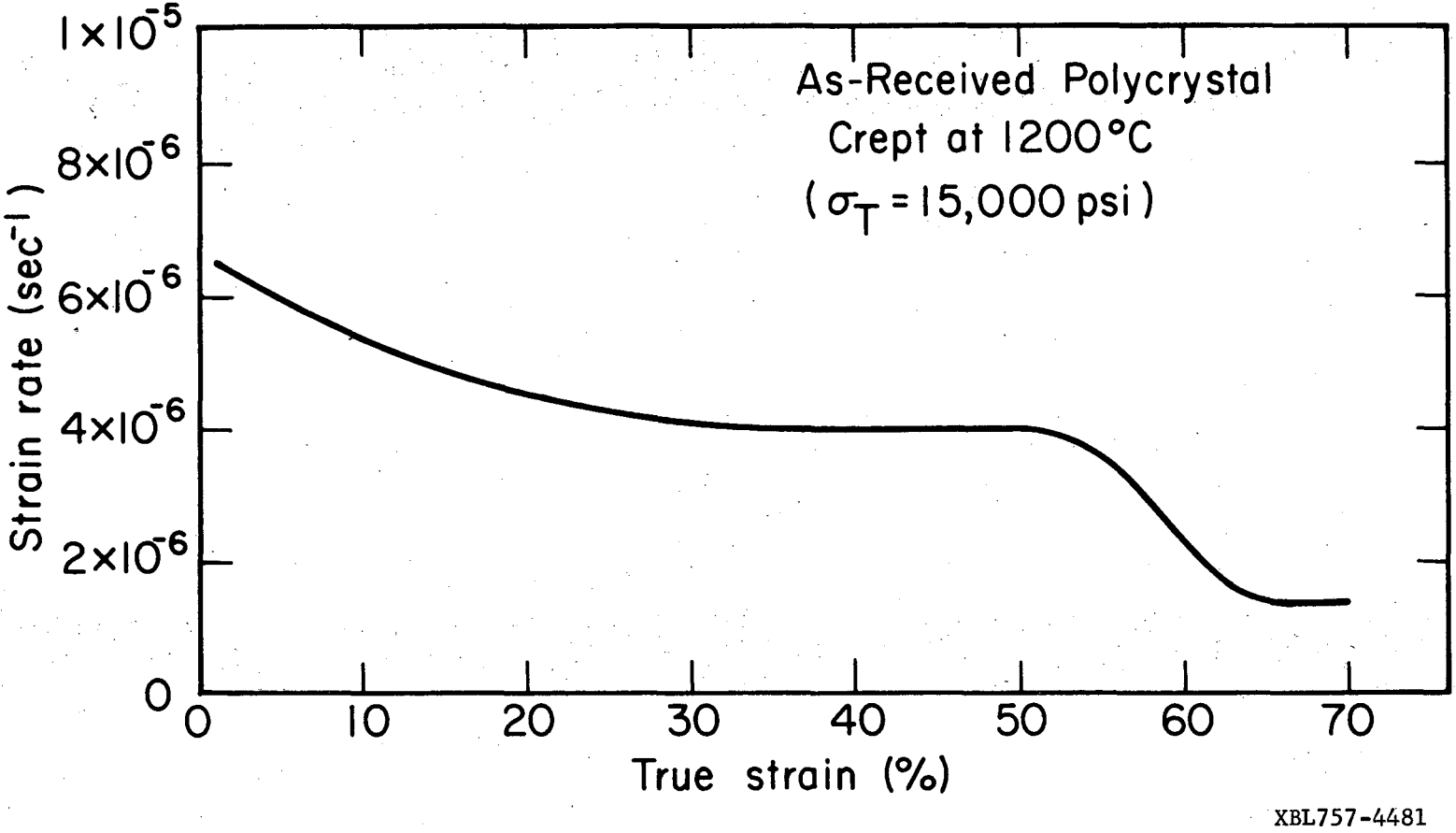
As-Received Polycrystal
Crept at 1200°C
(σ_T = 15,000 psi)
Strain rate (sec^{-1})
1×10^{-5}
8×10^{-6}
6×10^{-6}
4×10^{-6}
2×10^{-6}
0
0
10
20
30
40
50
60
70
True strain (%)
XBL757-4481

Fig. 33.

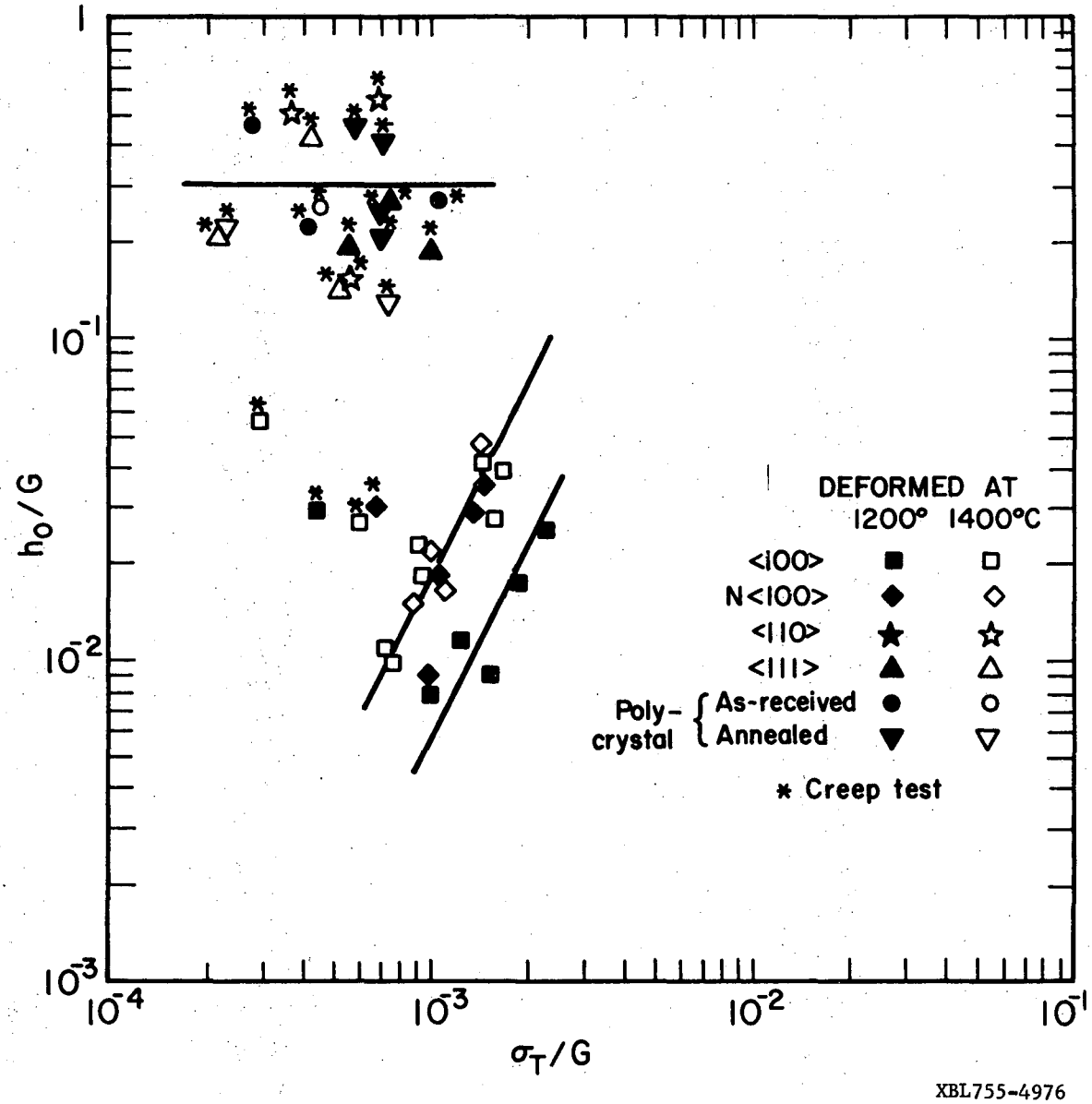

Fig. 34.

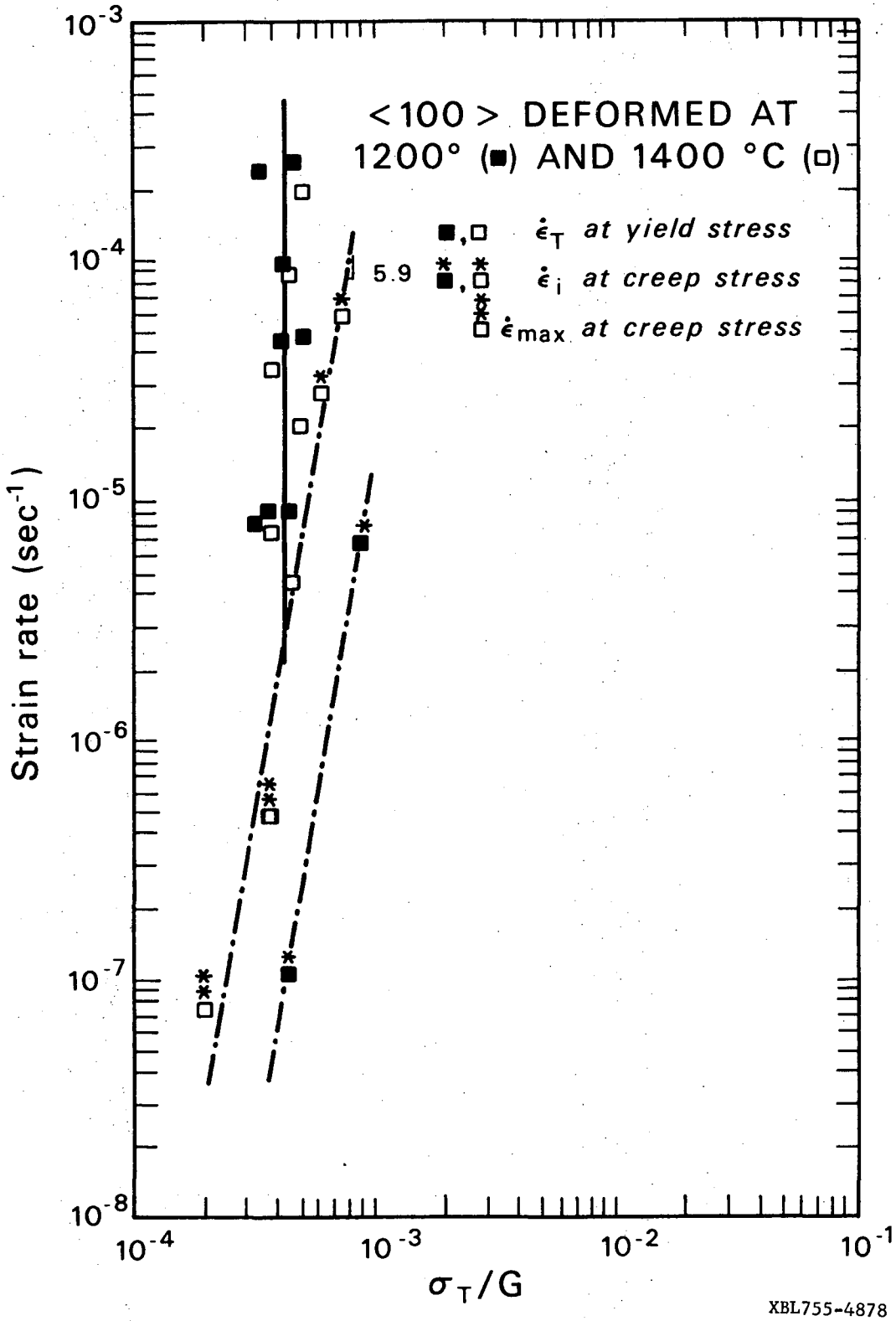
<100> DEFORMED AT
1200° (■) AND 1400 °C (□)
■,□ $\dot{\epsilon}_T$ at yield stress
5.9 ■,□ $\dot{\epsilon}_i$ at creep stress
□ $\dot{\epsilon}_{max}$ at creep stress
Strain rate (sec^{-1})
10^{-3}
10^{-4}
10^{-5}
10^{-6}
10^{-7}
10^{-8}
10^{-4}
10^{-3}
10^{-2}
10^{-1}
σ_T/G
XBL755-4878

Fig. 35(a)

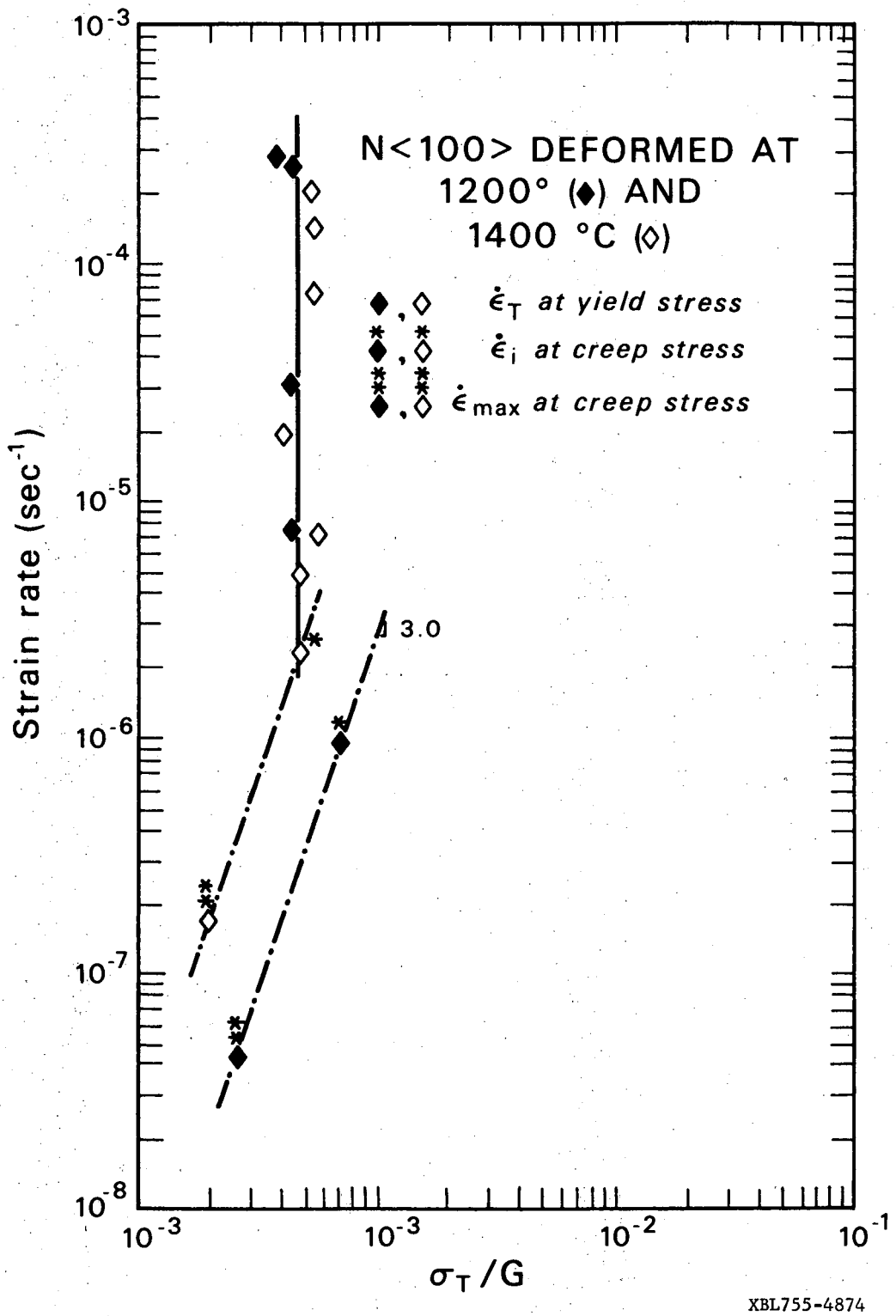

Fig. 35(b)

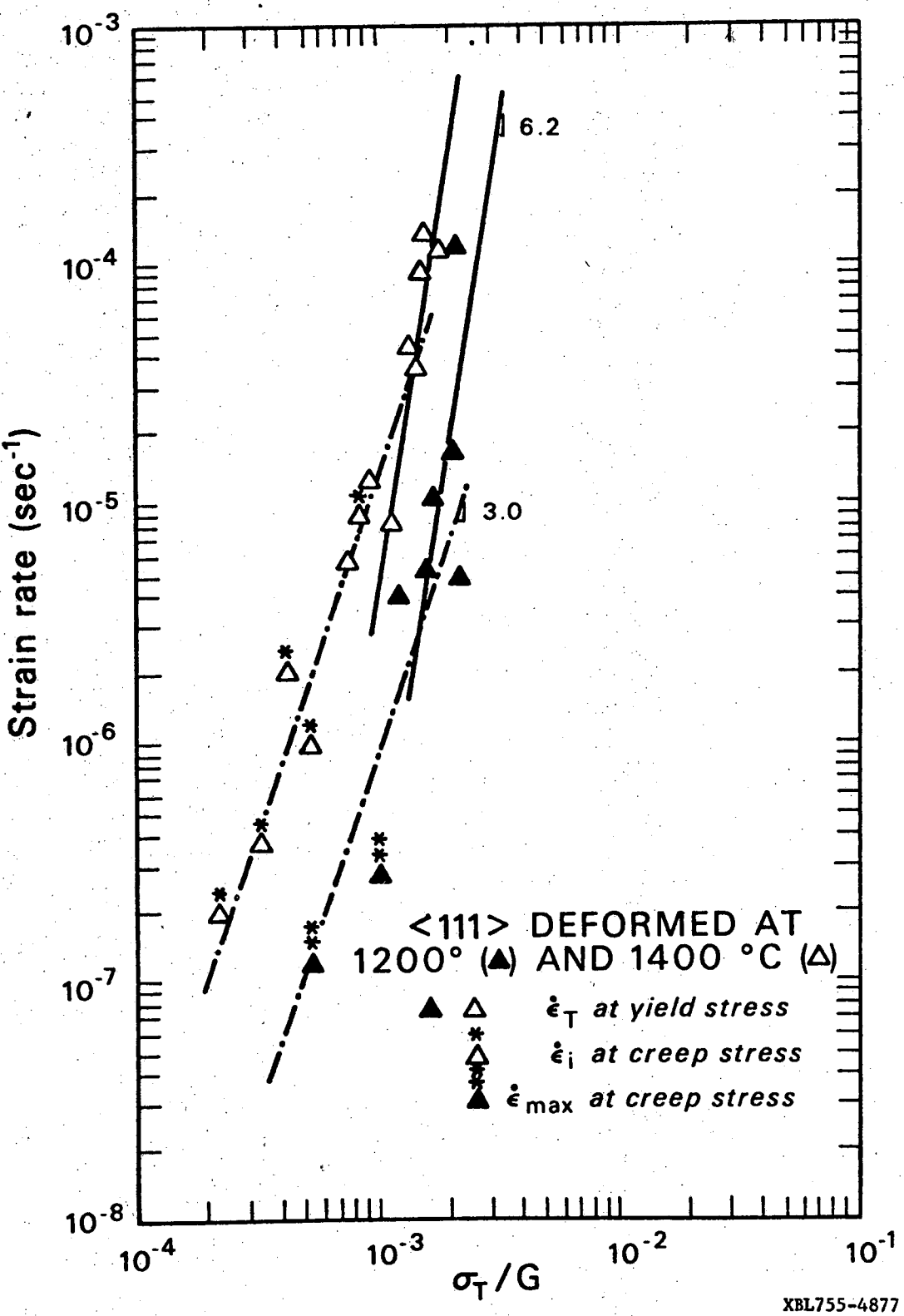
Strain rate (sec^{-1})
10^{-3}
10^{-4}
10^{-5}
10^{-6}
10^{-7}
10^{-8}
6.2
3.0
<111> DEFORMED AT
1200° (▲) AND 1400 °C (△)
$\dot{\epsilon}_T$ at yield stress
$\dot{\epsilon}_i$ at creep stress
$\dot{\epsilon}_{max}$ at creep stress
10^{-4}
10^{-3}
10^{-2}
10^{-1}
σ_T / G
XBL755-4877

Fig. 35(c)

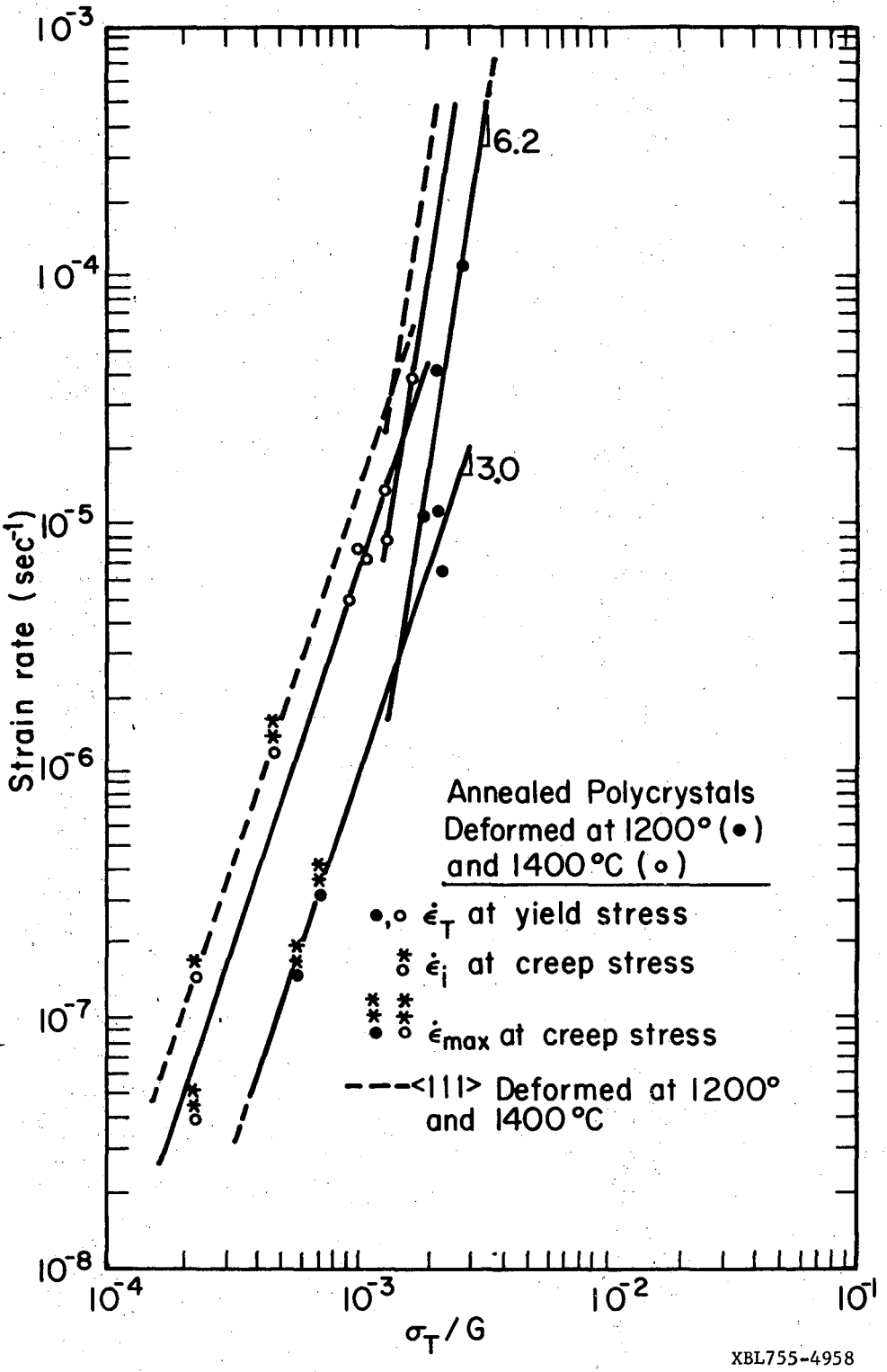

Fig. 35(d)

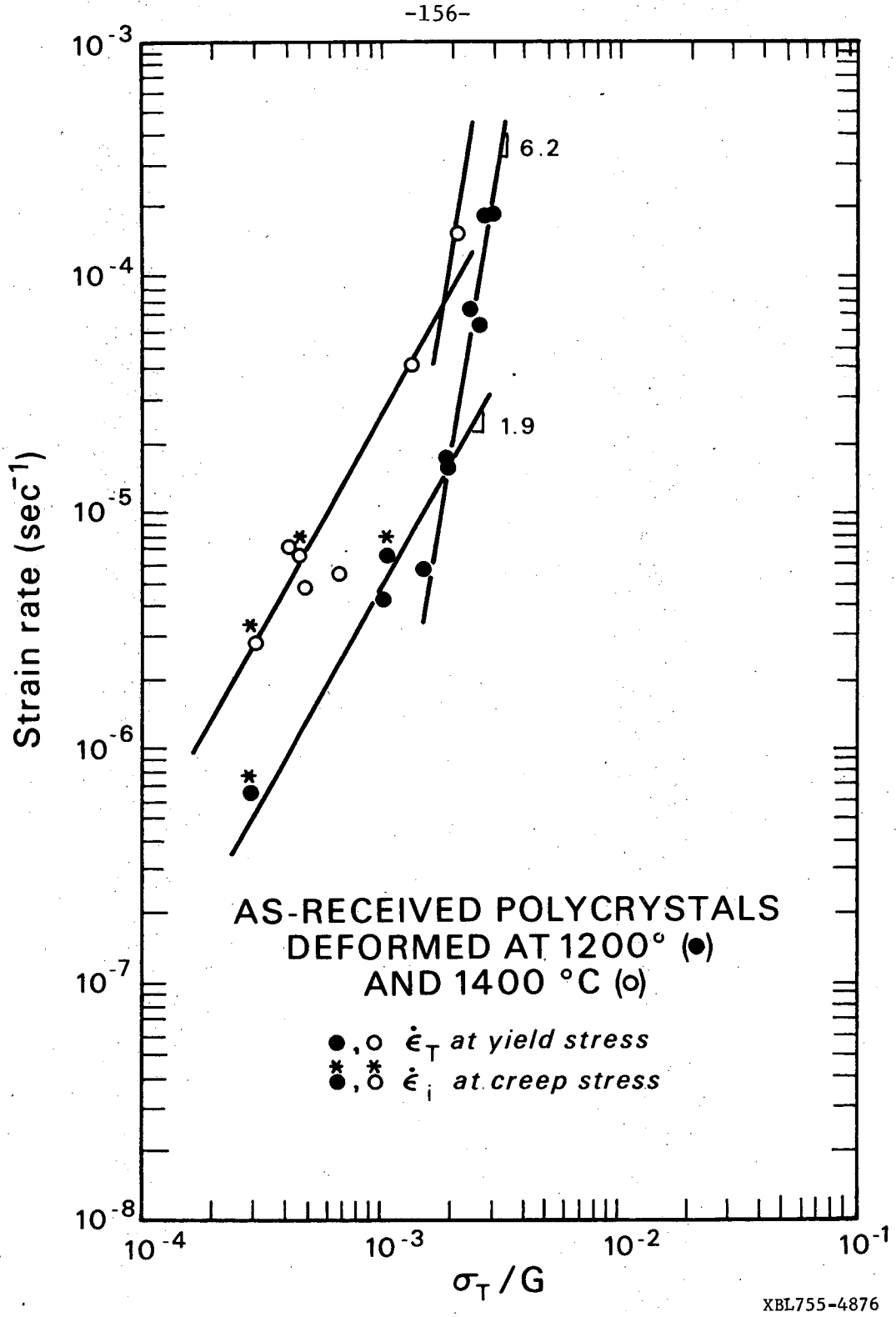
Strain rate (sec^{-1})
10^{-3}
10^{-4}
10^{-5}
10^{-6}
10^{-7}
10^{-8}
6.2
1.9
AS-RECEIVED POLYCRYSTALS
DEFORMED AT 1200° (●)
AND 1400 °C (o)
●, o $\dot{\epsilon}_T$ at yield stress
✱, ✱ $\dot{\epsilon}_i$ at creep stress
10^{-4}
10^{-3}
10^{-2}
10^{-1}
σ_T / G
XBL755-4876

Fig. 35(e)

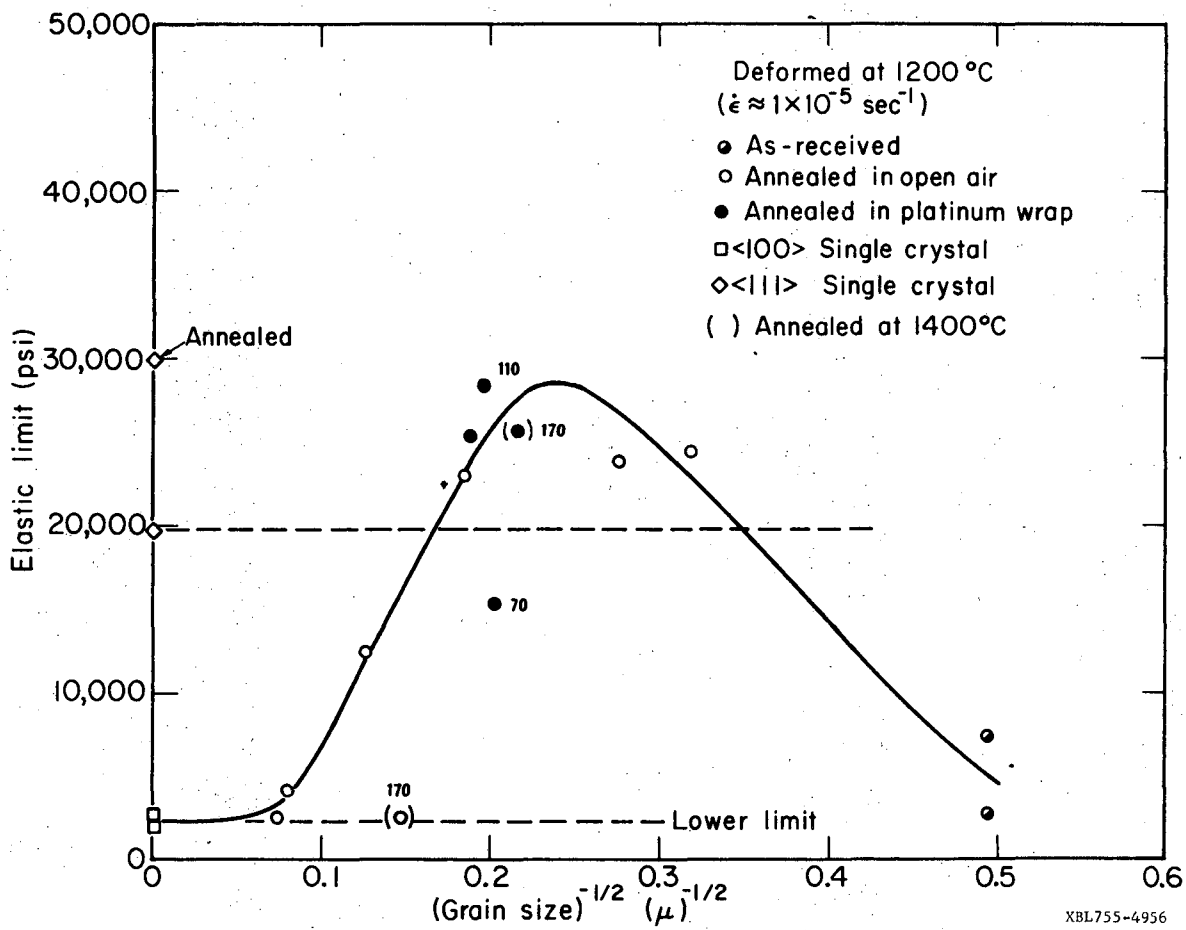

Fig. 36(a)

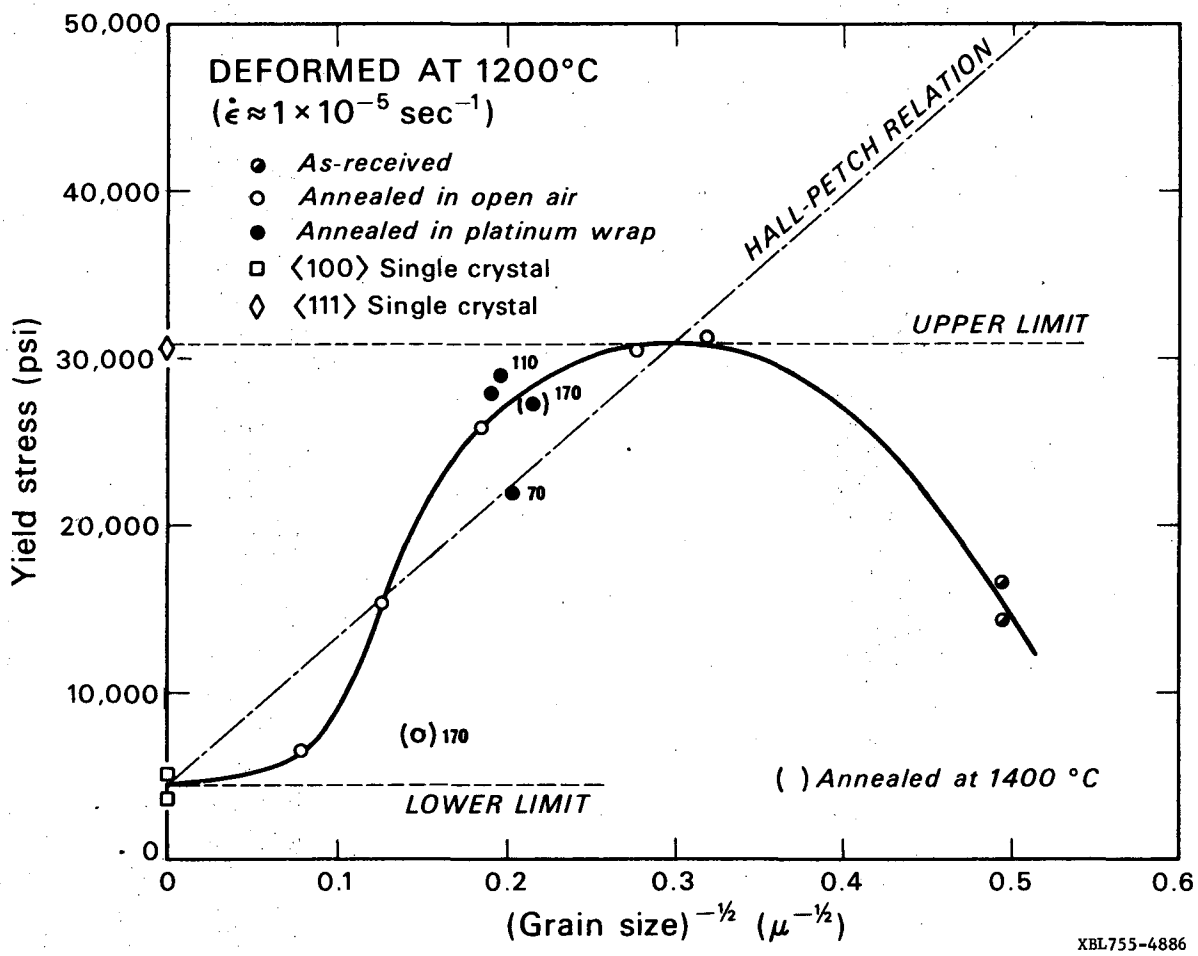
DEFORMED AT 1200°C
($\dot{\epsilon} \approx 1 \times 10^{-5}$ sec^{-1})
As-received
Annealed in open air
Annealed in platinum wrap
⟨100⟩ Single crystal
⟨111⟩ Single crystal
HALL-PETCH RELATION
UPPER LIMIT
LOWER LIMIT
110
170
70
(o) 170
( ) Annealed at 1400 °C
Yield stress (psi)
50,000
40,000
30,000
20,000
10,000
0
0
0.1
0.2
0.3
0.4
0.5
0.6
(Grain size)$^{-½}$ ($\mu^{-½}$)
XBL755-4886

Fig. 36(b)

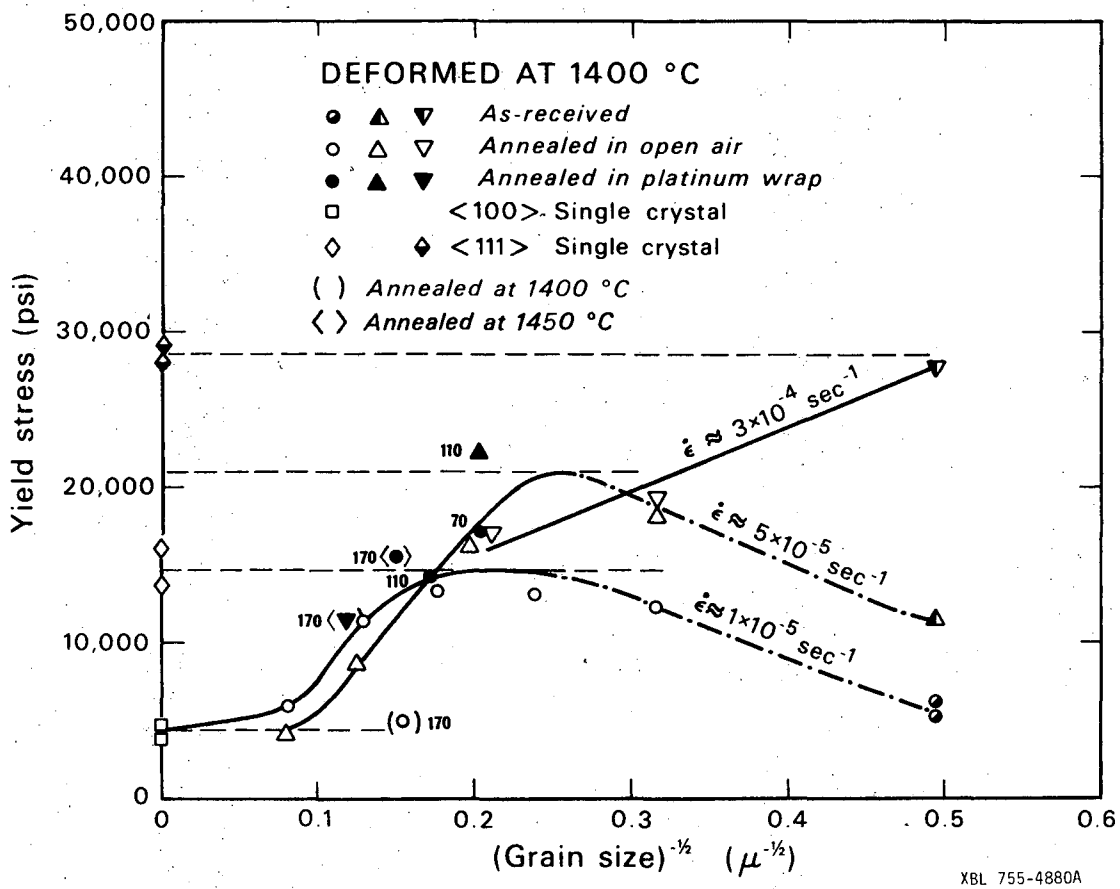

Fig. 36(c)

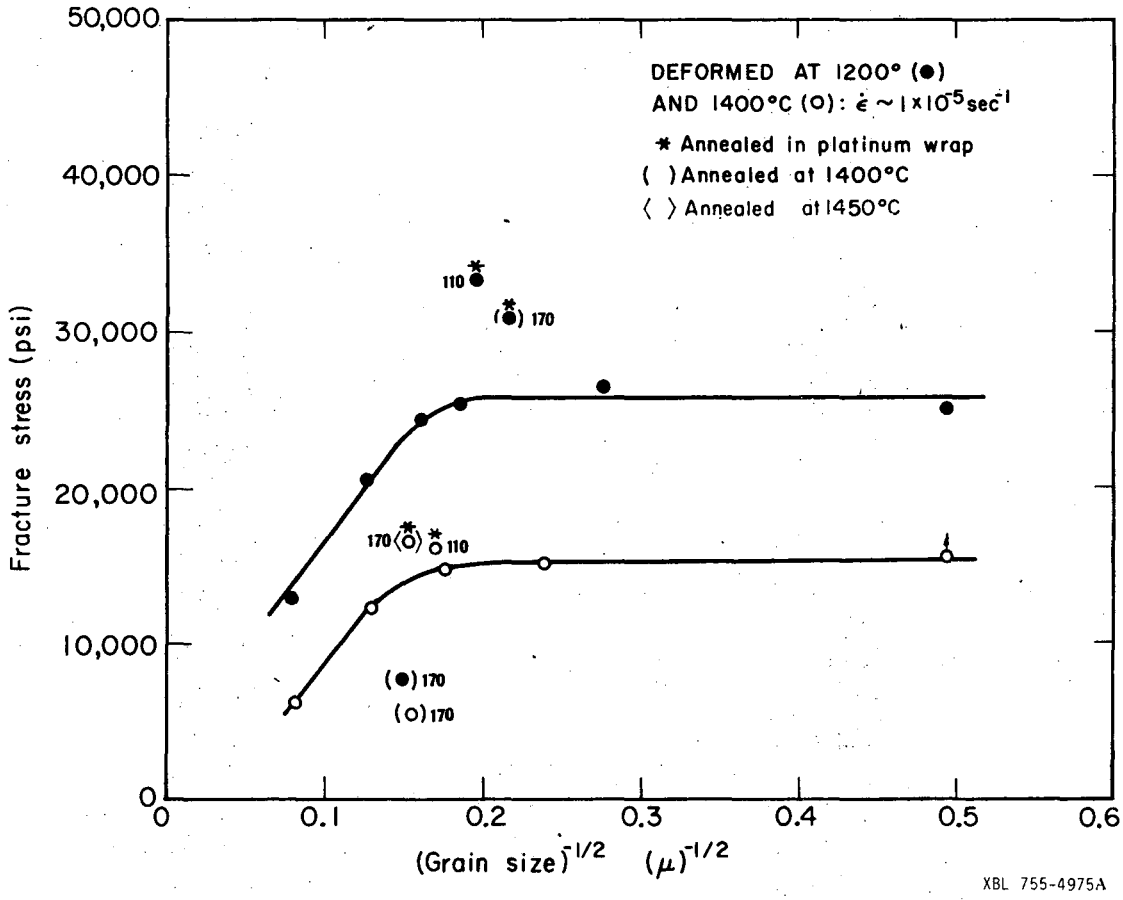
DEFORMED AT 1200° (●)
AND 1400°C (○): $\dot{\epsilon} \sim 1 \times 10^{-5} sec^{-1}$
* Annealed in platinum wrap
( ) Annealed at 1400°C
⟨ ⟩ Annealed at 1450°C
Fracture stress (psi)
50,000
40,000
30,000
20,000
10,000
0
0
0.1
0.2
0.3
0.4
0.5
0.6
(Grain size)$^{-1/2}$ (μ)$^{-1/2}$
110
170
170
110
(●) 170
(○) 170
XBL 755-4975A

Fig. 37.

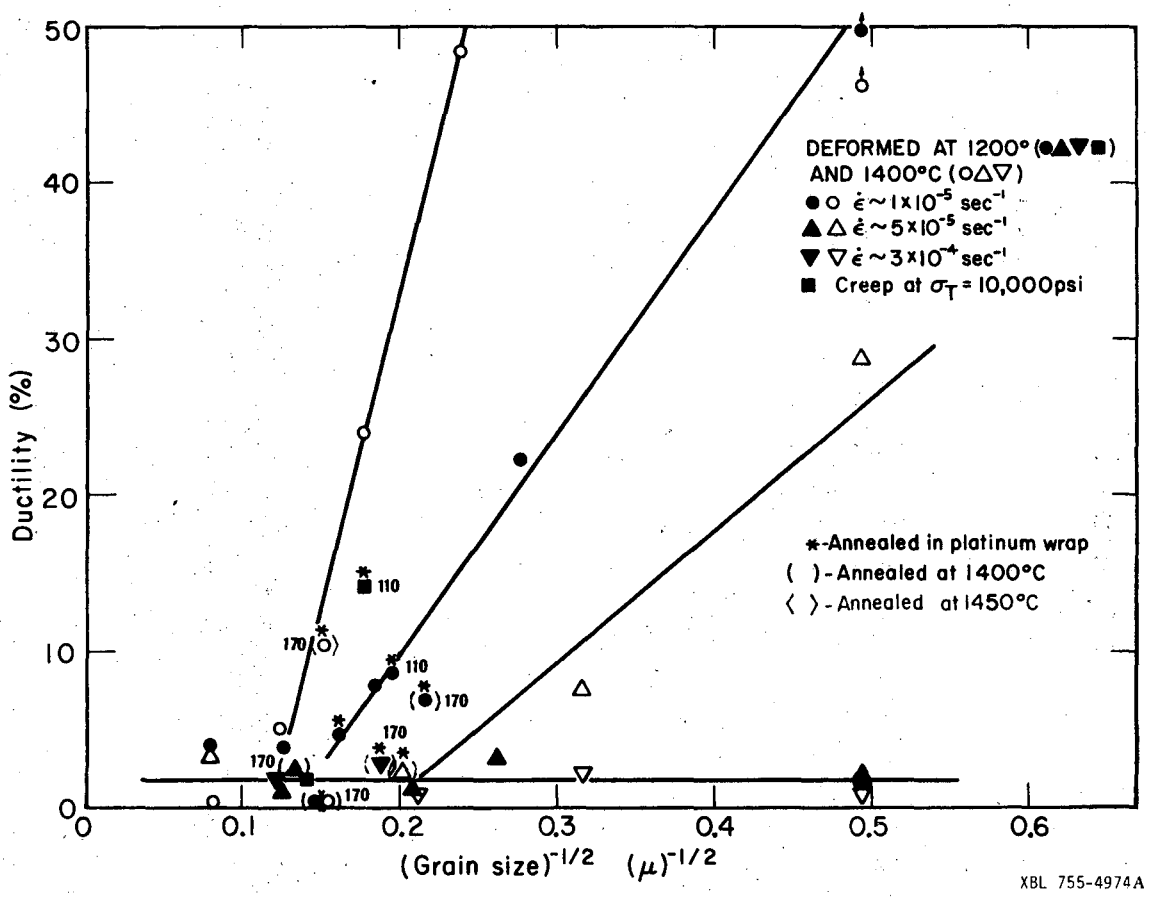

Fig. 38.

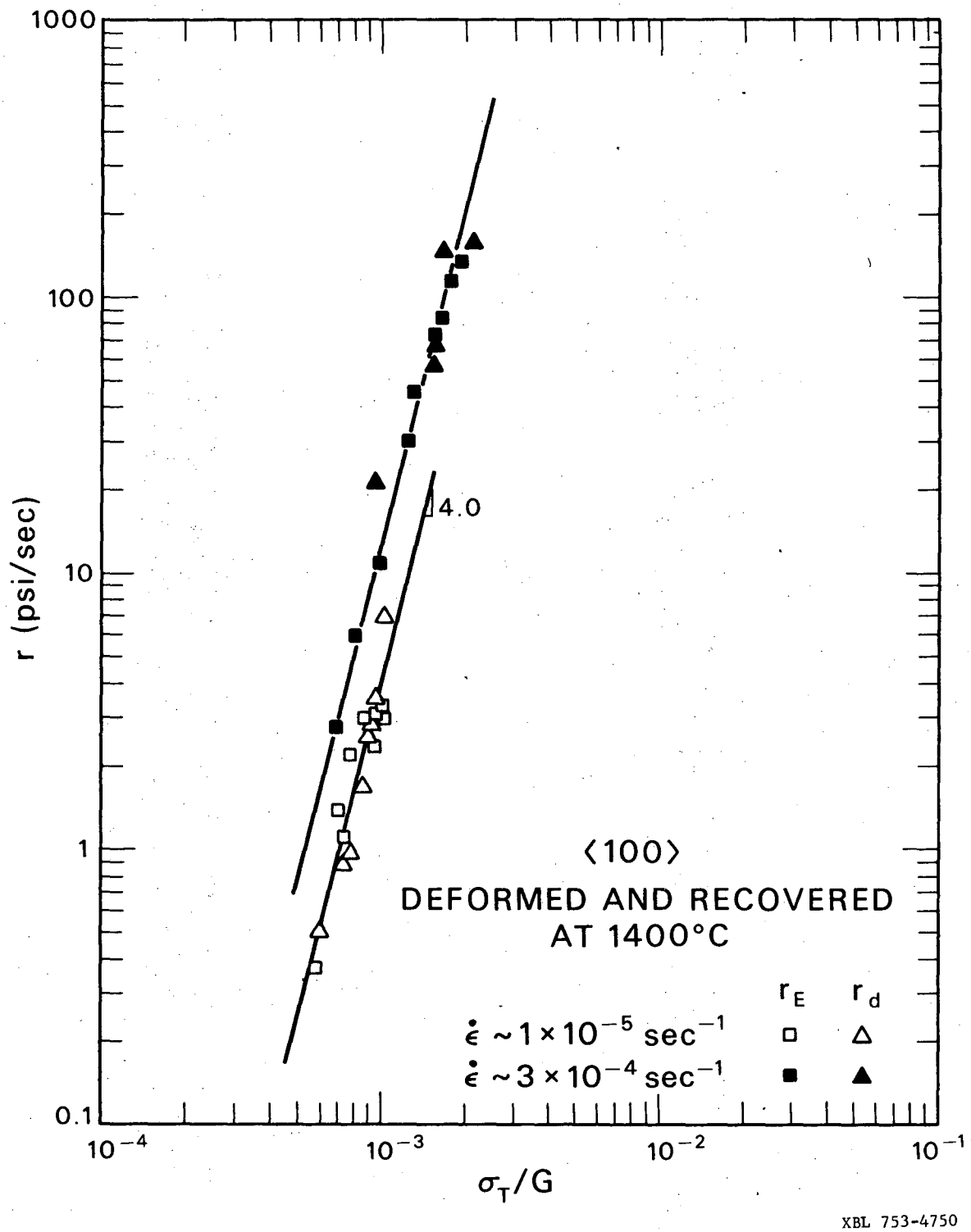
1000
100
10
1
0.1
r (psi/sec)
4.0
⟨100⟩
DEFORMED AND RECOVERED
AT 1400°C
r_E r_d
$\dot{\epsilon} \sim 1 \times 10^{-5}$ sec^{-1}
$\dot{\epsilon} \sim 3 \times 10^{-4}$ sec^{-1}
10^{-4}
10^{-3}
10^{-2}
10^{-1}
σ_T/G
XBL 753-4750

Fig. 39.

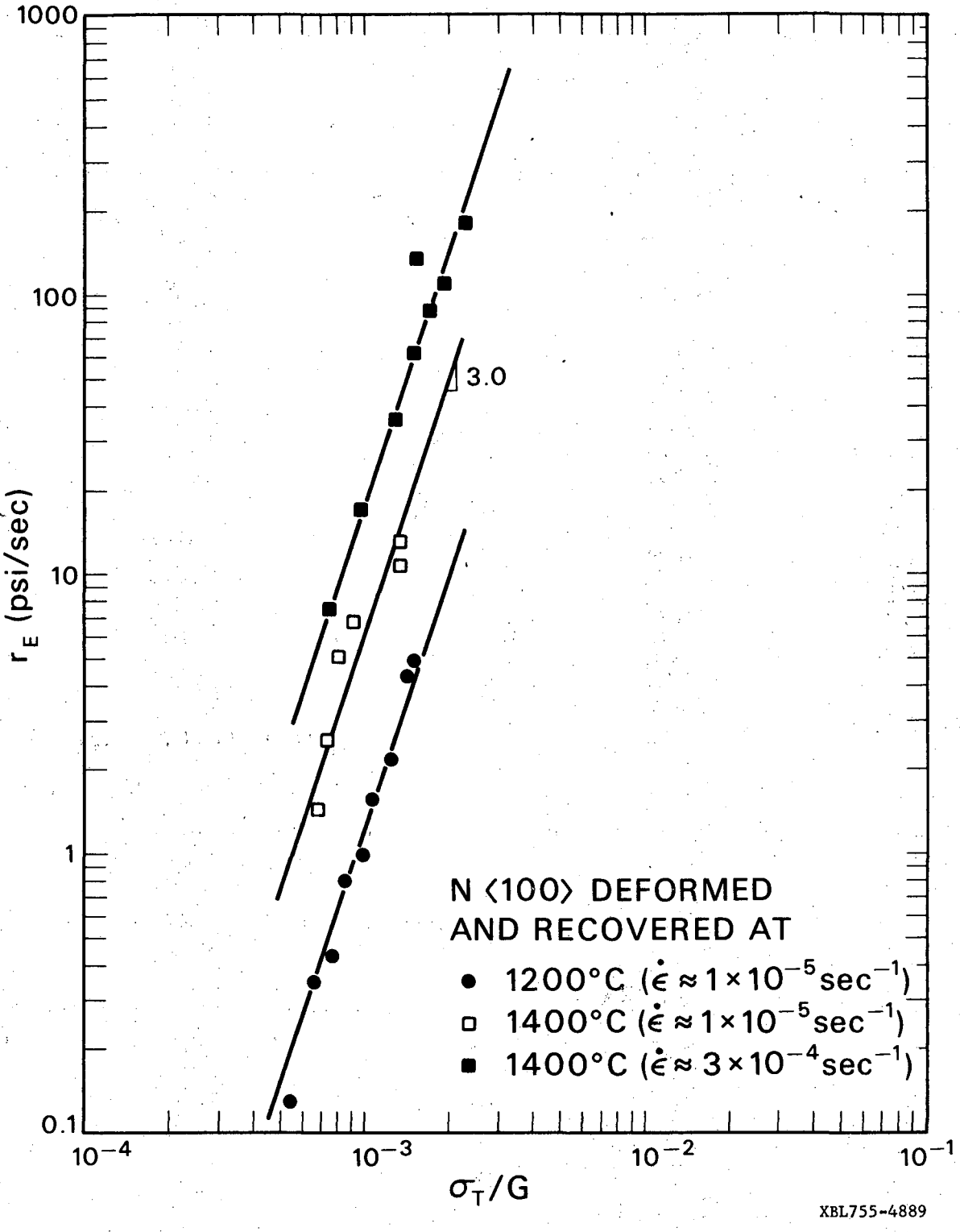

Fig. 40.

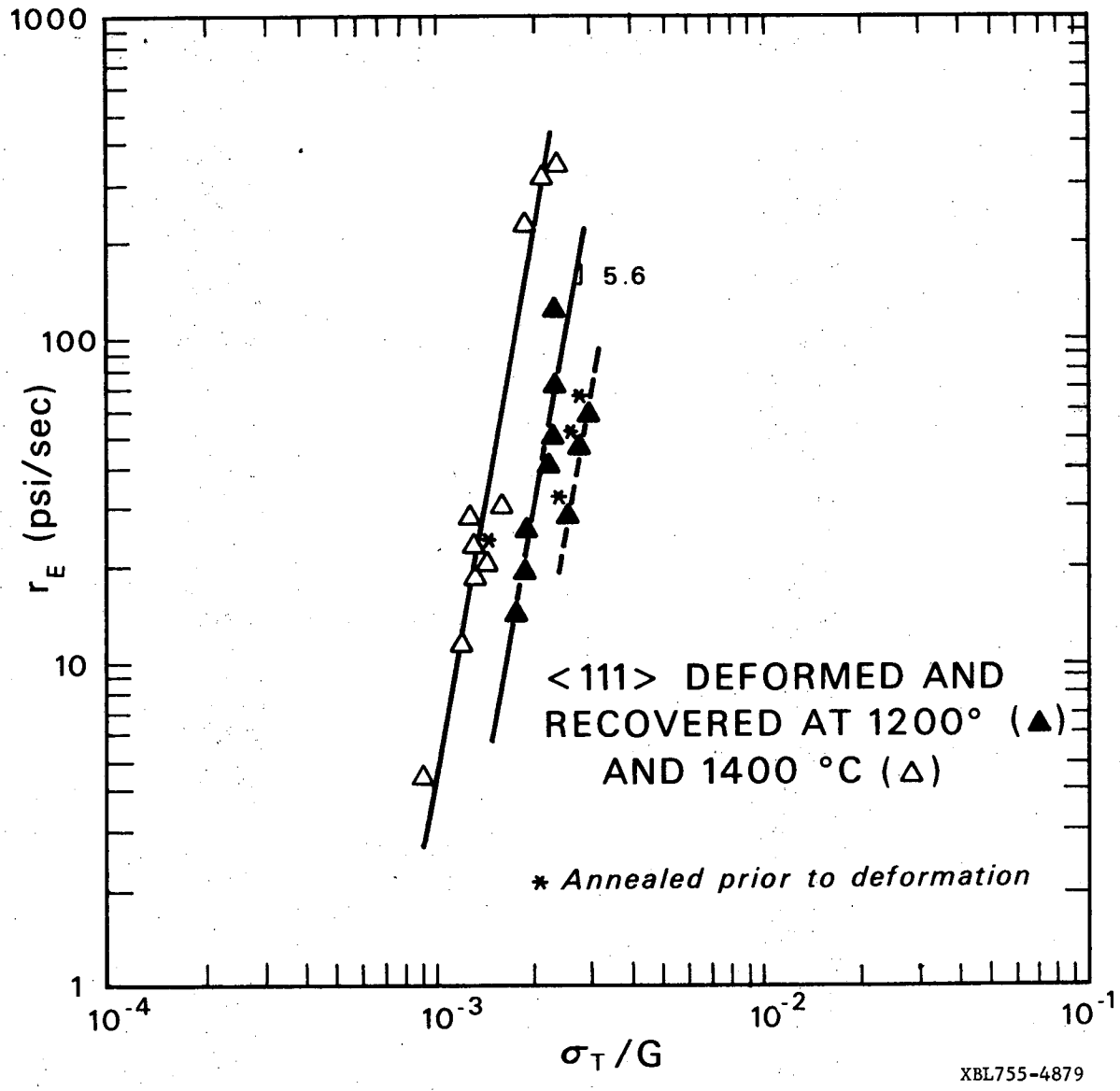
1000
100
10
1
r_E (psi/sec)
5.6
<111> DEFORMED AND
RECOVERED AT 1200° (▲)
AND 1400 °C (△)
* Annealed prior to deformation
10^{-4}
10^{-3}
10^{-2}
10^{-1}
σ_T / G
XBL755-4879

Fig. 41.

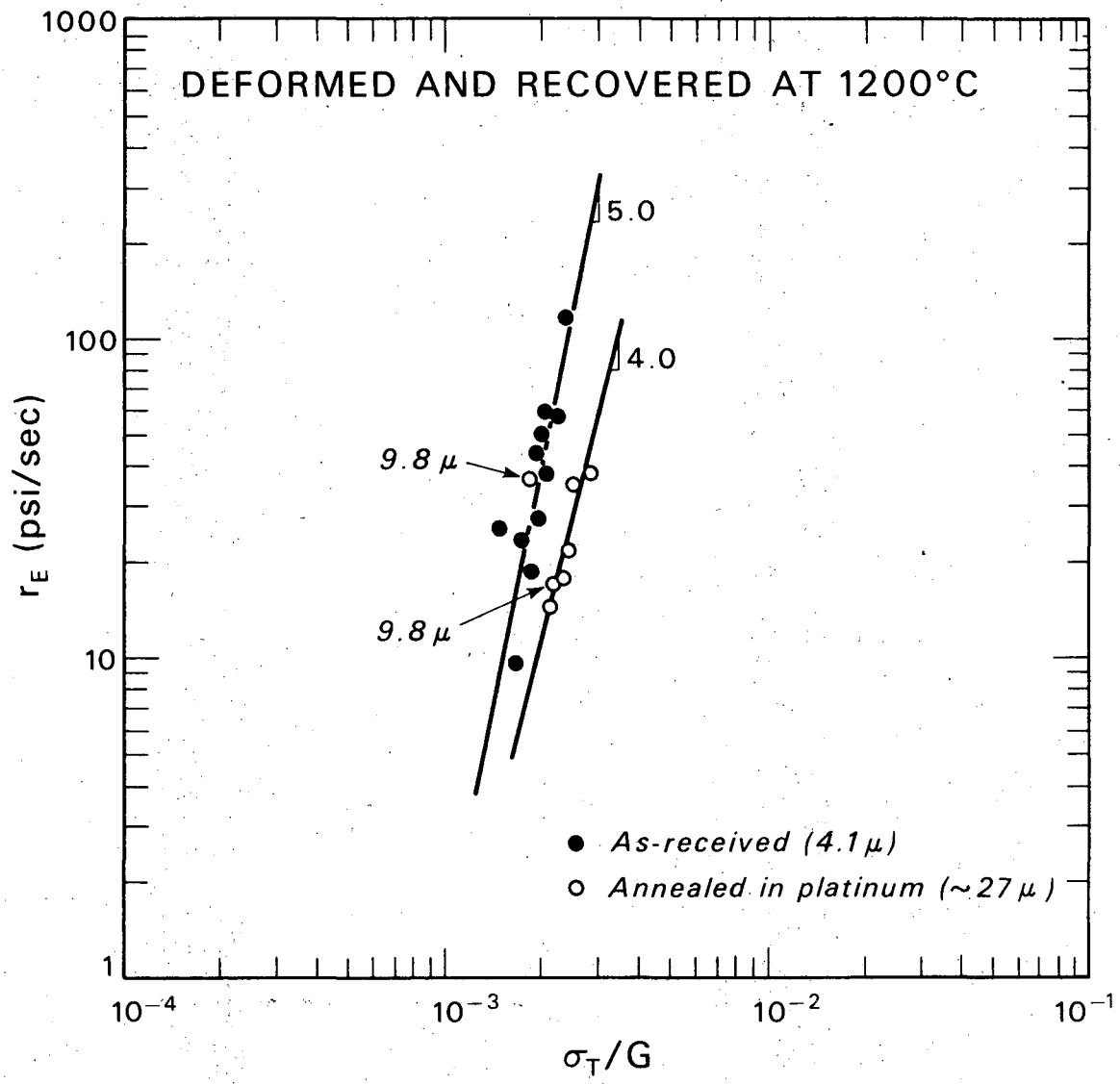

Fig. 42(a)

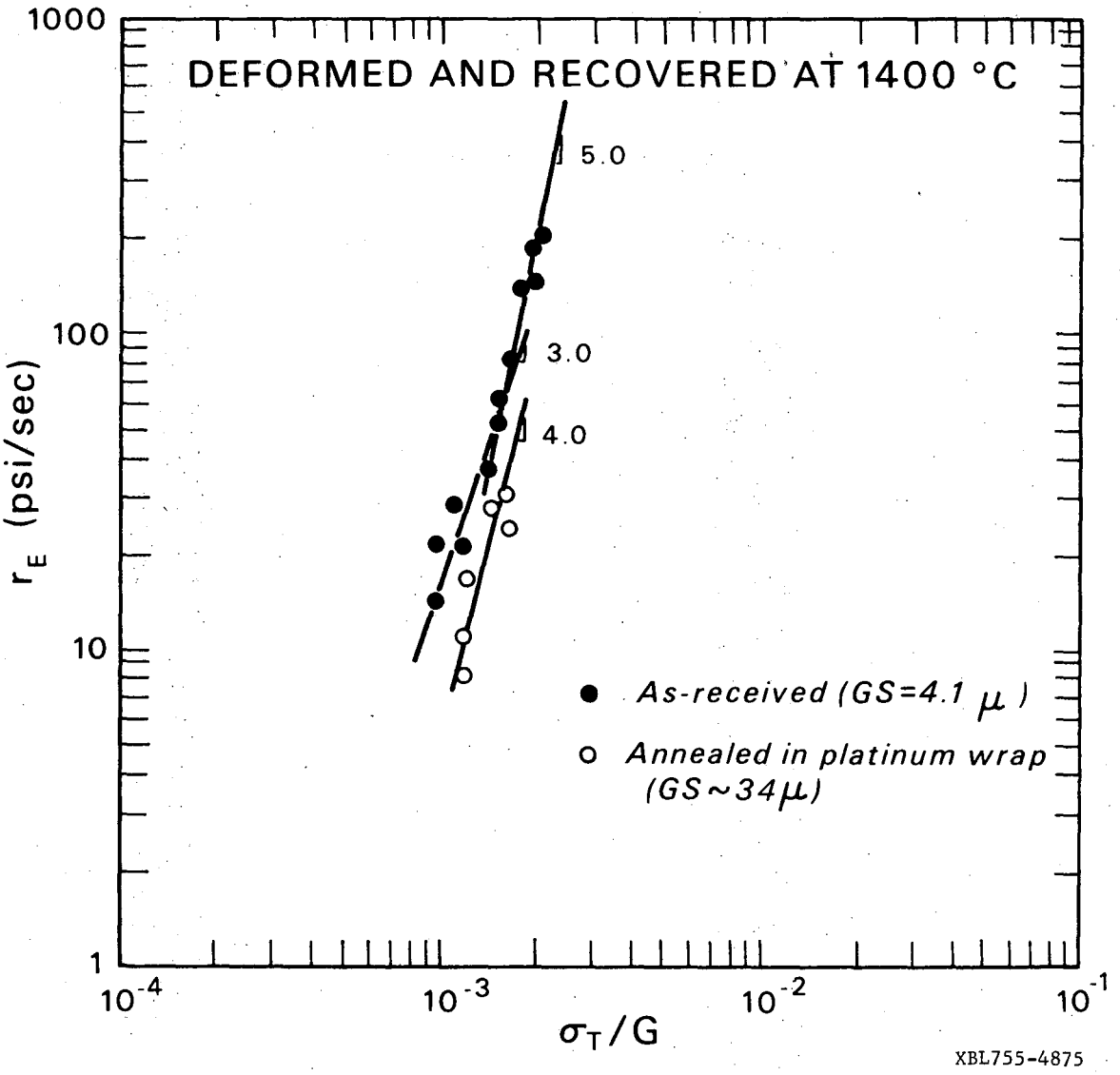
DEFORMED AND RECOVERED AT 1400 °C
5.0
3.0
4.0
As-received (GS=4.1 μ)
Annealed in platinum wrap (GS~34μ)
1000
100
10
1
r_E (psi/sec)
10^{-4}
10^{-3}
10^{-2}
10^{-1}
σ_T/G
XBL755-4875

Fig. 42(b)

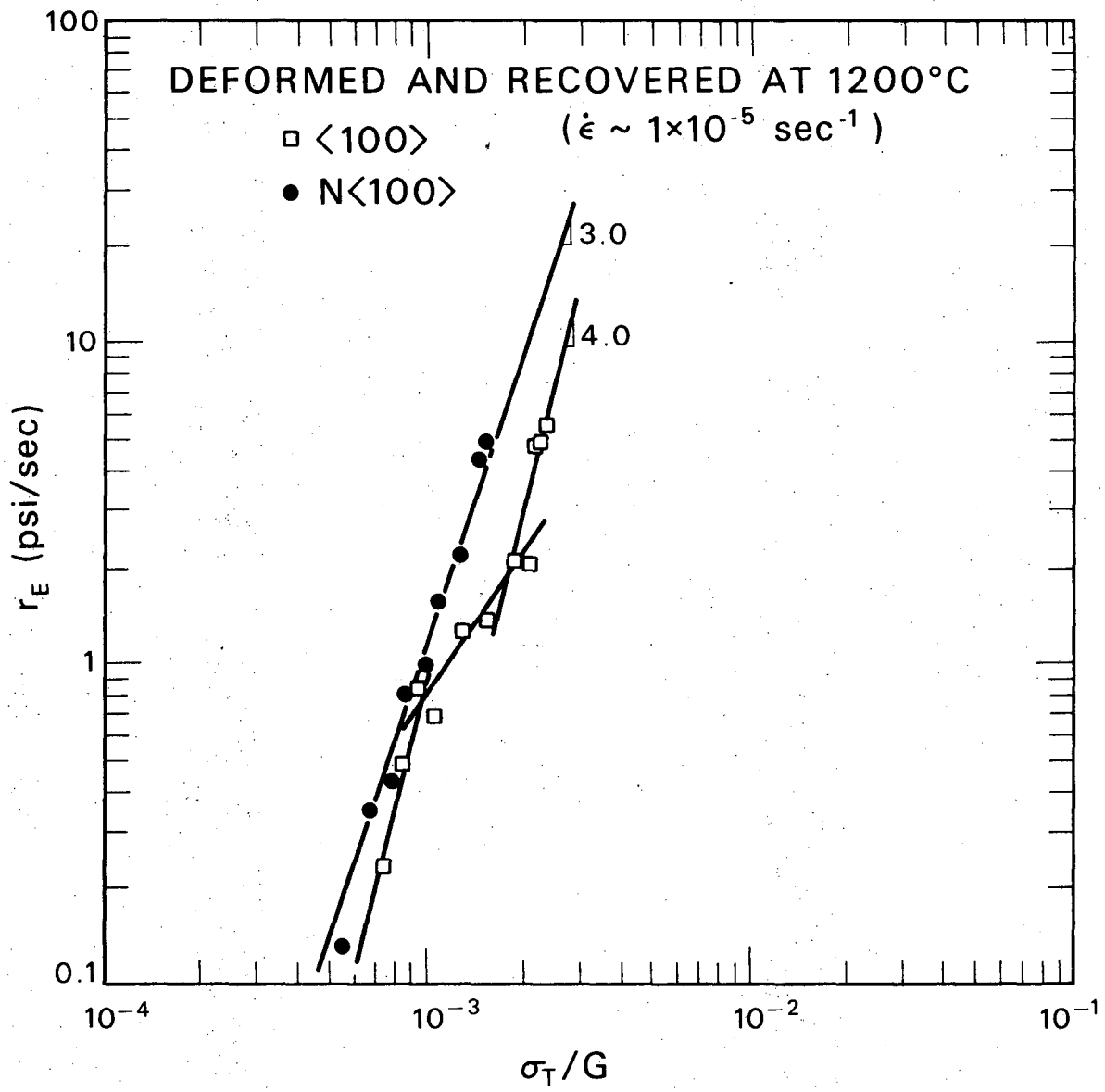

Fig. 43.

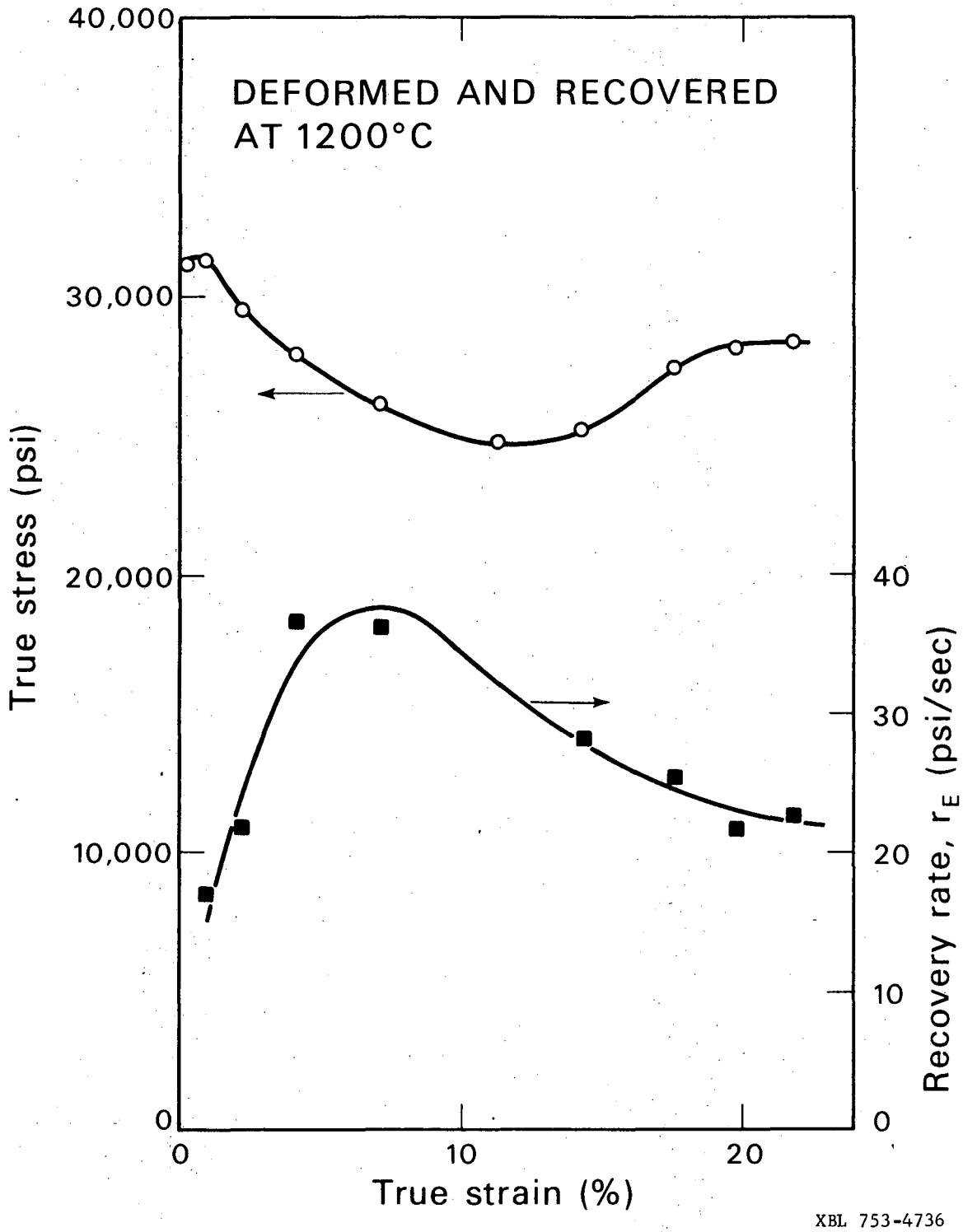
DEFORMED AND RECOVERED
AT 1200°C
40,000
30,000
20,000
10,000
0
True stress (psi)
0
10
20
True strain (%)
40
30
20
10
0
Recovery rate, r_E (psi/sec)
XBL 753-4736

Fig. 44.

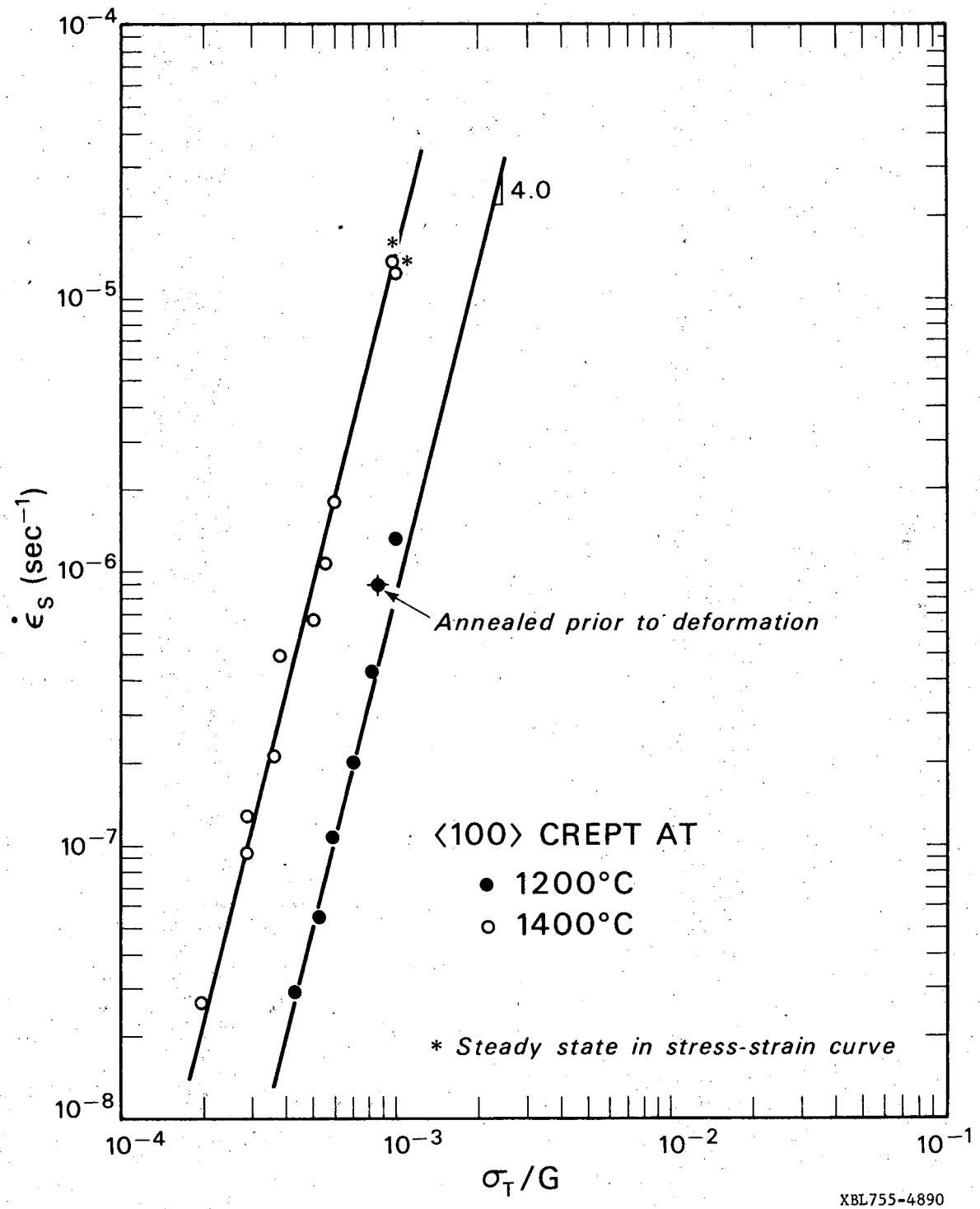

Fig. 45(a)

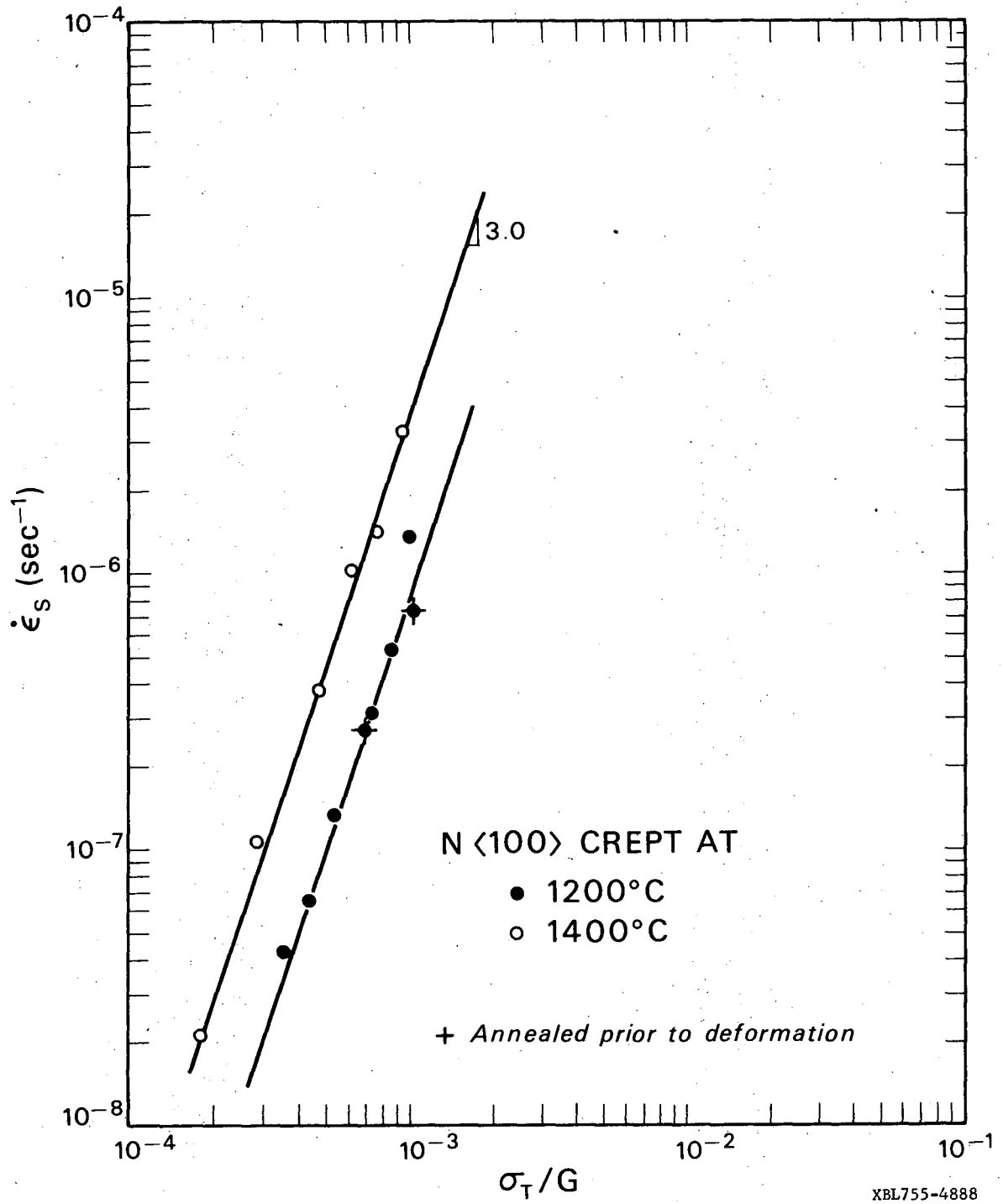
10^{-4}
10^{-5}
10^{-6}
10^{-7}
10^{-8}
$\dot{\epsilon}_s$ (sec^{-1})
3.0
N ⟨100⟩ CREPT AT
● 1200°C
○ 1400°C
+ Annealed prior to deformation
10^{-4}
10^{-3}
10^{-2}
10^{-1}
σ_T/G
XBL755-4888

Fig. 45(b)

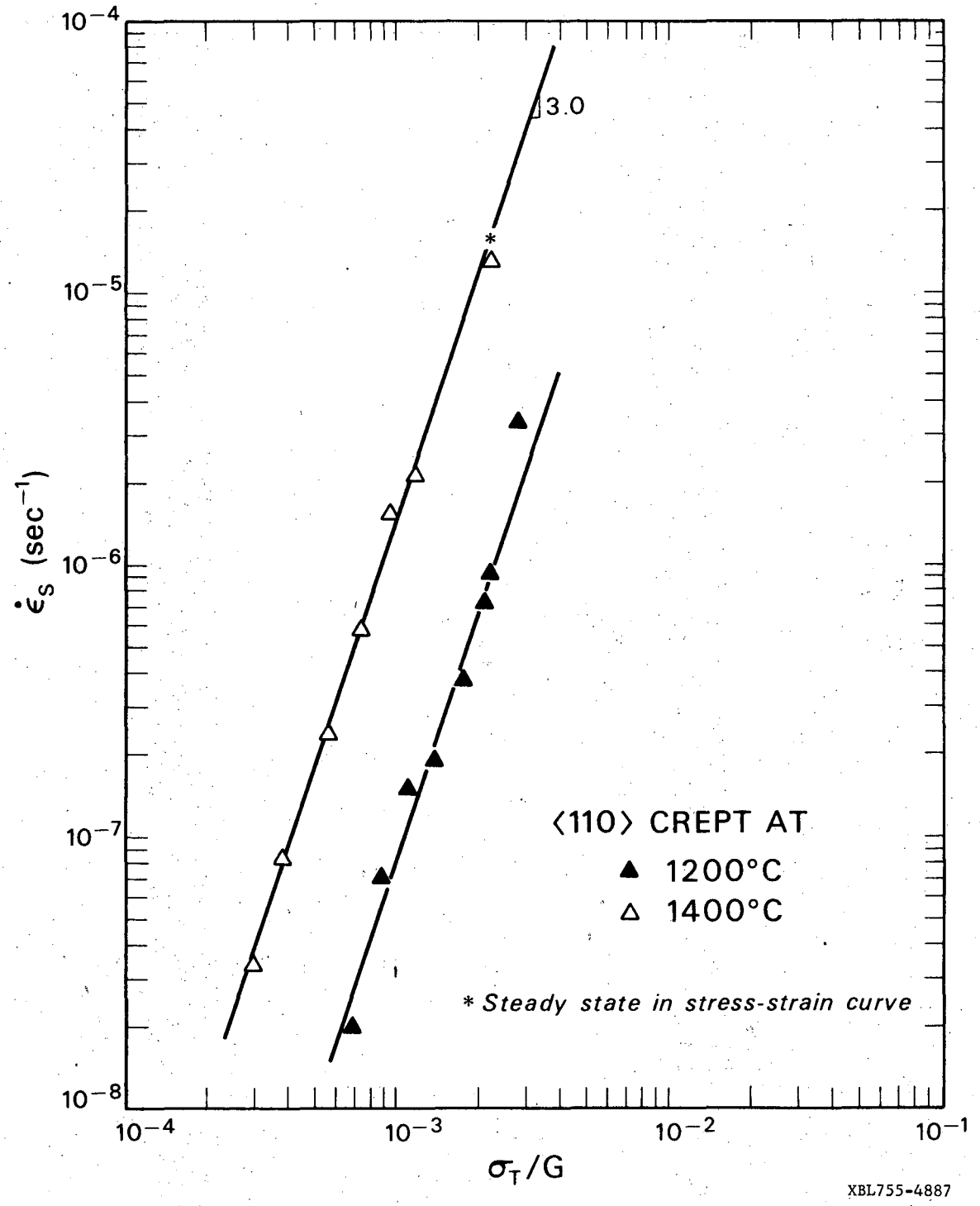

Fig. 45(c)

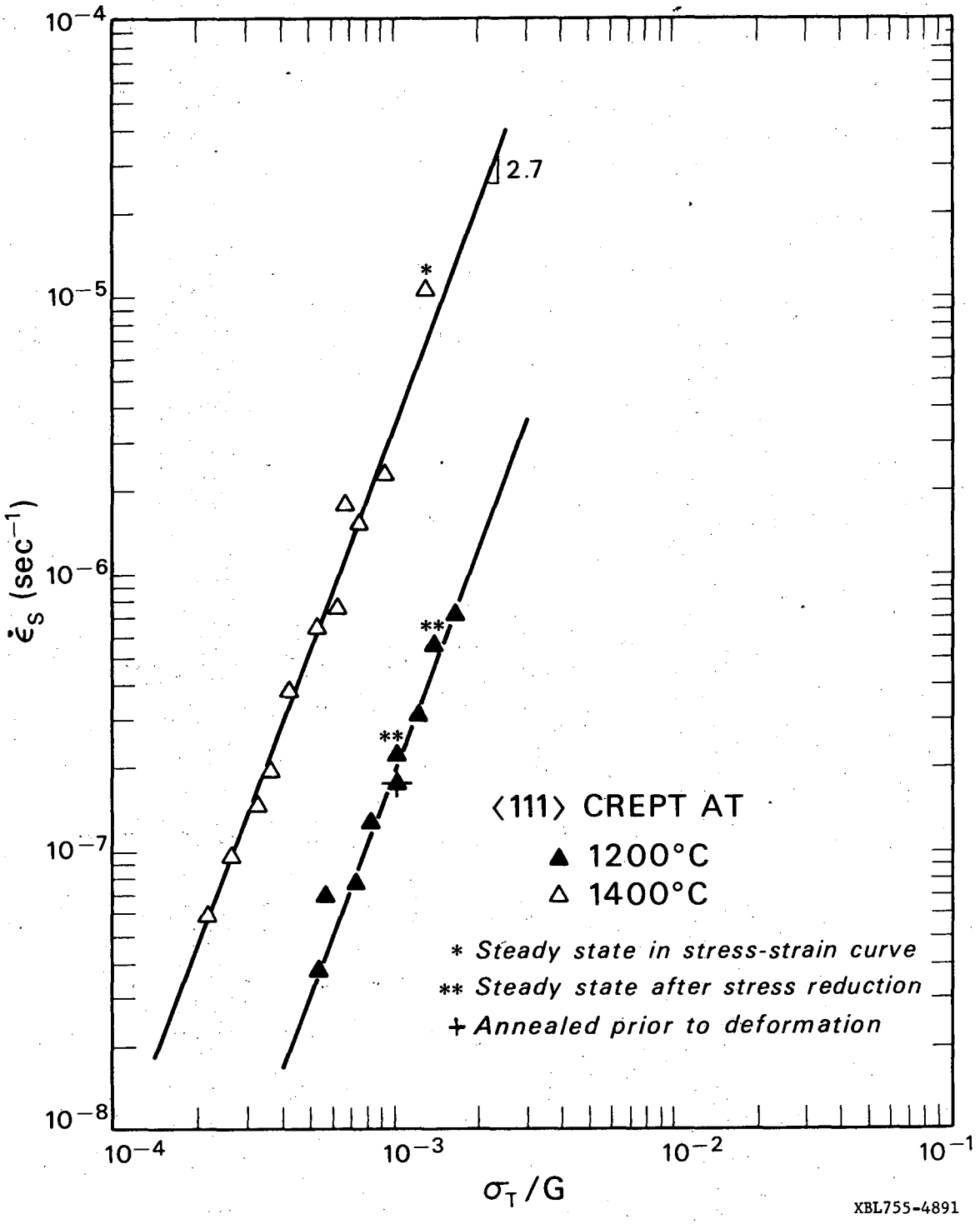
10^{-4}
10^{-5}
10^{-6}
10^{-7}
10^{-8}
$\dot{\epsilon}_s$ (sec^{-1})
2.7
*
**
**
+
⟨111⟩ CREPT AT
▲ 1200°C
△ 1400°C
* Steady state in stress-strain curve
** Steady state after stress reduction
+ Annealed prior to deformation
10^{-4}
10^{-3}
10^{-2}
10^{-1}
σ_T /G
XBL755-4891

Fig. 45(d)

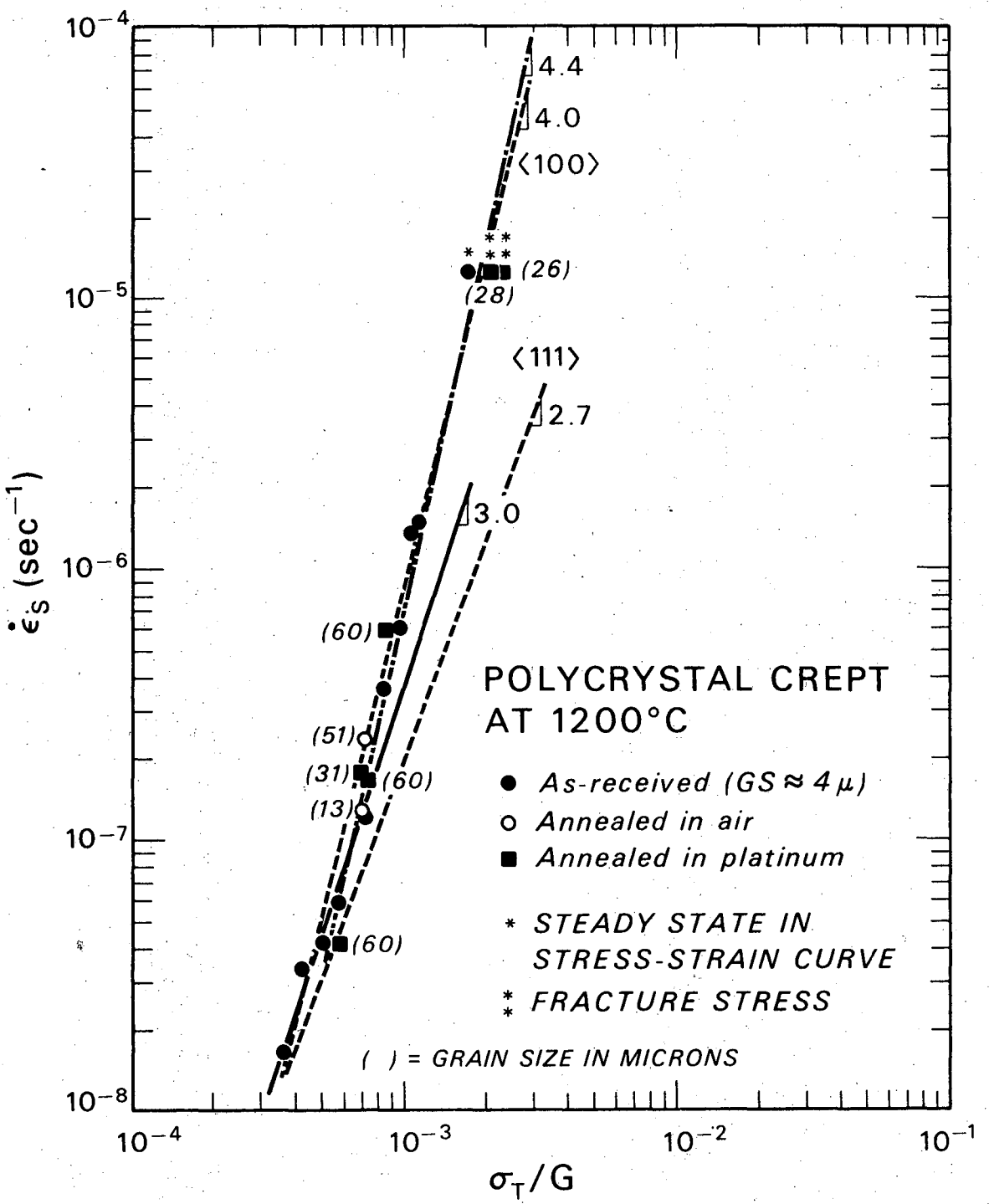

XBL 753-4752

Fig. 46(a)

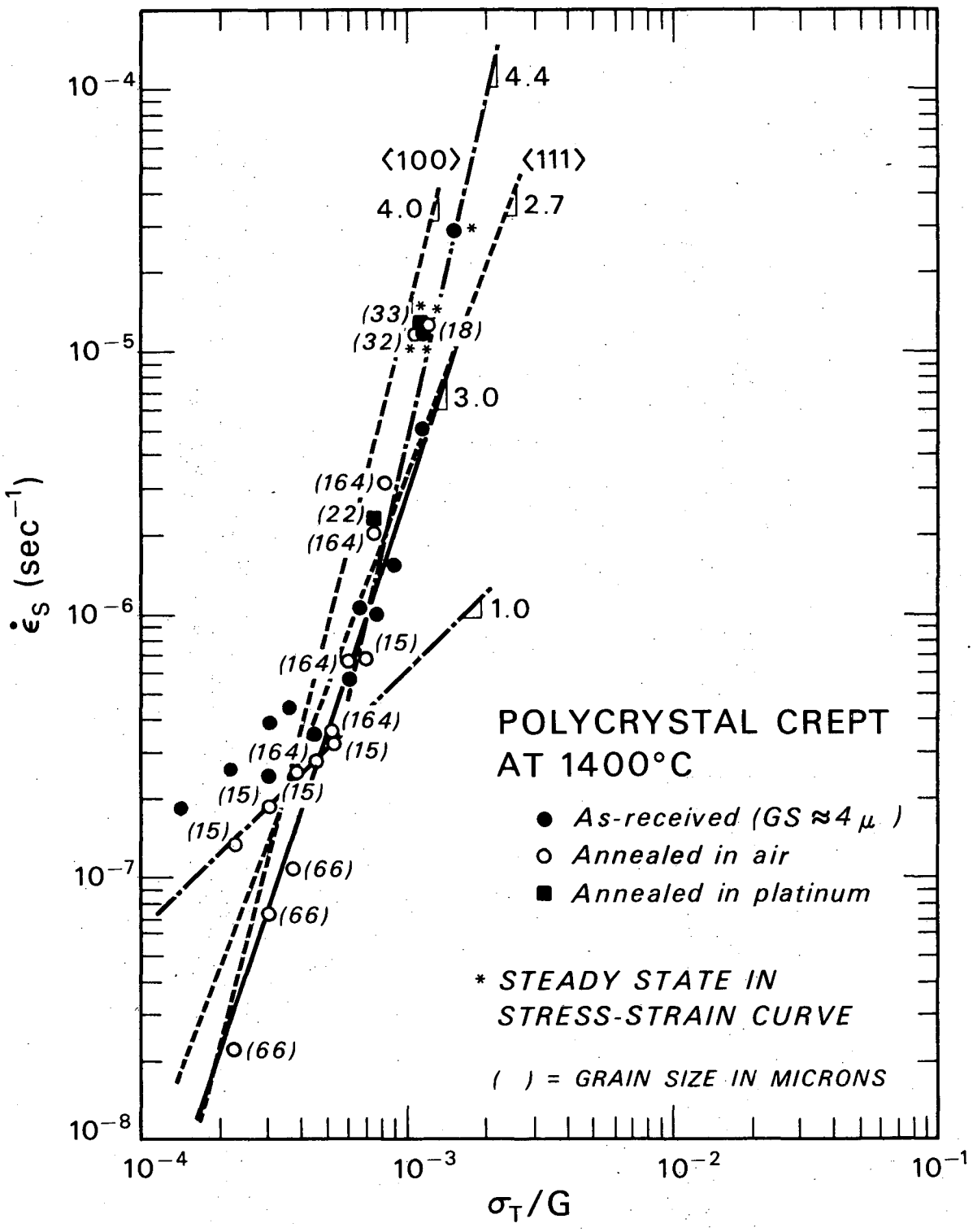
10^{-4}
10^{-5}
10^{-6}
10^{-7}
10^{-8}
$\dot{\epsilon}_S$ (sec^{-1})
10^{-4}
10^{-3}
10^{-2}
10^{-1}
σ_T/G
4.4
4.0
2.7
3.0
1.0
⟨100⟩
⟨111⟩
(33)
(32)
(18)
(164)
(22)
(164)
(15)
(164)
(164)
(15)
(164)
(15)
(15)
(15)
(15)
(66)
(66)
(66)
POLYCRYSTAL CREPT
AT 1400°C
● As-received (GS ≈4 μ)
○ Annealed in air
■ Annealed in platinum
* STEADY STATE IN
STRESS-STRAIN CURVE
( ) = GRAIN SIZE IN MICRONS
XBL 753-4753

Fig. 46(b)

TECHNICAL INFORMATION DIVISION
LAWRENCE BERKELEY LABORATORY
UNIVERSITY OF CALIFORNIA
BERKELEY, CALIFORNIA 94720